The nature and timing of postglacial valley fill incision, Fraser River, Big Bar to Watson Bar, British Columbia

by

Travis Gingerich

BSc (Hons.), University of the Fraser Valley, 2018

Thesis Submitted in Partial Fulfillment of the
Requirements for the Degree of
Master of Science

in the
Department of Geography
Faculty of Environment

© Travis Gingerich 2021
SIMON FRASER UNIVERSITY
Summer 2021

Copyright in this work rests with the author. Please ensure that any reproduction or re-use is done in accordance with the relevant national copyright legislation.

Declaration of Committee

Name:	**Travis Gingerich**
Degree:	**Master of Science (Geography)**
Thesis title:	**The nature and timing of postglacial valley fill incision, Fraser River, Big Bar to Watson Bar, British Columbia**
Committee:	**Chair:** Bing Lu Assistant Professor, Geography
	Tracy Brennand Supervisor Professor, Geography
	Olav Lian Committee Member Professor, Land Use and Environmental Change University of the Fraser Valley
	John Clague Examiner Professor Emeritus, Earth Sciences

Abstract

Since deglaciation, Fraser River through the southern British Columbia (BC) interior has undergone episodic aggradation and incision to create a series of distinct stepped terraces. This study employed optical dating to date different terrace levels in the Big Bar and Watson Bar reaches of Fraser River to calculate the rate of postglacial incision through glacial valley fill. This incision rate was developed to explore correlation of Fraser River incision with terrace-forming drivers such as climate, local base level change, and glacioisostatic adjustment. The oldest age in this study corresponds to the outburst flood of glacial Lake Fraser at 11.3 ± 1.5 ka, consistent with other independent ages for the event. From this event, Fraser River incised through ~180 m of glacial valley fill to reach its present-day level, where it now flows on bedrock. The average incision rate during the last ~11 ka was 15 mm/a, though this study speculates that during the last ~11 ka, Fraser River incision rates may have varied, roughly following postglacial climatic phases imprinted on the paraglacial cycle. For example, fast incision rates (30 m/a) were present through the cooler and wetter middle Holocene (7-4 ka) due to the reduction of upland paraglacial sedimentation and high flow power due to wetter conditions. Local aggradation resulted upstream of landslides and large paraglacial fans that temporarily increased local base level. Fraser River incised to bedrock sometime in the last 4 ka. This is the first detailed chronological study of postglacial Fraser River terraces.

Keywords: Fraser River; optical dating; river terraces; Holocene; paraglacial sedimentation

Acknowledgements

A thesis is not a one-person show and there are many who made this project possible. Tracy Brennand has been an incredible support both in the field teaching me sedimentology and fluvial processes, as well as in the office helping me craft arguments and tighten up my writing. Olav Lian, whom I have known since the first semester of my geography undergraduate journey, taught me the ropes of optical dating, has provided numerous learning opportunities and adventures, and was kind enough to share part of his PhD study area with me for this thesis. John Clague as the examiner provided many excellent comments and suggestions which greatly improved the final thesis.

Many thanks to Jonathan Cripps, whose calm and steady demeanour was so appreciated as I fumbled through fieldwork-on-the-fly. Christina Neudorf was very helpful in guiding me through some of the finer nuances of optical dating software. My palaeoglaciology lab mates Meaghan Dinney and Jordan Bryce were invaluable moral support throughout the journey. Cassandra Shewchuk and Vanessa Brewer helped process samples in the UFV luminescence dating lab. Funding for the project was provided by NSERC Discovery Grants to Tracy Brennand and Olav Lian, as well as generous support from NSERC and SFU through grants and scholarships.

Land access was generously granted by High Bar First Nation, Rebecca Tilley and Danny Phillips at Big Bar, the Joiner family of OK Cattle Ranch, and the Albietz family of Watson Bar Ranch. The study area is located on the traditional unceded territories of the Secwépemc, St'at'imc, and Tsilhqot'in people.

Last but certainly not least I must thank my family and friends. First and foremost, thanks to my wife Lauren. Lauren has endured the marathon journey of living with me, a stressed, preoccupied, indecisive, insecure, and anxious graduate student. Her steadfast character, patience, care, and encouragement have helped me press on. My parents, Bryan and Colleen, have never ceased in their support and I count them as tremendous blessings in my life. My brother, Denver, has inspired me with his curiosity and love of maps, and my sister-in-law Naomi provided encouragement from her own journey to PhD. Thanks to all my friends and associates for great questions, continued interest, and steady encouragement to continue along the narrow path.

Table of Contents

List of Tables

List of Figures

Fraser River terraces at Watson Bar, looking downstream

All the rivers run into the sea, yet the sea is not full.

To the place where the rivers flow, there they flow again.

Ecclesiastes 1:7 (WEB)

Chapter 1.

Introduction

1.1. Introduction

The landscape in British Columbia (BC) is undergoing adjustment as a result of the last glaciation. This interval of adjustment, known as the paraglacial period (Church and Ryder 1972), is defined as the time during which landscape response is conditioned by glaciation through processes not directly related to it. As the glacial ice disappeared sediments that were left in unstable positions, especially in upland regions of valleys, were distributed by fluvial and mass wasting processes to valley bottoms causing rivers to aggrade, adding sediments to the pre-existing glacial valley fill. As the quantity of easily erodible sediment in upland regions decreased and discharge increased from changing climate rivers incised through postglacial (paraglacial) and glacial sediments, and terraces formed. In many places, prominent alluvial and mudflow fans developed on these terraces (Ryder and Church 1986, Lian and Hicock 2001) upon which aeolian sediments were deposited (Lian and Huntley 1999).

Terrace development occurs as a combination of river aggradation and incision. Rivers aggrade when sediment supply is greater than the river's ability to carry the sediment, which is a function of competence, the size of material a river is able to entrain and transport, and capacity, the total amount of sediment a river can transport. Both competence and capacity vary according to discharge and river slope. When sediment supply increases to an amount greater than what a river can carry, such as through inputs from mass wasting and tributary streams, a river must rework this additional sediment and aggradation occurs. Additionally, if base level increases, such as through local damming from landslides or the development of glacial lakes from advancing or retreating ice, river slope is reduced, reducing the river's ability to move sediment. Rivers incise when the river has enough power to move material in the river bed and transport it downstream. Incision can occur when discharge increases, such as during especially wet climate periods. It can also be brought on by the lowering of base level through glacioisostasy or the drainage of glacial lakes.

During the postglacial period in BC, many factors have been involved in this complex interplay contributing to aggradation and incision resulting in terrace formation. Palaeoecological information (e.g., Mathewes and King 1989) has shown that during postglacial time major climate fluctuations occurred in southcentral BC. These fluctuations would have resulted in variations of river discharge and sedimentation which might be reflected in the current landscape. For example, during wet periods, increased sedimentation from tributary streams and valley side mudflows may have increased fluvial sediment load, while increased moisture may also have caused higher discharge, increasing river capacity. In warmer, drier periods, when sedimentation decreased, rivers might incise through their floodplains, albeit with decreased fluvial capacity from reduced precipitation.

Other regional factors could also contribute to terrace formation during the postglacial period. Local base level may have changed due to the formation of local landslide dams (Ryder and Church 1986, Ryder et al. 1990), causing temporary base level rise followed by rapid fall. Glacial lakes also formed during the postglacial period, with some of them known to have drained down the present-day Fraser River valley (Johnsen and Brennand 2004, Perkins and Brennand 2015, Clague *et al.* 2021), which would have led to fluvial aggradation as sediment-laden water rushed through valleys and incision when flow became channelized. Furthermore, glacioisostatic uplift occurred rapidly in previously glaciated regions of BC (Clague and James 2002, Shugar *et al.* 2014), further decreasing relative base level and encouraging incision. Finally, autogenic processes (Muto and Steel 2004) such as periodic armoring of bed surfaces followed by subsequent breaching of channel armor (Iseya and Ikeda 1987; Faulkner *et al.* 2016) can also contribute significantly to periods of aggradation and incision that cannot be explained by the above-mentioned external (i.e., allogenic) factors.

On the timescale of thousands to tens of thousands of years, however, climate has been regarded as the primary driving factor in river terrace development (Bull 1990, Blum and Törnqvist 2000). To further explore the potential impact of postglacial climate on terrace formation in British Columbia, terrace formation can be constrained with absolute dating methods to potentially correlate known postglacial climate phases with river incision. A detailed postglacial fluvial terrace dating study has not yet been conducted in British Columbia.

A suite of terraces along Fraser River between Big Bar and Watson Bar (Figure 1.1) was chosen for study. Fraser River is a crucial waterway as it is the longest river in BC, draining ~25% of BC's land area, and it is one of the most productive rivers for salmon in the world. The reach between Big Bar and Watson Bar has been investigated in previous studies; the underlying valley fill sedimentology has been described (Lian and Hicock 2001) and aeolian caps overlying paraglacial fans and fluvial sediments resting on terrace surfaces have been investigated in a preliminary optical dating study (Lian and Huntley 1999). However, the fluvial sand in the terraces associated with postglacial Fraser River activity has only been studied at a cursory level with few limiting ages associated with them (Lian and Clague 2009). The Big Bar and Watson Bar area is an ideal study site for this work because previous research on the character of the postglacial valley fill has been completed, terraces were accessible on both sides of the river, the landscape has not been drastically altered by anthropogenic development, and preliminary optical dating studies provided confidence that the method is applicable for this dating study.

This study seeks to (i) provide limiting ages for terrace formation in Fraser River valley at Big Bar and Watson Bar (Figure 1.1), (ii) determine the rate of incision of Fraser River through its valley fill, and (iii) look for correlation between the timing of terrace formation, the rate of incision, and existing information on the paraglacial cycle, postglacial climate change and changes in local base level.

The dating information from this study will also provide insight for future researchers that will aid in understanding how incision rates, and therefore the rate of evacuation of a considerable amount of Fraser River valley fill, near Big Bar and Watson Bar might affect downstream sedimentation rates on Fraser River and its tributaries. Further, this study provides a baseline for future studies on landslides and slope stability along Fraser River associated with the Big Bar landslide and its impact on salmon fisheries (Province of British Columbia 2021). Currently, there is a paucity of absolute dating information associated with glacial valley fill incision from Fraser River in the BC Interior to tie the upriver incision history to the downriver deposition history (Kovanen and Slaymaker 2015). This study will provide a piece of that puzzle. The outcomes of this study are also important because sediments evacuated by Fraser River and its tributaries contributed, and continue to contribute, significantly to the formation of the

Fraser delta (Clague *et al.* 1983, Kovanen and Slaymaker 2015), which is now densely populated.

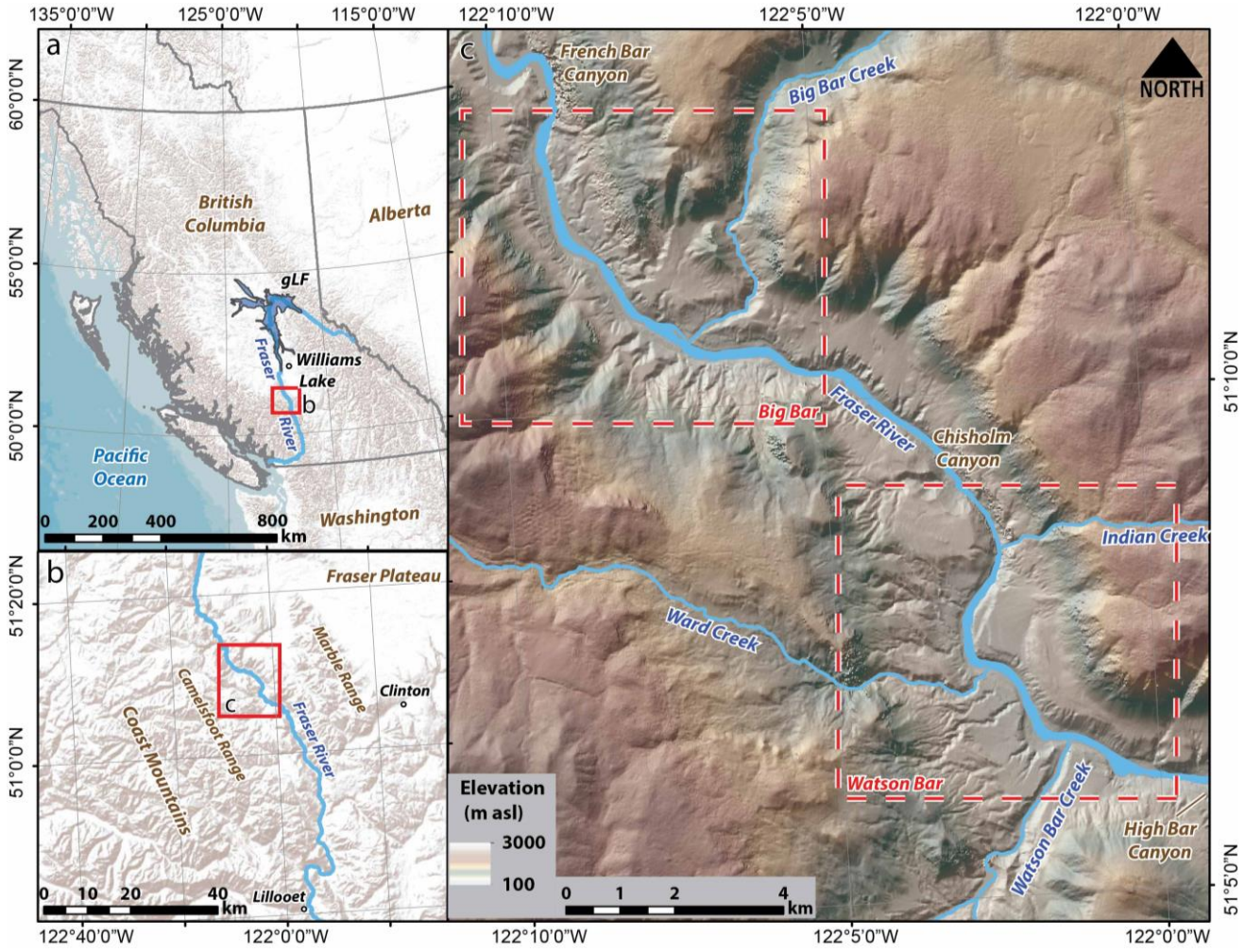

Figure 1.1. The study area in southwestern British Columbia. The sites are along a remote stretch of Fraser River, north of Lillooet and south of Williams Lake between French Bar Canyon and High Bar Canyon. Two terraced reaches, Big Bar and Watson Bar (dashed boxes), are the focus of this study. Glacial Lake Fraser (gLF) (extent from Clague *et al.* 2021) is depicted in (a). Elevation from 2019 TanDEM-X data.

1.2. Research conception, rationale, and contributions

The project idea was suggested by Dr. Tracy Brennand and Dr. Olav Lian, from observations made by Lian during his PhD research in the area. I, Travis Gingerich, collaborated with them to come up with the initial research questions and fieldwork strategy. I conducted fieldwork with assistance from Jonathan Cripps. I have processed all optical dating samples on my own in the University of the Fraser Valley Luminescence Laboratory, with the assistance of laboratory assistants Cassandra Shewchuk and Vanessa Brewer. I developed and tested my own optical dating protocols and analyzed and interpreted the data myself. Radiocarbon dating was performed by the A.E. Lalonde Accelerator Mass Spectrometry (AMS) Laboratory. Justin Song (Simon Fraser University) assisted in processing survey data in Excel to construct terrace longitudinal profiles.

1.3. Thesis overview

This thesis has three chapters. Chapter 1 lays out the basis for the thesis. Chapter 2 is written in journal manuscript form. As this chapter is part of a thesis it is written in more detail than the anticipated version that will be submitted for publication. Moreover, as a stand-alone manuscript there is some necessary repetition with other chapters. Chapter 3 assesses the success of the project based on the research objectives, outlines changes that could have been made to improve it and provides suggestions for future research. Appendices contain supplementary data.

Chapter 2.

The nature and timing of postglacial valley fill incision, Fraser River, Big Bar to Watson Bar, British Columbia

2.1. Introduction

The landscape in British Columbia (BC) is undergoing adjustment as a result of the last glaciation. This interval of adjustment, known as the paraglacial period (Church and Ryder 1972), is defined as the time in which landscape response is conditioned by glaciation through processes not directly related to it. As the glacial ice disappeared sediments that were left in unstable positions, especially in upland regions of valleys, were distributed by fluvial and mass wasting processes to valley bottoms causing rivers to aggrade. As the quantity of easily erodible sediment in upland regions decreased and discharge increased from changing climate, rivers incised their floodplains and terraces formed. In many places, prominent alluvial and mudflow fans developed on these terraces (Ryder and Church 1986, Lian and Hicock 2001) upon which aeolian sediments were deposited (Lian and Huntley 1999).

River terrace formation occurs as an interplay between river incision and aggradation which are driven by changes in climate and tectonics. On the timescale of thousands to tens of thousands of years (in this case, the postglacial period), climate has been regarded as the primary driving factor in river terrace development in general (Bull 1990, Blum and Törnqvist 2000). Climate can affect river terrace formation by: increasing sedimentation and thus aggradation by destabilizing valley walls through increased precipitation; increasing incision through higher precipitation resulting in greater discharge, or; increasing incision through warming, causing increased rates of glacial melt and thus greater discharge. Postglacial climate history in British Columbia is relatively well-known (e.g., Hebda 1995).

Tectonic changes most affect terrace formation on timescales orders of magnitude higher than this study focuses on, and thus will not be explored in this study. Glacioisostatic adjustment (Clague and James 2002; Shugar *et al.* 2014), however, may

have some effect. Glacioisostatic adjustment can change river slope and thus affect base level, with lowering base levels driving incision and rising base levels influencing aggradation. The timing of glacioisostatic adjustment is well-constrained along the coast of BC (Shugar *et al.* 2014), although inland it is less conclusive (Clague and James 2002).

Fraser River is the longest river within BC at 1375 km long. It originates in the east-central part of BC, high in the Rocky Mountains, first running northwest before turning and running south through the southern half of BC. It terminates in the Pacific Ocean near Vancouver, BC, and has created floodplains and a delta near which most of BC's population now resides. It drains around 25% of BC's land area, is one of the world's most productive salmon-bearing rivers and, as such, is an important cultural and economic hub for BC. A detailed study outlining the timing of postglacial Fraser River incision has not yet been performed. A reach was selected for study from within this long river system between Big Bar and Watson Bar creeks where terraces are easily accessible and previous work had identified sedimentary exposures that could be studied.

This study thus seeks to: (i) date a selection of Fraser River terrace tops using optical dating methods, (ii) estimate incision rates of Fraser River over the postglacial period using these optical ages, and (iii) correlate these incision rates to the paraglacial cycle, known postglacial climate periods and local base level changes. This study presents the first detailed chronology of postglacial Fraser River terrace formation and incision.

2.1.1. Study area

In the Big Bar-Watson Bar area (Figure 2.1), Fraser River has incised through the BC interior plateau and subsequent valley fill (~500 m thick, Lian and Hicock 2001). The Coast Mountains rise directly to the west with the Camelsfoot Range the closest range on the western edge of Fraser River. The Marble Range rises to the east between Fraser River and Clinton. Fraser River flows at an elevation of ~270 m asl, with adjacent peaks reaching elevations of more than 2000 m asl (Figure 2.1). Major tributaries along these reaches are Big Bar Creek, Ward Creek, Indian Creek, and Watson Bar Creek (Figure 2.1). Through these reaches, the Fraser River follows the Fraser Fault (Mathews

and Rouse 1984), navigating bedrock canyons at French Bar Canyon, Chisholm Canyon, and High Bar Canyon (Figure 2.1). In wider non-canyonized reaches, it has produced a series of stepped terraces during its incision.

Fraser River between Big Bar and Watson Bar creeks has well-defined river terraces that are accessible from both sides of the river via gravel roads and a reaction ferry at Big Bar. Past studies in the area have identified fluvial terraces inset into glacial valley fill sediments (Lian and Hicock 2001). The terraces contain ancestral Fraser River sediments, which are, in turn overlain in places by paraglacial fan and aeolian deposits (Lian and Huntley 1999, Lian and Hicock 2001). Optical dating has been used in preliminary studies to date aeolian caps (Lian and Huntley 1999) and ancestral Fraser River sand (Lian and Clague 2009).

2.1.2. Glacial retreat and postglacial history

The valley fill in the study area and its vicinity has been characterized by several studies. Lian and Hicock (2001) provide a stratigraphic description of the area between Big Bar and Watson Bar that identifies glaciofluvial sand and gravel, glacially-derived gravity flow diamicton, and glaciolacustrine silt and sand as the major components of the valley fill. Limiting optical ages suggest that deposition of these units occurred during the Fraser Glaciation (Lian and Hicock 2001), although older units may exist, based on evidence found ~40 km north of the study area (e.g., unit A of Eyles and Clague 1991). Further stratigraphic descriptions of the valley fill immediately upstream of the study area are provided by Huntley and Broster (1994), who report stratigraphy like that of Lian and Hicock (2001) and suggest glacial lake formation in the study areas during both advance and retreat stages of the Fraser Glaciation.

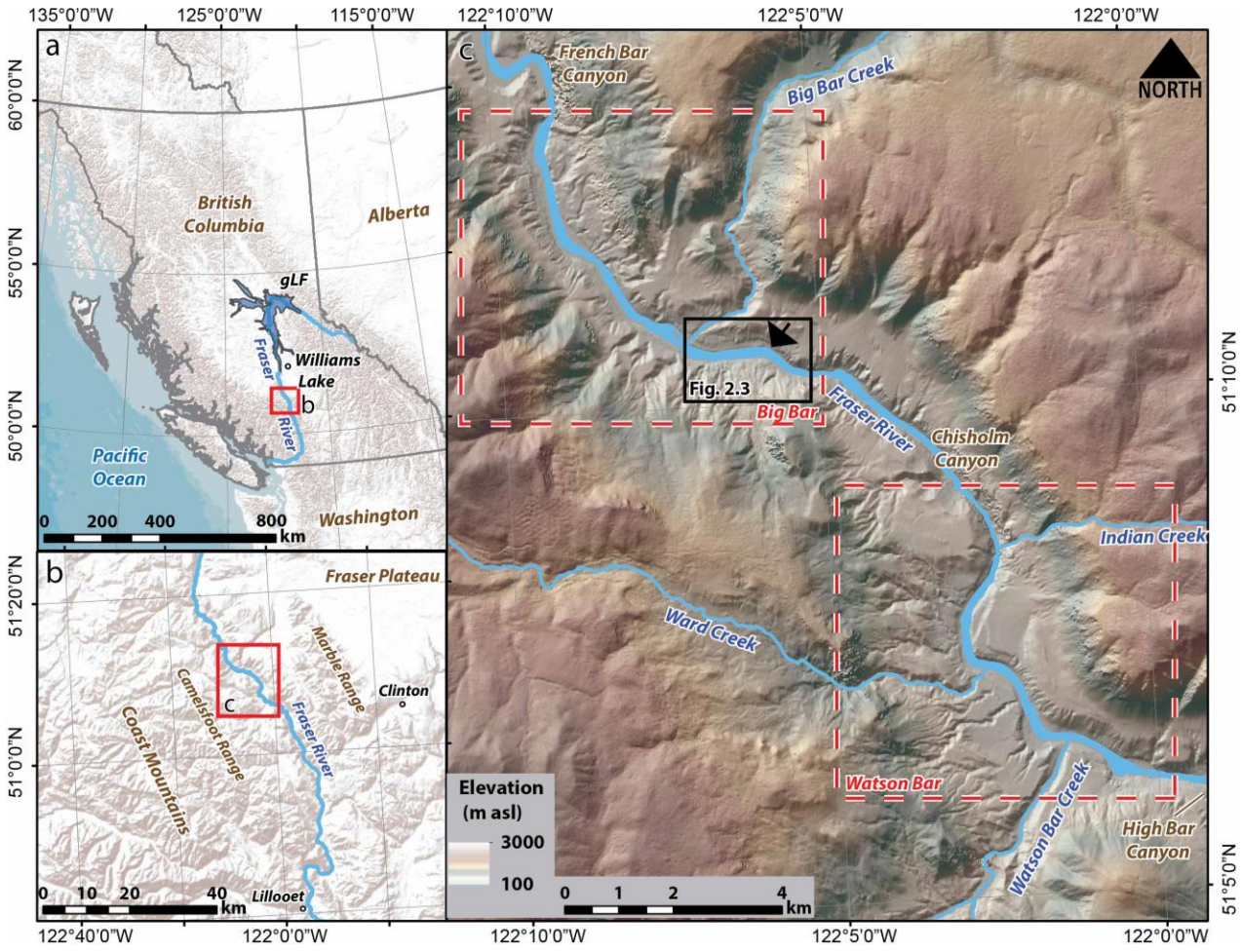

Figure 2.1. The study area in southwestern British Columbia. The sites are along a remote stretch of Fraser River, north of Lillooet and south of Williams Lake between French Bar Canyon and High Bar Canyon. Two terraced reaches, Big Bar and Watson Bar (dashed boxes), are the focus of this study. Glacial Lake Fraser (gLF) (extent from Clague et al. 2021) is depicted in (a). Elevation from 2019 TanDEM-X data. Figure 2.3 extent is shown with the arrow denoting the perspective of the image.

During the Fraser Glaciation, the Cordilleran Ice Sheet (CIS) covered most of BC, reaching its maximum southern limit in Puget Sound ~16.5 ka ago (Clague 2017) (Note: all ages are reported in calendar years, with any radiocarbon [^{14}C] ages from the literature calibrated using OxCal 4.4 and denoted “cal ka”). Deglaciation was a combination of complex frontal retreat of the ice sheet and stagnation within the BC interior (Clague 2017). Margold *et al.* (2014), using ^{10}Be exposure ages from erratics high in the Marble Range adjacent to the study area (Fig. 2.1b), suggest that high-elevation ice in this locale disappeared 14.5 ± 1.0 ka ago. This is much earlier than expected, given the furthest southern extent of the CIS occurred around 18 ka ago (Clague 2017). Menounos *et al.* (2017) further note the complexity of CIS retreat, with two readvances recorded in high mountain moraines in northern BC during the Bølling-Allerød period (14.6 – 12.9 ka) and in both northwestern and southwestern BC during the Younger Dryas (12.9-11.7 ka) period. Although retreat was complex and much debate continues regarding its timing and nature, consensus is that most areas in the BC interior had substantially less ice by 14 ka (Margold *et al.* 2014; Menounos *et al.* 2017), and that all but the major mountain ranges were nearly ice-free by ~11 ka ago (Clague 2017).

During deglaciation, meltwater was trapped in a series of glacial lakes in the BC interior; the largest that affected this study was glacial Lake Fraser (gLF). Glacial Lake Fraser was in central British Columbia (Figure 2.1a), its extent described in Clague *et al.* (2021). It was dammed by the retreating CIS and grew during deglaciation, the ice dam being ~20 km south of the city of Williams Lake (Clague *et al.* 2021), ~100 km upstream of the study area. The ice dam failed and gLF drained catastrophically, sending hundreds of cubic kilometres of water down the present-day Fraser River drainage path. It is possible that a second outburst flood occurred soon after the first event when a landslide dam triggered by the first flood temporarily blocked drainage of gLF, then also gave way (Clague *et al.* 2021). The timings of these floods are constrained by terrestrial cosmogenic nuclide (TCN) ages from flood-transported boulders within the Fraser River valley (Clague *et al.* 2021) and by ^{14}C ages from silty clay layers in Saanich Inlet interpreted to have formed from sediment washed over ancestral Strait of Georgia (Blais-Stevens *et al.* 2003). Clague *et al.* (2021) reported a median age for the flood of 11.1 ± 0.6 ka from nine TCN samples, while Blais-Stevens *et al.* (2003) bracket the timing of this event as younger than 12.3 ± 0.3 cal ka (GSC ^{14}C sample 1034E-9H1, 69,

Blais-Stevens *et al.* 2003) and older than 11.9 ± 0.5 cal ka (GSC ^{14}C sample 1033B-6H4, 110, Blais-Stevens *et al.* 2003).

This cataclysmic event would have occurred in the initial stages of paraglacial fluvial activity in the study area, with paraglacial fluvial activity commencing after the outburst flood of gLF. As glaciers retreated out of valleys, they left large quantities of sediment perched on valley sides and within tributary valleys. During the next several thousand years, tributary stream sedimentation and mass wasting processes dominated the fluvial sedimentary regime as unstable sediment moved downslope, some of it developing into alluvial and mudflow fans at positions lower in the valley. These fans supplied rivers with high sediment loads, and thus fluvial aggradation occurred (Church and Ryder 1972, Clague 1981, Jackson Jr. *et al.* 1982). Upland paraglacial sedimentation peaked as glaciers began their retreat, with sediment supply being highest when the landscape was least stable (Church and Ryder 1972, Ballantyne 2002) and continued at a high rate for thousands of years afterwards. Aeolian deposition has occurred after the stabilization of paraglacial fans (Lian and Huntley 1999), marking the reduction of upland sedimentary inputs into the fluvial system. Church and Slaymaker (1989) argue that, although paraglacial sedimentation from upland areas may have been drastically reduced shortly after deglaciation, this sediment continues to be reworked in larger basins, and likely still dominates the sedimentological regime in large rivers.

2.1.3. Fraser River terraces

In the Fraser River valley between Big Bar and Watson Bar, the interaction between paraglacial processes and fluvial reworking by Fraser River is seen in a series of stepped terraces that are situated high above the present-day course of the river. During the postglacial period in the region (~12 ka to present), paraglacial processes have dominated, adding sediment to the fluvial system and causing Fraser River to undergo cyclic processes of aggradation, creating floodplains, and incision, which abandons floodplains, creating terraces. In past studies of the region, Holocene gravel and sand were observed in many valley side exposures through river terraces indicating postglacial Fraser River floodplain development and subsequent incision (Ryder and Church 1986; Lian and Hicock 2001). The terraces are in places overlain by paraglacial alluvial and debris flow fans (Lian and Hicock 2001) which are, in turn, commonly capped by aeolian deposits up to several metres thick (Lian and Huntley 1999).

In Lillooet, ~60 km south of the study area (Figure 2.1b), Ryder and Church (1986) investigated a series of terraces along Fraser River within 100 m elevation from the current Fraser River level. In their study, four upper unpaired terraces were identified, along with two sets of paired terraces nearer present-day river level. Ryder and Church (1986) observed multiple small channel traces and no overbank deposits on the four upper terraces. They concluded that these sediments were deposited in a braided system, consistent with a proglacial river during deglaciation. Further, they argued that, because these upper terraces are unpaired and narrowing with depth into the valley, they were formed during a period of sustained incision. The lower terraces contain downstream-thickening floodplain sediments, suggesting that floodplain aggradation was controlled by backwater processes consistent with potential downstream blockages causing upstream aggradation. It is suggested that these blockages were a result of landslides initiated from creeks 6 and 17 km downstream from Lillooet (Ryder and Church 1986, Ryder *et al.* 1990). It is possible that terrace formation in the study area was affected by similar processes.

Few chronological controls have been established for the formation of Fraser River terraces in the region, so the timing of their formation and river incision is largely unknown. At Lillooet, ancestral Fraser River had abandoned a terrace at 103 m above present-day Fraser River more than 7.5 ± 0.1 cal ka ago due to the presence of Mazama ash (Egan *et al.* 2015) in the contact between fluvial overbank deposits and an aeolian cap (Ryder and Church 1986). Ryder and Church (1986) speculate that downcutting began at the end of the Holocene xerothermic interval (HXI), ~7 cal ka ago (Mathewes 1985, Hebda 1995), but no absolute age controls are provided apart from the Mazama ash identified by Ryder and Church (1986) and a single ^{14}C age of 1.1 ± 0.2 cal ka on a terrace at 28 m above present-day river level, derived from charcoal overlain by 2 m of river gravel. Although the study by Ryder and Church (1986) did much to provide a case for why terraces formed at different stages, the paucity of chronological controls makes it difficult to tie to other longer time-scale drivers such as climate, glacioisostatic adjustment, and local base level changes that may have contributed.

At Big Bar and Watson Bar, three studies have used optical dating to date different sedimentary facies to provide absolute ages where there is a paucity of material suitable for radiocarbon dating. Lian and Huntley (1999) use optical dating to date an aeolian cap overlying a paraglacial fan ~400 m above Fraser River at Big Bar. A

minimum age of 11 ± 1 ka was calculated from near the bottom of the aeolian cap, providing a minimum age of paraglacial fan stabilization and the onset of aeolian deposition at ~400 m above present-day river level. Lian and Hicock (2001) characterize the valley fill at Big Bar and provide limiting optical ages for valley fill deposition, placing it as during the Fraser Glaciation. Lian and Clague (2009) provide preliminary ages of Fraser River terrace abandonment from three terraces at Big Bar. Their site 76 at 440 m asl, 170 m above present-day river level, has a maximum optical age of terrace abandonment of 11.6 ± 0.6 ka from fluvial sand and a minimum optical age of 5.0 ± 0.1 ka from aeolian sediment overlying a thick sequence of paraglacial sediments. Their site 88 at 330 m asl, 40 m above present-day river level, has a maximum optical age of terrace abandonment of 6.3 ± 0.4 ka from fluvial sand. Their site 79 at 290 m asl, 20 m above present-day river level has a minimum ^{14}C age of terrace abandonment of 3.69-4.08 cal ka, based on a bone fragment found at the base of a paraglacial fan and a minimum optical age of 3.4 ± 0.1 ka from aeolian sediment overlying the paraglacial fan. Optical ages use the central age model (CAM), which may overestimate fluvial sediment that has an incomplete bleaching history (Galbraith et al. 1999). Past preliminary optical dating studies at Big Bar demonstrate that optical dating can be used to date both fluvial and aeolian sediments in the area, though models other than the CAM could be employed, where appropriate, to provide more accurate ages.

2.1.4. Drivers of terrace formation

The drivers of terrace formation that most likely affected Fraser River are climate, glacioisostatic adjustment, and local base level changes. Although extensive placer mining has occurred on lower terraces, anthropogenic impacts on terrace formation are likely negligible and isolated to terraces <15 m above river level. Postglacial climatic fluctuations in British Columbia have been documented using palaeoecology (e.g., Mathewes and Heusser 1981; Mathewes 1985; Mathewes and King 1989). These studies indicate that different regions in BC experienced changes in climate at slightly different times, although regional trends prevail and have been summarized for the last ~10 cal ka by Hebda (1995). Prior to ~10 cal ka ago, climate for the coast and interior of British Columbia was cold and dry before 12 cal ka, then shifted to cool and moist until ~10.5 cal ka when the HXI began (Mathewes 1985) (Figure 2.2). The HXI is typified by warm and dry climate across British Columbia (Mathewes 1985, Hebda 1995), and

although the end of this period fluctuated across the province, it was generally thought to have ended by ~7 cal ka in the regions upstream and downstream of Fraser River at Big Bar and Watson Bar (Figure 2.2). At this time in the middle Holocene, climate began to moisten and in regions other than the Southern Interior, cool to temperatures lower than those in the HXI (Hebda 1995). Specifically in the Central Interior Plateau and Northern BC regions upstream of Big Bar and Watson Bar, climate was wetter than present (Figure 2.2). This wetter period lasted until ~4 cal ka ago when climate shifted to near-modern, which is drier than the middle Holocene, especially when compared to the Central Interior Plateau and Northern BC regions (Figure 2.2). The Holocene glacial record provides higher resolution climate information (e.g. Menounos et al. 2009), with periods of glacial advance occurring between 8.59-8.18, 7.36-6.45, 4.40-3.97, 3.54-2.77, 1.71-1.30 ka, and during the last thousand years. The age resolution in this study, however, is not sufficient to infer drivers of terrace formation from these higher resolution recorded advances, especially in the last ~5 ka.

Glacioisostatic adjustment can lower relative base level as depressed landscapes rebound after deglaciation, encouraging incision as rebound progresses. Identified in the BC interior using glacial lake shoreline tilt as a proxy (Fulton and Walcott 1975), Clague and James (2002) report that the BC interior plateaus (immediately adjacent to this study area) would have been glacioisostatically depressed by as much as 400 m. The amount of glacioisostatic depression is also alluded to by Johnsen and Brennand (2004) who report tilts of 1.7-1.9 m km $^{-1}$ dipping NNW (toward this study area) along glacial Lake Thompson shorelines. Although the timing of interior glacioisostatic adjustment is poorly constrained, it began while ice was thinning and retreating (Clague and James 2002), with most adjustment concluding shortly after deglaciation in a span of <2 ka (Clague and James 2002). Glacioisostatic adjustment was also experienced along the BC coast during and shortly after deglaciation, causing uplift and lowering relative sea level by as much as 200 m at the mouth of Fraser River (Clague and James 2002; Shugar *et al.* 2014).

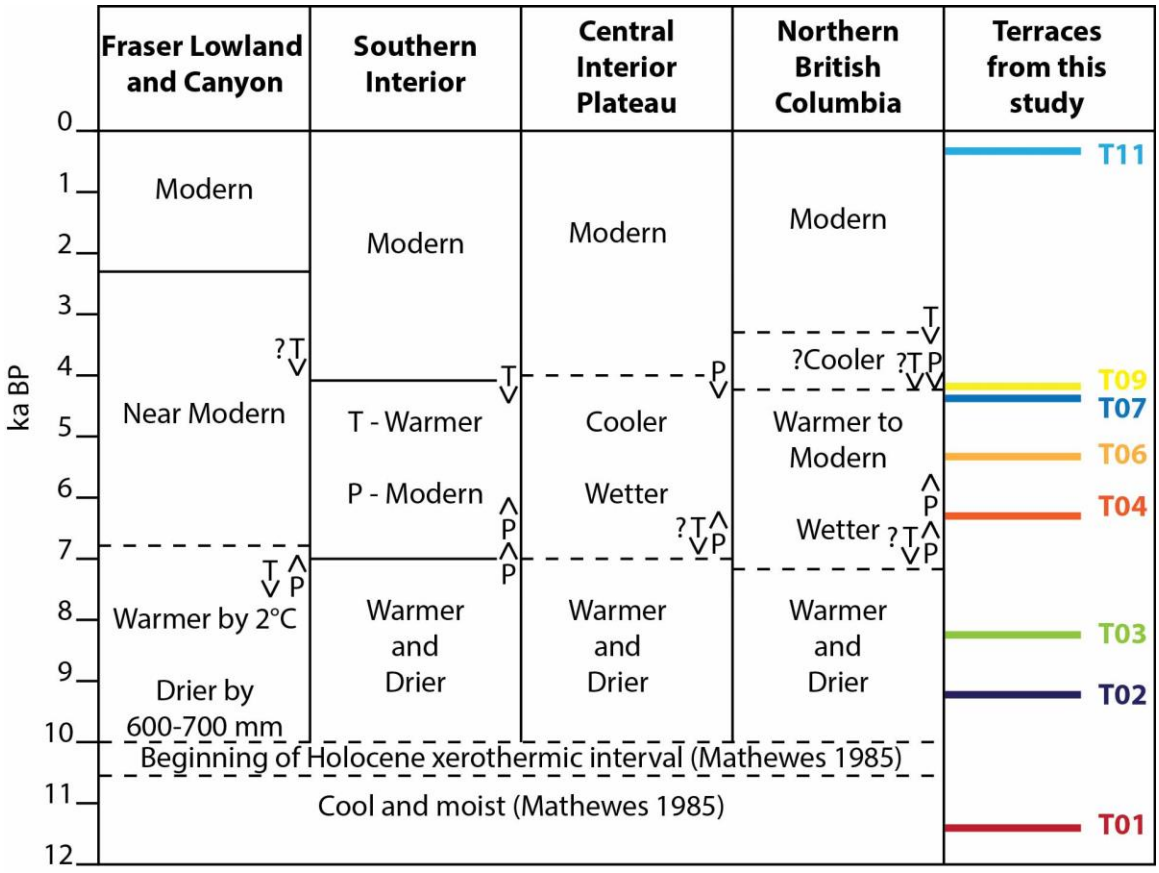

Figure 2.2. Postglacial climate in four different regions of British Columbia directly upflow or downflow from the study area, modified from Hebda (1995) with early Holocene BC climate from Mathewes (1985). Temperature and precipitation descriptions are in comparison to modern climate. Solid lines denote marked change, while dashed lines denote gradual or uncertain change (Hebda 1995). Blocks of time can be considered climate states or periods, while arrows associated with (T) or (P) infer localized trends for temperature and precipitation, respectively. Terrace ages from this study provided in the right hand column and discussed in sections 2.3 and 2.4.

Additionally, local base level can change due to increased paraglacial sedimentation from tributary valleys, the formation of local landslide dams, and/or the formation and drainage of glacial lakes associated with CIS retreat. Paraglacial sedimentation from tributary valleys is well-documented in the Fraser River valley and other trunk stream valleys in southwestern British Columbia (Ryder 1971). This sediment, experienced peak mobility shortly after deglaciation (Church and Ryder 1972), inundating Fraser River, causing local base level increases and excess sediment for Fraser River to rework. Downstream of the study area at Lillooet, Ryder and Church (1986) suggest that lower terraces in their study were formed from backwater processes

associated with landslides at Texas Creek, further described by Ryder *et al.* (1990). Upstream of the study area, gLF was impounded first by ice and then by a landslide dam (Clague et al. 2021) which resulted in catastrophic drainages down the Fraser River valley, depositing large swaths of sediment as it went. Finally, autocyclic processes (Muto and Steel 2004, Faulkner *et al.* 2016) within a river system can also contribute significantly to periods of aggradation and incision that cannot be explained by the above-mentioned external (i.e., allogenic) factors.

2.2. Methods

2.2.1. Geomorphology

Terraces in the southern Fraser River region, formed on and in glacial valley fill sediments consist of floodplains that were abandoned as Fraser River incised (Ryder and Church 1986; Lian and Hicock 2001). These floodplain sediments are commonly overlain by paraglacial fans formed by fluvial and debris flow processes that are, in turn, capped by aeolian sediments that may be several metres thick (Lian and Hicock, 2001).

Terraces are mapped around Big Bar and Watson Bar using digital terrain models (TanDEM-X elevation data: 12 m grid, >1 m vertical resolution) and field checked. These terraces are correlated in space, and the elevations of their floodplain surfaces determined using a combination of digital elevation model (DEM) analyses and differential global positioning system (dGPS) surveys. Because dGPS surveys were conducted on multiple days and no local benchmarks were available, each survey was overlapped with those from preceding days using shared points to ensure high accuracy and repeatability. Additionally, dGPS surveys included measurements at river level so elevations above river level could be calculated and river levels could be correlated between dGPS surveys and DEM data. Once gathered, dGPS data were corrected using the Canadian Spatial Reference System (CSRS) Precise Point Positioning (PPP) tool, which uses precise satellite orbit data from the time of survey to correct floating GPS data points to high accuracy and precision (<0.1 m grid, <0.2 m vertical resolution).

TanDEM-X data use the WGS84 G1150 datum, while dGPS data use the NAD83 CSRS datum, so a datum transformation was performed on dGPS data to ensure all data were in WGS84 G1150 format. The TanDEM-X data is considerably lower

resolution than the dGPS data (12 m grid, >1 m vertical vs. <0.2 m grid, <0.2 m vertical, respectively) and because of this, horizontal coordinates should be considered at ±10 m precision and vertical measurements should be considered ±1 m precision unless explicitly stated that they were only derived from dGPS surveys.

Because many terraces are capped by paraglacial fans emanating from tributary valleys, the terrain is steep and gullied, some areas are affected by past placer mining activity (Figure 2.3) and the study area is large, it was challenging to precisely verify palaeofloodplain elevations throughout the study area. To approximate palaeofloodplain elevations beyond dGPS measurements, terrace edge elevation data was extracted from the DEM and compared to dGPS elevations. Minimum and mean elevations from the terrace edges in each terrace DEM polygon are used to estimate palaeofloodplain elevations. Mean DEM elevations are used for terraces with fluvial sediments exposed at the surface. Minimum DEM elevations are used in cases where fan sediments occur at the surface. Using this method, the elevation estimates of palaeofloodplains were within 10 m of dGPS elevations in ~80% of cases, the exceptions being where fans were >10 m thick. These elevations were used to correlate palaeofloodplains downvalley and identify potential paired terraces.

Terraces are correlated in space through analysis of photographs, elevation-classed DEMs, hillshaded DEM imagery, and the results of the palaeofloodplain elevation analysis described previously. Terraces are correlated downvalley by identifying elevations of terrace clusters at Big Bar and Watson Bar, then tying them together based on palaeoslope of the ancestral Fraser River. It is assumed that the slope of the Fraser River has not changed substantially over the time that this study covers (~12 ka), and any changes in the slope are likely masked within the measurement uncertainty. Composite cross-valley topographic profiles were created for Big Bar and Watson Bar using seven and eight DEM-generated individual topographic profiles, respectively (Appendix D). The final cross-valley profiles included dGPS-checked palaeofloodplain elevations. Paired terraces are correlated by palaeofloodplain elevations using the composite cross-valley topographic profiles. Once correlated, terraces were named from the highest (T01), and presumably oldest investigated in this study, to the terraces nearest present-day river level (T12), which are presumed to be the youngest.

Figure 2.3. Big Bar terraces from the east side of Fraser River. Paraglacial fans overlie river sediment on most of these terraces. Gullies and slumping complicate terrace mapping and correlation. Past placer mining on some T09-T12 terraces, as outlined by the dashed line, has removed or disturbed some terrace sediments. Terrace levels visible on the west side of Big Bar are annotated and discussed in sections 2.3 and 2.4.

2.2.2. Lithostratigraphy

Lithostratigraphic analysis was conducted at metre to decimetre scale using standard sediment description procedures (e.g., Evans and Benn 2021; Lindholm 1987) to differentiate between depositional environments at the study sites, which included 1) pre-terrace valley fill, 2) postglacial Fraser River sand and gravel, 3) paraglacial fans, and 4) aeolian caps. Unit thicknesses and optical dating sampling depths were determined by measuring tape and/or dGPS surveys. Gravel fabrics were determined from clast *ab*-plane dip angle and trend measurements (Appendix B), and these were plotted on lower hemisphere equal-area Schmidt projections using Stereonet v. 10.4.2 (Allmendinger *et al.* 2011; Cardozo and Allmendinger 2013). Unit numbering reflects palaeoenvironmental units and differs from lithostratigraphic units established during

past studies of the area. Unit 1, pre-terrace valley fill sediments, has been previously described and interpreted in the study area (units I-IV of Lian and Hicock 2001) and in adjacent study areas (Eyles and Clague 1991; Huntley and Broster 1994). This study focuses on postglacial Fraser River activity thus the underlying valley fill units are not described in further detail here.

2.2.3. Dating

Radiocarbon dating

Radiocarbon (^{14}C) dating can provide high-precision ages of fossil organic materials which, if found in growth position, correspond with depositional ages of associated sedimentary layers. If the materials are detrital and not found in growth position, radiocarbon dating will typically give maximum ages, but these may approximate true ages if sedimentological analysis suggests the detrital material was generated at a similar time as deposition. A paucity of organic materials suitable for radiocarbon analysis has been observed in past studies of the area (Lian and Huntley 1999) and fieldwork in 2019 confirmed this. However, at site 1966, charcoal fragments were found in several beds, and some of these were collected for radiocarbon analysis. Samples were collected with trowels and placed in clean plastic bags. The charcoal was kept refrigerated until it could be dried to prevent contamination.

Samples were dried in an oven at 80°C for ~8 hr, then cleaned with a synthetic bristled brush to remove any sand or contaminating modern organic material from their surfaces. Samples were sent to the A.E. Lalonde AMS Laboratory to undergo processing and analysis. Sample pre-treatment techniques were performed as per Crann *et al.* (2017) and Murseli *et al.* (2019). Radiocarbon ages were calibrated using OxCal v.4.4.2 (Bronk Ramsey 2009) and the IntCal 20 calibration dataset (Reimer *et al.* 2020).

Optical dating

Organic materials for ^{14}C dating are rare in the study area. Additionally, detrital organic materials may not always be chronologically consistent with deposition in fluvial sedimentary strata, thus providing age discrepancies (e.g., Blong and Gillespie 1978). Due to these concerns, optical dating was employed as the main method to provide age

estimates for Fraser River palaeofloodplain development and subsequent incision. Optical dating measures the time elapsed since mineral grains, typically quartz and feldspar, were last exposed to light, which is usually consistent with stabilization ages of sedimentary landforms. Detailed account of the technique can be found in Lian and Roberts (2006) and Wintle (2008).

Sampling

Optical dating samples were collected from palaeofloodplain sand units and aeolian caps (Lian and Huntley 1999; Lian and Hicock 2001). Ancestral Fraser River sand units typically overlie fluvial gravel units and are inferred to be overbank sediments (Brennand *et al.* 2014). Optical ages from ancestral Fraser River sand thus provide maximum limiting ages for fluvial activity before incision and floodplain abandonment at each site. At some sites aeolian samples were collected from the base of aeolian units to provide minimum limiting ages of fluvial activity, thus bracketing the timing of floodplain abandonment and terrace formation between fluvial maximum ages and aeolian minimum ages. Aeolian samples also provide minimum ages for the cessation of paraglacial fan formation when overlying fans at associated terraces, and further, they provide a test of the optical dating procedure as these samples are expected to have received sufficient sunlight exposure prior to burial and they were collected stratigraphically below Bridge River tephra (BRT; 2.36 ka; Clague *et al.* 1995). Samples were collected by inserting opaque tubes into cleaned section faces. The tubes ranged in size from 3 to 10 cm diameter by 15 to 30 cm length, depending on the thickness and texture of the sediments collected.

Preparation

Sample tubes were opened in the University of the Fraser Valley luminescence dating laboratory under dim orange light conditions and prepared using standard procedures (e.g., Wintle 1997). Approximately 5-10 cm of sediment was removed from both ends of each tube to prevent light-contaminated sand grains from being incorporated into the material to be analyzed for dating, with some of this material reserved for water content and radionuclide concentration measurements. Fine sand between 180-250 µm diameter was isolated using wet-sieving procedures, then treated with HCl acid and H_2O_2 to remove carbonates and organic material, respectively. Lithium metatungstate (LMT) heavy liquid separation was employed to concentrate quartz (2.62-

2.70 g/cm^3) and potassium feldspar (KF; 2.58-2.60 g/cm^3). Samples were etched with HF acid to remove the α-effected portion of the grain surfaces, followed by an HCl acid rinse to remove precipitated fluorides. Quartz samples were treated with a 50% HF solution for 40 minutes with a 5-minute HCl rinse and KF samples were treated with a 10% HF solution for 4 minutes with a 1-minute HCl rinse. The etched sand grains were then mounted as aliquots to 10 mm diameter aluminum discs on a circle of silicone spray measuring either 1 mm or 3 mm diameter, corresponding to 40 ± 20 or 140 ± 30 grains per aliquot, respectively. The aliquot size was dependent on whether evidence of partial bleaching was present, which is discussed in the next section.

Measurement of equivalent dose

Samples were measured using a Risø TL/OSL DA-20 reader/irradiator equipped with a calibrated ^{90}Sr/^{90}Y source delivering β radiation to samples at a rate of ~4.8 Gy/min. Quartz grains were stimulated with 45 mW/cm^2 blue (~470 nm) light and ultraviolet (~350 nm) luminescence emissions were detected using a 9235QA photomultiplier tube (PMT) fitted with a 7.5 mm thick Hoya U-340 optical filter to absorb reflected and scattered light from the stimulation beam. KF grains were stimulated with 130 mW/cm^2 infrared (IR) light (~880 nm) and violet (~400 nm) luminescence emissions were detected using the same PMT fitted with Schott BG-39 and Corning 7-59 optical filters. The BG-39 filter absorbs reflected and scattered IR light from the stimulation beam and the 7-59 filter absorbs yellow-green light (~570 nm) emitted by plagioclase feldspars.

This study employed the single-aliquot regenerative dose (SAR) method to determine equivalent dose (D_e) on quartz (Murray and Wintle 2000) and KF (Wallinga *et al.* 2000). The generalized procedure can be found in Table 2.1. Several parameters inherent to the SAR protocol were adjusted through pilot experiments to find the SAR protocol best suited for the minerals specific to the study area.

When mineral grains are dosed in the environment, only some traps will reliably store electrons over timescales of interest. These traps are known as thermally stable or ‘deep’ traps, and they must be isolated from thermally unstable or ‘shallow’ traps in the SAR procedure as they are filled by exposure to laboratory radiation but remain empty in the environment. This is done by employing a preheat to empty any thermally unstable traps and it is performed both on the naturally dosed aliquots and after subsequent

laboratory doses (Table 2.1). Preheat procedures can vary based on the local mineralogy of a sample, and thus a preheat plateau test is performed. The goal of this test is to find a temperature and heating duration that sufficiently empties thermally unstable traps while not significantly emptying the thermally stable traps that are of interest for dating. Preheat plateau tests on quartz and KF were performed using guidelines laid out by Neudorf *et al.* (2015) using a range of preheat temperatures that ranged from 140-260°C at 20 C° increments for 10 seconds. From these tests, it was determined that a 220°C preheat and a 160°C preheat was most suitable for quartz and KF, respectively. The efficacy of the chosen preheat temperature and duration is further tested by dose-recovery experiments.

Table 2.1. SAR procedure for KF used for this study. Each aliquot receives this treatment, starting with the preheat and stimulation of the sample without a laboratory dose to measure its natural signal. After the natural signal is measured, the aliquot is given various doses of laboratory radiation and stimulated each time to generate data points to construct a dose response curve. The test dose is used to correct for sensitivity change from repeated dose and stimulation cycles, and a test dose of ~2.4 Gy was chosen to provide a luminescence signal significantly greater (>3x) than the background signal to minimize the influence of instrument error.

Step	Procedure	Measurement
1	Laboratory dose (omitted during first run: sample already dosed with natural dose)	
2	Preheat: 160°C, 10 s	
3	Stimulation: IR, 50°C, 100 s	L_n, then L_x
4	Test dose: ~2.4 Gy	
5	Preheat: 160°C, 10 s	
6	Test dose stimulation: IR, 50°C, 100 s	T_n, then T_x
7	Repeat steps 1-6	

L_n: Luminescence signal of the natural dose
L_x: Luminescence signal of subsequent laboratory doses
T_n: Luminescence signal of the test dose associated with the natural dose
T_x: Luminescence signal of the test doses associated with subsequent laboratory doses

Quartz from sample 1951-TG-01 was tested to assess the viability of quartz as a chronometer in the study area. The first tests of quartz used linearly-modulated-optically-stimulated-luminescence (LM-OSL, Bulur 1996) to assess the presence of a so-called 'fast component' of the luminescence signal which is thermally stable and is quickly reset (bleached) in daylight and is thus desired for use in optical dating of quartz. These

measurements are also used to assess the magnitude of unwanted slowly-bleached and/or thermally-unstable medium and slow components of the signal (Singarayer and Bailey 2003) as these may interfere with (contaminate) the fast component. Initial LM-OSL curves indicated that few aliquots possessed an obvious fast component (Appendix C, Figure C.14), and this made the use of quartz impractical. Quartz was thus abandoned, and the focus was turned to KF.

Pilot SAR experiments on KF using a few aliquots were completed to provide a preliminary assessment of the protocol. To this end dose recovery tests were performed. Dose recovery tests use known laboratory doses as an estimate of the natural dose and a SAR run is conducted to assess the reliability of recovering the known dose as the D_e. Subsamples of prepared KF were first bleached in natural daylight for ~3 hr, then SAR tests were performed, each using a single laboratory dose value, ranging from ~1-20 Gy. Dose recovery tests yielded given dose to recovered dose ratios of 1.02 ± 0.01 when the laboratory dose was 8-20 Gy (Appendix C, Table C.1). Laboratory doses of 1 Gy yielded given-to-recovered dose ratios of 1.31 ± 0.03 and tended to overestimate the recovered dose (Appendix C, Table C.1). As most samples in this study are expected to have D_e values >5 Gy, the results from the 8-20 Gy dose recovery tests showed that the chosen SAR protocol could be used successfully to date the samples. Samples with D_e values in the 1 Gy range had independent age control which could be used to assess optical ages. With the dose recovery test confirming that the SAR procedure was suitable for KF in the study region, full SAR runs were constructed to estimate the D_e of each sample.

Internal quality-control tests inherent to the SAR method, namely recycling ratio and recuperation tests were used to determine whether individual aliquot data could be used in final age calculations. The recycling ratio test, which assesses the effectiveness of the chosen test dose, is performed by repeating one of the laboratory doses in a SAR sequence. The measured luminescence after each dose is then compared. The common acceptance criterion for the recycling ratio is 1.0 ± 0.1, or no more than 10% from unity (Murray and Wintle 2000, Wintle and Murray 2006), which is what was used in this study. Recuperation values are assessed by measuring the aliquot at the end of a SAR cycle without dosing it beforehand; this is known as the zero-dose point. The amount of luminescence measured after a zero dose is due to thermal transfer, and it is acceptable if it is 5% or lower than the natural signal (Murray and Wintle 2000; Wintle and Murray 2006). Only aliquots that pass these two criteria are used for D_e calculations.

For each sample 24 or 48 aliquots were measured and those that passed the SAR quality control tests were used to determine D_e values. The D_e values form a distribution which is then plotted on radial or abanico plots (Dietze *et al.* 2016), and then analyzed to estimate a representative D_e for that sample which is used for the age calculation. The first step in analysis is measuring the D_e distribution's overdispersion value. Overdispersion (OD) describes the amount of variance in individual D_e values from the same sample that cannot be explained by analytical uncertainties (Galbraith *et al.* 2005, Galbraith and Roberts 2012). In general terms, the smaller the OD value, the more certain one is that all the D_e values belong to a single population, with 10% OD being nearly the lowest achievable value with a fully bleached aeolian sample using an aliquot size of ~200 grains (Cunningham *et al.* 2011). OD values are considered alongside visual analysis of D_e distributions on radial or abanico plots (Dietze *et al.* 2016); the latter are used here. An abanico plot includes a radial plot which provides a visual representation of the D_e distribution and the analytical uncertainty associated with each aliquot from a sample. Unlike a simple radial plot, it also includes a kernel density curve (Figure 2.4b). The abanico plot provides insight into whether the D_e distribution is normal, skewed, or multimodal. Considering both the OD value and the abanico plot, statistical models are chosen to best estimate the representative D_e value to be used to calculate the sample's optical age.

For a well-bleached sample with a low (<20%) OD, the central age model (CAM) is appropriate for determining a representative D_e value for the age calculation (Galbraith and Roberts 2012). This method provides a weighted average of all aliquots and considers the precision of each aliquot's D_e value. In a well-bleached sample, use of the CAM is likely reasonable as it is expected that each sand grain was adequately bleached before deposition. Aeolian deposits (and some littoral sediments) are most appropriate for this model, as grains comprising them are typically well beached before deposition and burial in a landform.

The CAM is an inappropriate model in cases where samples include enough partially bleached grains that retain residual signals from a past burial period(s) (Galbraith *et al.* 1999). The application of the CAM to such samples leads to an averaging of fully bleached signals and incompletely bleached signals, thus providing D_es that are higher than they should be. The minimum age model (MAM; Galbraith *et al.* 1999) is more appropriate for incompletely bleached samples. It assigns a higher weight

to aliquots with lower D_e values, thus providing a representative D_e that is skewed toward the lower end of the D_e distribution. To operate effectively, the MAM algorithm requires an estimate of the idealized spread of data value (σb), which is the amount of variance, associated with OD, expected in a sample if it had been fully bleached (Cunningham *et al.* 2011). A higher σb value will make the impact of the MAM lower and increase the error, while a lower σb value will provide a younger-skewed age which may end up being an underestimate of the D_e associated with the true burial age

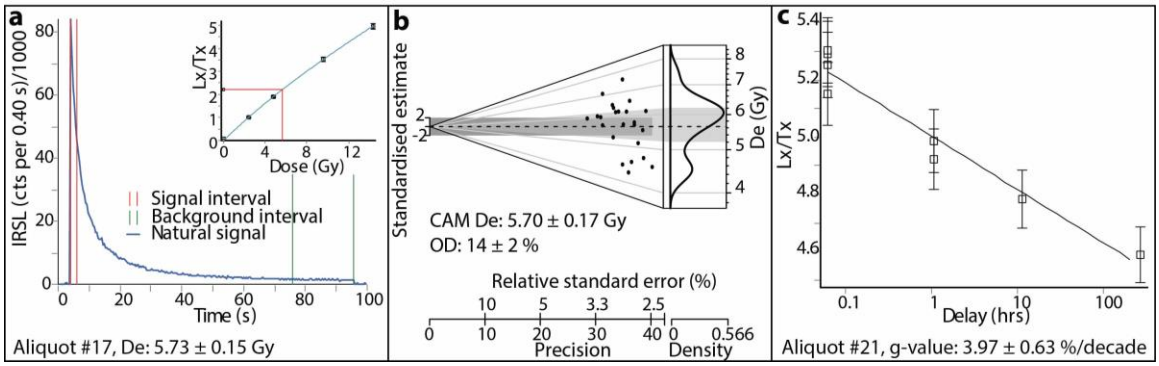

Figure 2.4. Optical dating summary for sample 1951-TG-02. a) A shinedown curve of the natural signal from an aliquot. Vertical lines indicate which portion of the shinedown curve was used for the signal (red lines) and background (green lines) measurements. Inset is a dose-response curve for the same aliquot with the normalized (L_x/T_x) "natural" luminescence interpolated onto its dose-repsonse curve (red line), its D_e value being read from the x-axis. b) An abanico plot of D_e values from all accepted aliquots for the sample. Abanico plots include a radial plot on the left and a kernel density curve on the right. The positions of the points are plotted based on their value and uncertainty; those with lower uncertainty plot further to the right on the radial plot. Radial plots are read by drawing a line from the origin at the left y-axis through each point and onto the y-axis to the left of the kernel density curve. Two sigma error values can be measured on the graph by drawing a straight line from each of the "2" and "-2" standardised estimate dashes on the left y-axis, through the point, and onto the axis to the left of the kernel density curve. The kernel density curve provides a visual representation of the spread of data. In this case, the data are skewed slightly to the bottom and are weakly bimodal. The representative D_e for this sample is found here using the central age model (CAM); overdispersion (OD) for the sample is also provided. c) A representative fading plot from one aliquot of the sample. Delay time on the logarithmic x-axis denotes the time between laboratory irradiation and stimulation, with longer delay times resulting in lower luminescence values as a result of anomalous fading. Additional summary figures can be found in Appendix C.

To choose the *σb* value, OD values from aeolian samples in the study were used as a starting point as they are considered to be fully bleached, thus they contained the lowest variance that could be expected for the sample area. These ranged between 14 ± 2% and 15 ± 2%, thus the *σb* value chosen for MAM calculation was 15%. Using the 20% OD threshold, the CAM was used for samples with OD values under 20%, and the MAM was used for samples with OD values over 20%. The modelled D_e s were then divided by an estimate of the environmental dose rate to produce optical ages (uncorrected for anomalous fading) for each sample.

Environmental dose rate

The environmental dose rate (commonly referred to as just 'dose rate'), is the rate at which the optical dating samples absorb ionizing radiation while *in situ* in the environment. This radiation comes from radionuclides (mainly U, Th, ^{40}K, and Rb) in the surrounding sediments, from within the minerals in the samples, and from cosmic rays. Ideally, most of the radioisotope concentrations are measured *in situ* at the time of sample collection using a portable gamma-ray spectrometer which measures gamma rays from the surroundings up to ~50 cm away. However, a gamma-ray spectrometer was not available for this study. Instead, radionuclide concentrations were determined by neutron activation analysis (NAA) at a commercial laboratory (Bureau Veritas Laboratories, Mississauga, Ontario) from a dried and milled subsample of the bulk sand matrix from which the KF grains were separated (Appendix C, Table C.2). This approach assumes that the dose received by the sample from bounding sediments is like that at the sample site, which was probably the case, or nearly so, at the sites sampled during this study. Samples were collected as far away from bounding strata as possible to reduce their effect (Appendix C, Table C.3).

Cosmic rays also contribute to the dose rate, but this contribution diminished quickly with depth. The contribution of cosmic rays to the total dose rate was calculated using present-day burial depths, elevation, and latitude (Appendix C, Table C.4) and the relationship of Prescott and Hutton (1994, their Appendix).

Pore water in the sediment matrix attenuates radiation, and this must be considered in the dose rate calculations. As the samples were collected in a semi-arid environment that is assumed to have changed little over the time of burial (Lian and Huntley 1999), and since samples were collected from well-drained sand units overlying

gravel, as-collected water content values were used. Water content analysis was performed by extracting a bulk subsample in a water-permeable container, fully saturating the sample over the course of 3-20 days, then fully drying over the course of ~1 week, while weighing the sample at various times (Appendix C, Table C.4).

For each sample the contributions of α, β, and γ radiation to the total dose rate were calculated using the measured radioisotope concentrations, the dose-rate conversion factors of Guérin *et al.* (2011), the attenuation and absorption factors of Brennan (2003), and standard dose-rate equations (e.g., Berger 1988; Lian *et al.* 1995). In each case an internal ^{40}K concentration of 12.5 ± 0.5% was assumed (Huntley and Baril 1997), and an estimate of the fraction of the β dose rate arising from Rb inside the KF grains was made using the estimate of 11% Rb from Huntley and Hancock (2001). For each sample the contribution of α radiation from inside K-feldspar grains was assumed to be 0.09 Gy/ka (Ollerhead *et al.* 1994). In practice, dose rate calculations were done using the Dose Rate and Age Calculator (DRAC, Durcan *et al.* 2015), which also allows for the input of CAM- and MAM-modelled SAR D_es to produce optical ages (uncorrected for anomalous fading) for each sample.

Correction for anomalous fading

K-Feldspars are susceptible to a phenomenon known as anomalous fading (Wintle 1973), wherein the IR-stimulated (violet) signal due to laboratory irradiation fades over time due to quantum-mechanical tunneling of electrons from thermally stable electron traps to those that are thermally unstable (Huntley and Lamothe 2001). This results in age underestimation unless anomalous fading is dealt with. Various methods for dealing with anomalous fading have been proposed and they can be categorized by either circumvention or correction. Circumvention of the problem of anomalous fading is done by assessing traps that do not fade, such as those measured using the post-IRIR technique (Thomsen *et al.*, 2008). These traps, however, require far more time to bleach sufficiently in the environment (Colarossi *et al.*, 2015). In turbid waters, such as those expected in the ancestral Fraser River, it is unlikely that these traps can reliably be bleached sufficiently for post-IRIR techniques to work well. Moreover, it has been found that in many cases the post-IRIR signal also fades (Jain *et al.* 2015), albeit usually at a lower rate than the IR-stimulated signal traditionally used for dating, and thus still requires correction.

For this study, therefore, the correction method of Huntley and Lamothe (2001) was chosen. A modified SAR procedure (Auclair *et al.* 2003) was used to determine fading rates (*g* values) for each sample (Table 2.2). After samples were dated, 12 aliquots from each sample were tested for anomalous fading. They each received a dose of ~14 Gy, similar to the median D_e of all samples, then delays of 1-10 hr were built into the sequence. To increase the storage time while allowing the Riso reader to be used for other experiments, the aliquots were given a dose of laboratory radiation at the end of the sequence and removed from the machine for 3-30 days. Once returned to the machine, the samples were stimulated and the signal that had faded over time was plotted. This created a fading plot (Figure 2.4c) from which the fading rate was determined from the slope of the lined fitted to the data. Acceptance criteria for individual aliquots' fading plots were an adequate fit of a line to the data points ($\chi^2 < 1.00$) and evidence of minimal grain loss determined by similarity of Tx/Tn values before and after the multi-day resting period.

The fading rates determined from accepted fading plots (Figure 2.4c) (n = 5-11, depending on the sample) were then analyzed using the CAM to provide an averaged fading rate for each sample. This method is efficient and has been found to produce ages within error of those determined from aliquots that had their D_e values corrected for fading using their own fading rates (Neudorf *et al.* 2015). An important criterion for applying the correction method of Huntley and Lamothe (2001) is that the sample's D_e must fall within the linear portion of its dose-response curve, and this was the case for all the samples in this study. The fading rate was then used to correct each age using the method of Huntley and Lamothe (2001) and the R program written by Kreutzer (2020).

Incision rate calculation

Optical dating ages were correlated with height above river level, then correlated using ordinary least squares regression on each fluvial data point without accounting for error. This was deemed acceptable as the precision of the incision rate is low given the relatively limited number of data points in the study. The incision rate is thus an estimation, considered reliable within one order of magnitude. The incision rate was further broken down into three time periods, discussed in Section 2.4.3.

Table 2.2. SAR procedure used for constructing fading plots. Each aliquot receives this treatment, allowing for pauses between some steps to provide storage time in which to assess the rate of fading. Aliquots are removed from the instrument for the longer (>100 hr) storage times and then are returned to it for measurement. The test dose is used to correct for sensitivity change from repeated dose and stimulation cycles, and ~2.4 Gy was chosen to provide a luminescence signal significantly greater (>3x) than the background signal to minimize instrumental error.

Step	Procedure	Measurement
1	Dose: ~14 Gy	
2	Preheat: 160°C, 10 s	
3	Pause: 1 to >100 hr	
4	Stimulation: IR, 50°C, 100 s (Measures faded signal)	L_x
5	Test dose: ~2.4 Gy	
6	Preheat: 160°C, 10 s	
7	Test dose stimulation: IR, 50°C, 100 s	T_x
8	Dose: ~14 Gy	
9	Preheat: 160°C, 10 s	
10	Stimulation: IR, 50°C, 100 s (Prompt signal)	L_x
11	Test dose: ~2.4 Gy	
12	Preheat: 160°C, 10 s	
13	Test dose stimulation: IR, 50°C, 100 s	T_x
14	Repeat steps 1-13	

L_n: Luminescence signal of the natural dose
L_x: Luminescence signal of subsequent laboratory doses
T_n: Luminescence signal of the test dose associated with the natural dose
T_x: Luminescence signal of the test doses associated with subsequent laboratory doses

2.3. Results

2.3.1. Geomorphology

Terraces occur in wider reaches directly downstream of bedrock canyons, namely French Bar Canyon and Chisholm Canyon for Big Bar and Watson Bar, respectively (Figure 2.5). Fraser River has incised to bedrock throughout the study area. Paraglacial fans emanate from steep tributary valleys, commonly capping terraces. Around Watson Bar, there is a prominent streamlined bedrock landform (Figure 2.5, 2.6) on the east side of the river measuring ~1.4 km long and ~0.3 km wide, ~220 m above present-day river level and ~20 m higher than the highest terrace, with its long axis aligned with that of Chisholm Canyon.

Clearly identifiable terraces are found at elevations from ~450 m asl to river level at ~260-270 m asl. The highest terraces in this study are ~190 m above present-day river level. Based on clearly identifiable terraces, twelve distinct floodplain stages (T01 – T12) are identified for the Fraser River in the study area. All twelve are depicted in a map (Figure 2.5), illustrated in composite cross-sections (Figure 2.7), and shown on a longitudinal profile (Figure 2.8). There are eight instances of paired terraces (T01, T04, T06, T07 T08, T09, T10, and T11) and six terraces could be correlated in the downstream direction (T04, T05, T08, T10, T11, and T12; Table 2.3). Many of the terraces <50 m above present-day river level have been extensively excavated for placer mining. More subtle terraces exist but were not mappable at the scale of this study.

Around Big Bar, nearly all terraces are fan-covered. On the west side, all but the lowest terrace (T11, ~10 m above present day river level, Figures 2.5, 2.7) are fan covered. This is likely due to the proximity of these terraces to steep tributary valleys which have had debris flows and alluvial sediments emanating from them. On the east side of the river at Big Bar, few terraces were found without fan coverings, and those that lack fans include the terrace at site 1951 (T09, ~35 m above present day river level, Figures 2.5, 2.7) and terraces T11 and T12 closer to present-day river level and not directly adjacent to Big Bar Creek confluence. Near Big Bar Creek on the east side of Fraser River, T09 and T10 terraces are fan-covered, indicating that Big Bar Creek has contributed to the sedimentation on these terraces through debris flows and fluvial processes.

Around Watson Bar, all terraces on the west side are fan-covered due to the influence of both Ward Creek and Watson Bar Creek (Figure 2.5). These two high-volume creeks have deposited both debris flow and alluvial sediments, and recent debris flow sediments were even observed while measuring dGPS during the 2019 field season (Figure 2.9). On the east side of Fraser River at Watson Bar, fans are not typically present atop terraces due to the absence of tributary streams in those localities. At the north end of Watson Bar east, a large fan emanates from the valley wall along Indian Creek (Figure 2.5). This fan did not appear to reach the edges of terraces that were studied in the field, but on analysis of the DEM, it looks to have been truncated by the ancestral Fraser River during the T04 floodplain formation stage (Figure 2.5).

The valley downstream of Watson Bar was preliminarily analyzed for landslide scars that may have contributed to Fraser River blockage and subsequent fluvial aggradation. In the reach ~20 km downstream of Watson Bar, at least 5 landslide scars were identified (Figure 2.10), including one at High Bar Canyon ~5 km downstream of Watson Bar. The deposit at High Bar Canyon is associated with a meander in Fraser River and the top of the deposit measures ~100 m above present-day river level (Figure 2.10).

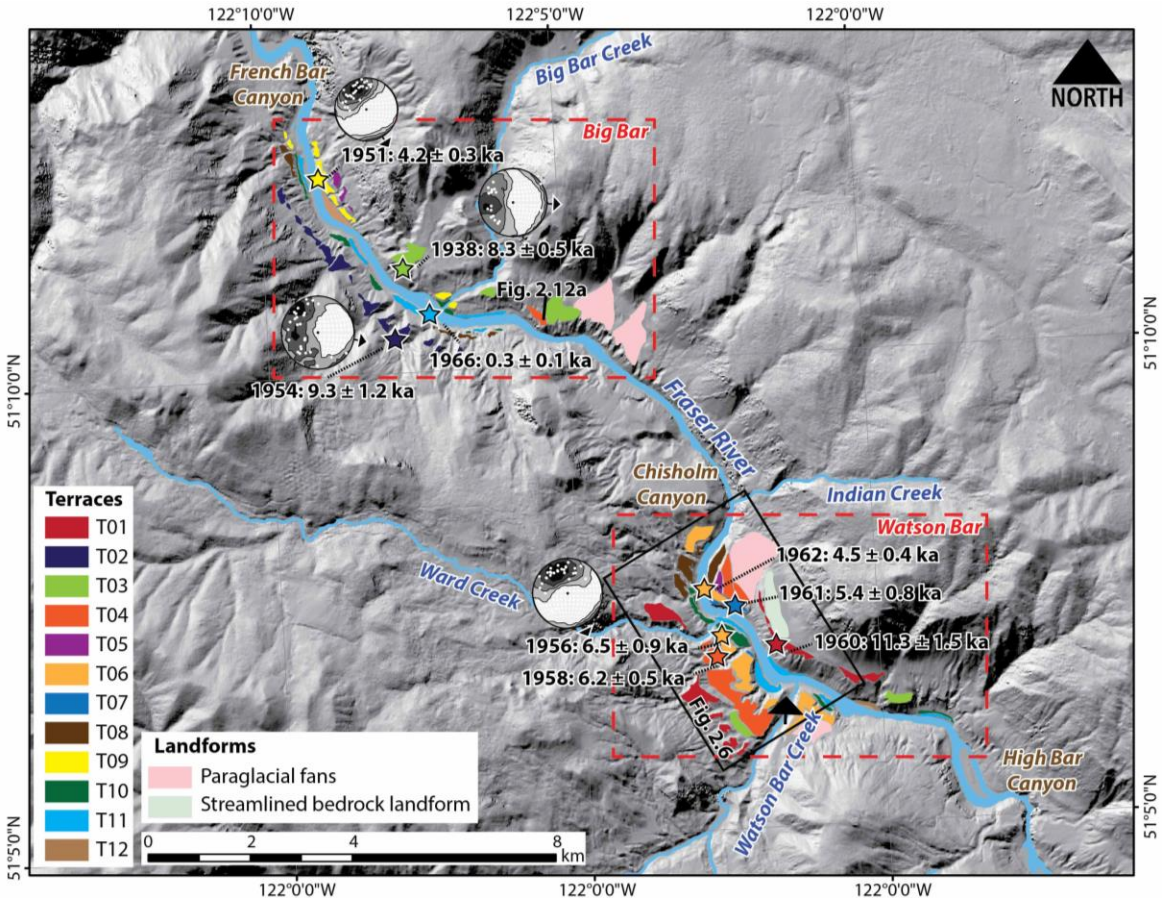

Figure 2.5. Terraces mapped at Big Bar and Watson Bar. Twelve terrace levels are indentified. Sample sites and optical ages are noted by star symbols on the map. Paraglacial fans with no observable underlying Fraser River sedimentsare delineated, as is a streamlined bedrock landform associated with site 1960 at Watson Bar. Plots of gravel a-b plane fabrics for sites 1951, 1938, 1954, and 1956 are plotted on lower hemisphere equal-area Schmidt projections. All palaeoflows from inferred ancestral Fraser River gravel are consistent with present-day river flow direction. Figure 2.6 extent is shown with the arrow denoting the perspective of the image. Figure 2.12a picture location at Big Bar is noted.

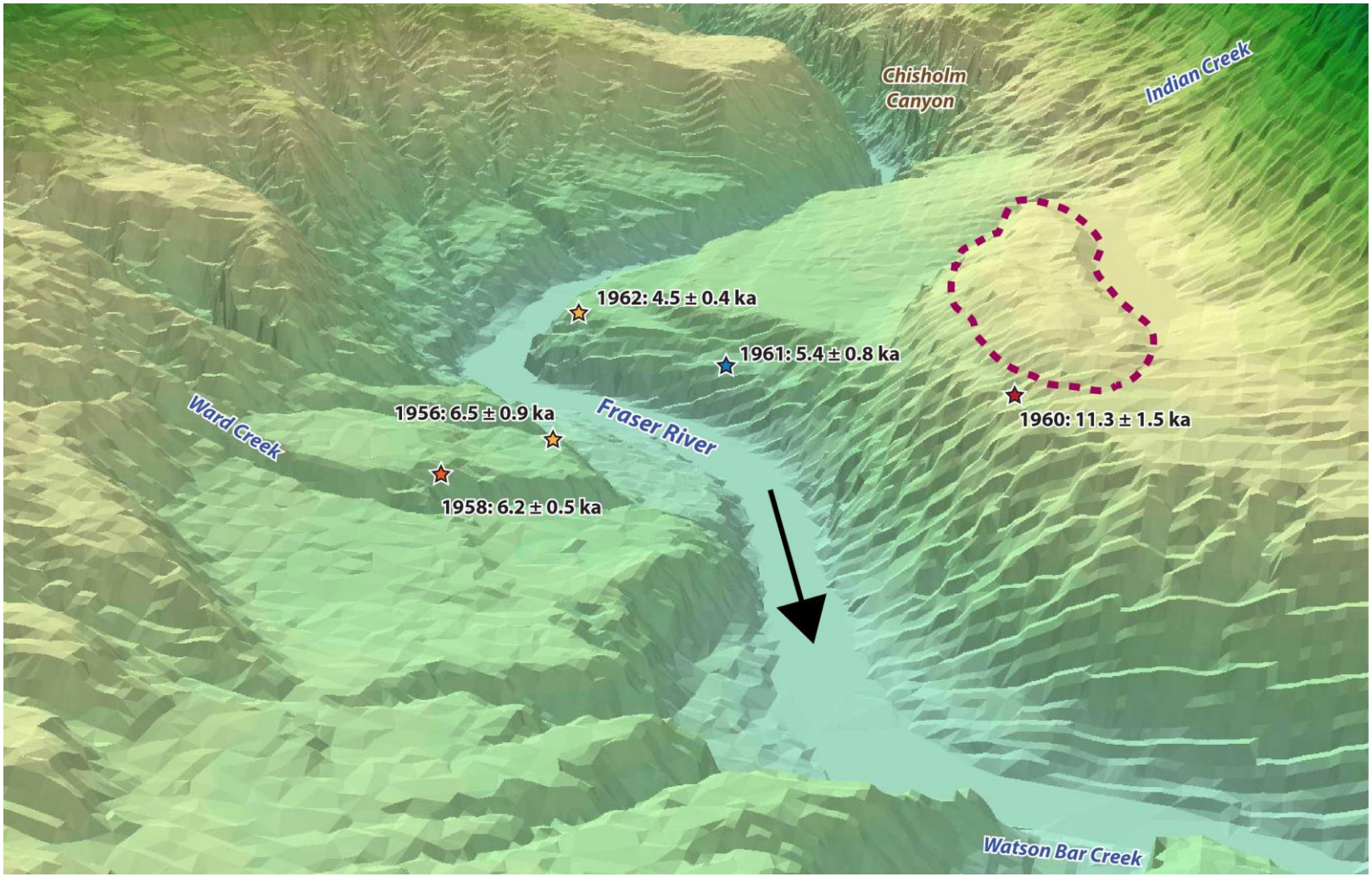

Figure 2.6. Oblique 3D view derived from DEM of Watson Bar terraces looking north, upstream toward Chisholm Canyon. Streamlined bedrock landform upstream from Site 1960 is delineated with a red dotted line. Extent of this figure shown on map in Figure 2.5.

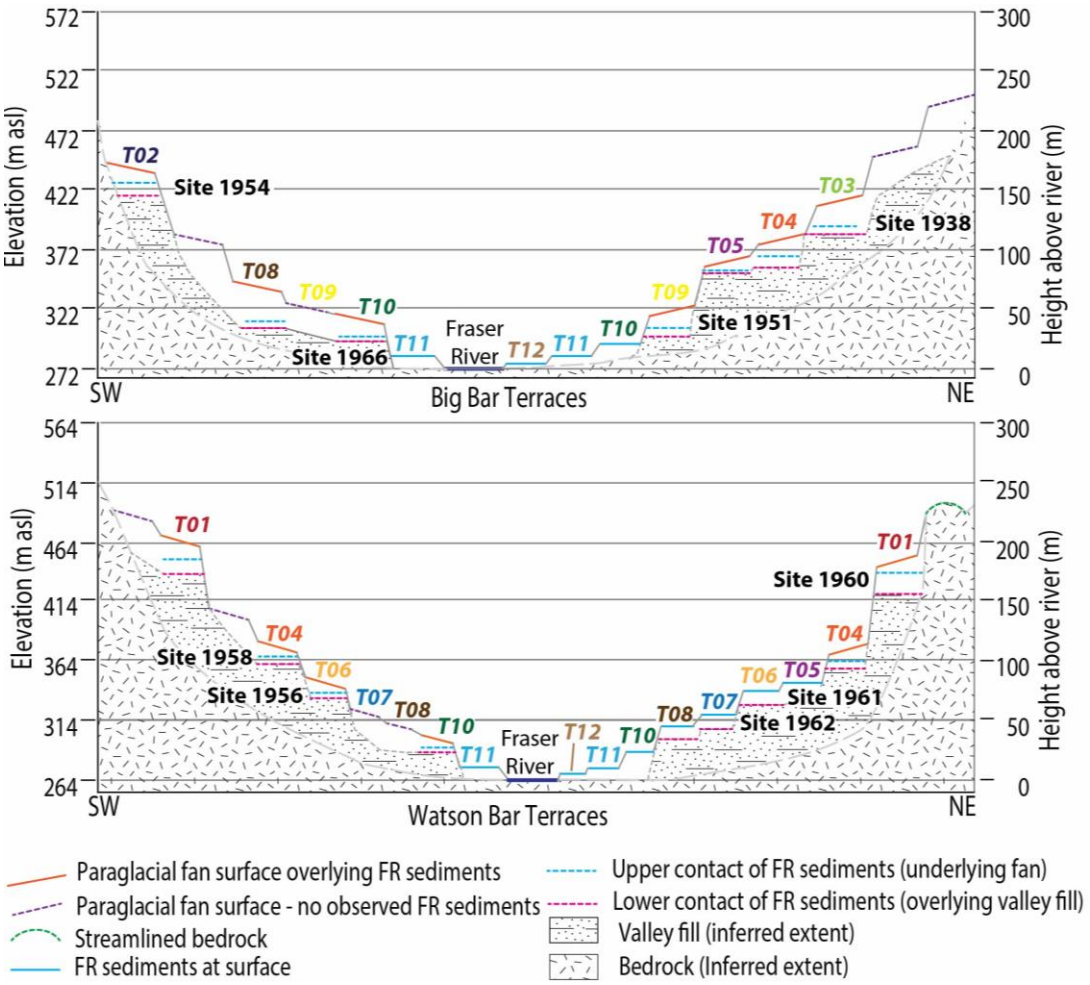

Figure 2.7. Composite cross-sections of terraces at Big Bar and Watson Bar. These cross-sections are developed from 7 and 10 individual DEM cross-sections at Big Bar and Watson Bar, respectively (Appendix D) and verified through DEM analysis, dGPS surveys, and photographic analysis. Exposed fluvial and valley fill contact elevations are from dGPS survey data. T09 on the west side of FR at Big Bar, T07 and T08 on the west side of FR at Watson Bar, and T10, T11, and T12 on the east side of FR at Watson Bar were observed through DEM analysis and visual confirmation in the field, but not dGPS surveyed due to access challenges. Bold text on each cross-section refers to the site where optical dating samples were collected (Figure 2.10, Table 2.3).

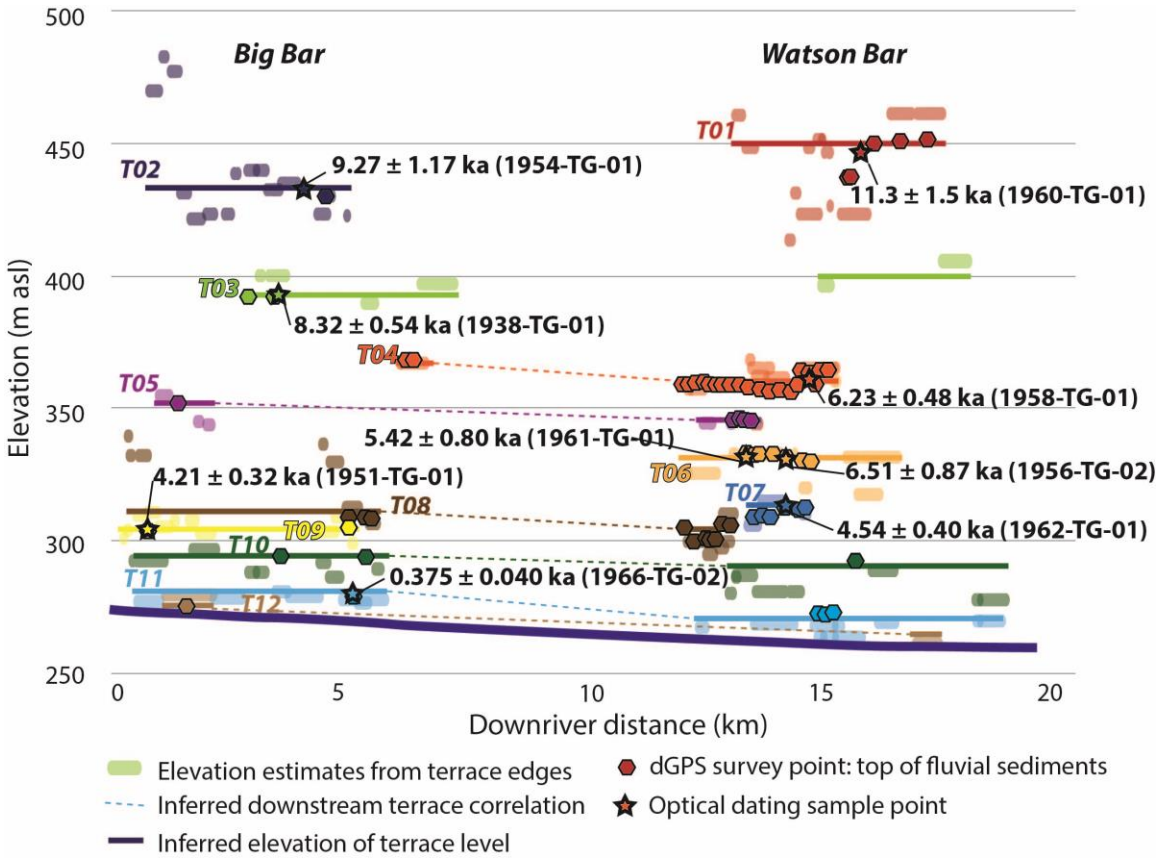

Figure 2.8. Downstream profile of Fraser River and ancestral Fraser River terraces between Big Bar and Watson Bar. Terraces are colour coded to correlate with mapped and numbered terraces (Figure 2.5). Faded dots behind solid lines are extracted elevations from DEM analysis. Solid lines are best-inferred elevations for each terrace level using dGPS points (hexagonal symbols) which are the highest precision indicators of past floodplain levels. Especially high T02 and T08 DEM elevations at Big Bar are anomalous due to the presence of thick fans, but their lateral continuity can be visually traced in the field and correspond best to the dGPS elevations provided above. Similarly, low T01 and T06 DEM elevations at Watson Bar are anomalous due to gullying and erosion of terrace edges, but their lateral continuity viewed in the field with adjacent dGPS-checked terraces places them at those respective terrace levels. Note that Watson Bar terrace correlation to T03 at Big Bar only appears higher downstream because Watson Bar T03 elevation is uncertain, based on DEM extraction only due to access restrictions, and these terraces are buried under thick fans.

Table 2.3. Terrace correlation summary. Terraces are considered paired if there were terraces at the same hieght above Fraser River on both sides of the same reach. Terraces are correlated downstream if there were terraces at Watson Bar that were similar height above present-day Fraser River level as at Big Bar. Confidence intervals are inferred based on thicknesses of observed fans. Question marks indicate possible, but not field verified, correlation.

Terrace ID	Height above river (m)	Optical dating site	BBE	BBW	WBE	WBW	Paired	Downstream correlation
T01	180 ± 10	1960	n	n	y	y	y	n
T02	160 ± 10	1954	n	y	n	n	n	n
T03	120 ± 10	1938	y	n	?	?	?	?
T04	100 ± 5	1958	y	n	y	y	y	y
T05	85 ± 5		y	n	y	n	n	y
T06	75 ± 5	1961, 1956	n	n	y	y	y	n
T07	55 ± 5	1962	n	n	y	y	y	n
T08	45 ± 5		n	y	y	y	y	y
T09	35 ± 2	1951	y	y	n	n	y	n
T10	15 ± 2		y	y	y	y	y	y
T11	10 ± 2	1966	y	y	y	y	y	y
T12	5 ± 2		y	n	y	n	n	y

BBE: Big Bar East; BBW; Big Bar West; WBE: Watson Bar East; WBW: Watson Bar West

Figure 2.9. Debris flow at Watson Bar that occurred during the 2019 field season. This, together with evidence of many other recent mass wasting events is affirmation that the landscape is still undergoing paraglacial adjustment.

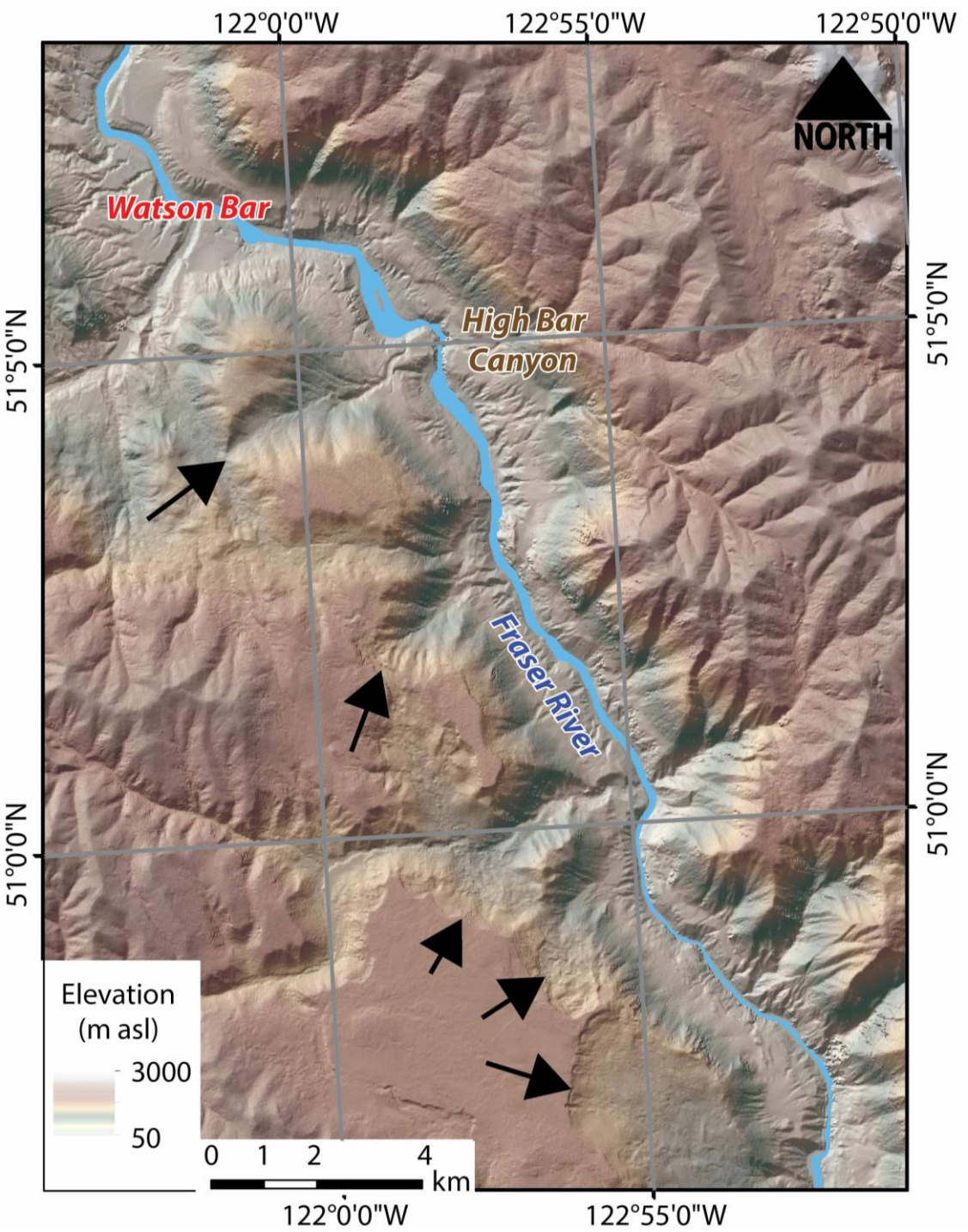

Figure 2.10. Landslide scars (scarps identified by black arrows) downstream of the study area. The toe of the landslide at High Bar Canyon is ~100 m above present-day river level.

2.3.2. Lithostratigraphy

The underlying stratigraphy of Fraser River terraces in the Big Bar and Watson Bar area can be generally subdivided into four palaeoenvironmental units (Figure 2.11, 2.12), each typically composed of similar lithofacies. Because terraces have formed by similar processes at different times, the sediment units that form them (unit 2, below) are often diachronous.

Unit 1: Pre-terrace valley fill

Unit 1 (Figure 2.11, 2.12) is pre-terrace valley fill and has been previously described in the study area by Lian and Hicock (2001), their units I-IV, and in adjacent study areas by Eyles and Clague (1991), and Huntley and Broster (1994). It consists mainly of glaciofluvial sand and gravel, glaciolacustrine silt and sand, and glacigenic diamicton (largely reworked till), deposited during the last (Fraser) glaciation. There is some evidence of sediments predating the Fraser Glaciation near the base of the valley fill to the north of the study area (Eyles and Clague 1991). Unit 1 forms the sediment in which ancestral Fraser River incised, formed terraces, and on which associated fluvial sediments were deposited.

Unit 2: Ancestral Fraser River floodplain sediments

Unit 2 contains three subunits (Figure 2.11). Unit 2a is found only at site 1960 (Figure 2.13), located on the southwest (downvalley) end of a streamlined bedrock landform near Watson Bar immediately downstream of Chisholm Canyon (Figure 2.5, 2.6). The site is on the highest terrace investigated in this study, standing ~180 m above present-day river level. At this site, Unit 2a is ~17 m thick and consists of clinoforms composed of poorly-sorted cobble to boulder gravel in a matrix of silty fine sand to granules with openwork pebble lenses that rest above a sharp, erosive contact with unit 1 (Figure 2.13). The clinoforms have an apparent dip of ~10-15° southward (downvalley) (Figure 2.13a). Diamicton intraclasts up to ~1m in diameter (b-axis) occur within the clinoforms (Figure 2.13b).

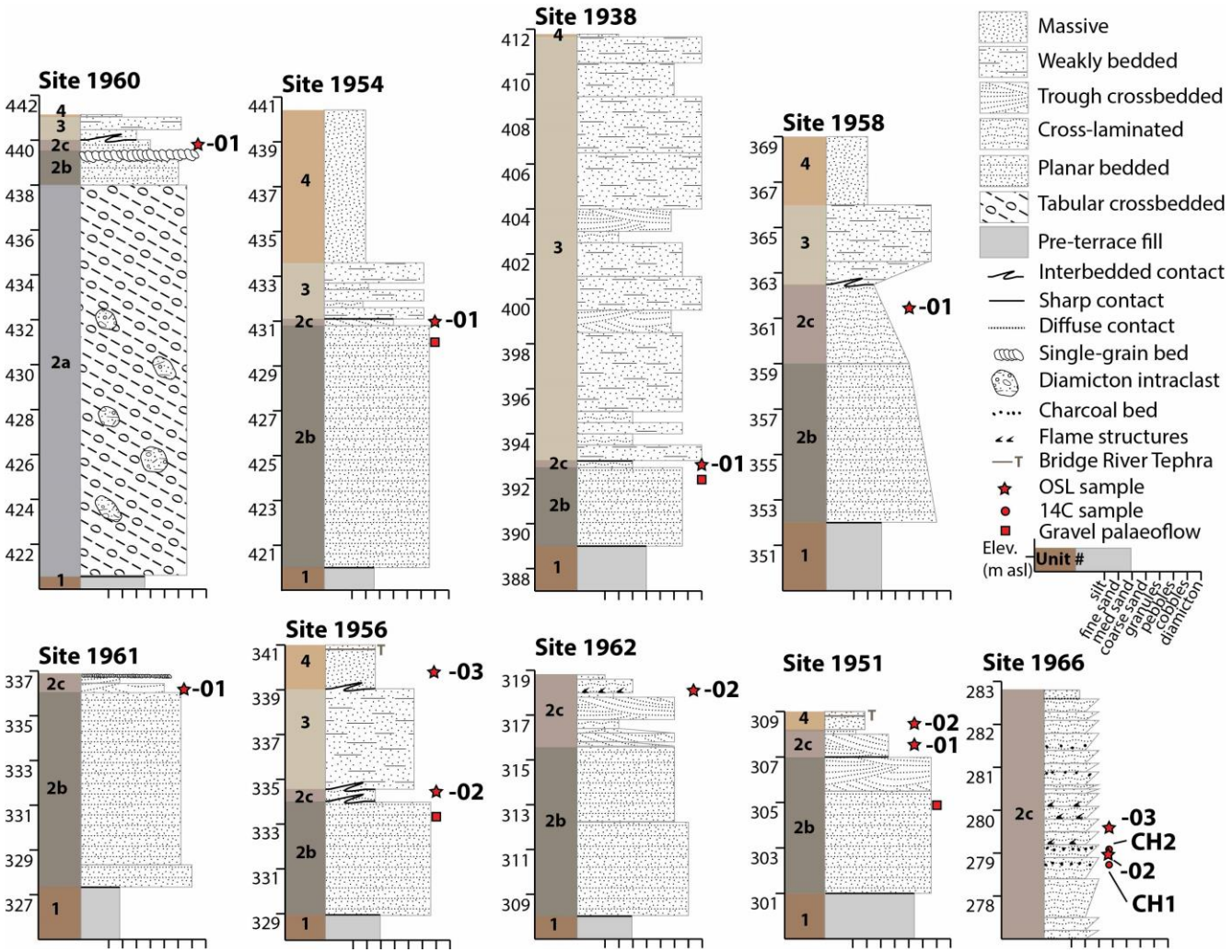

Figure 2.11. Stratigraphic logs from all optical dating sample sites. Unit numbers correspond to palaeoenvironmental units described in the text. Optical dating sample names have been shortened for the sake of space, their full notation being ([Site #]-TG-[# on stratigraphic log]). Gravel palaeoflows correspond to plots on Figure 2.5.

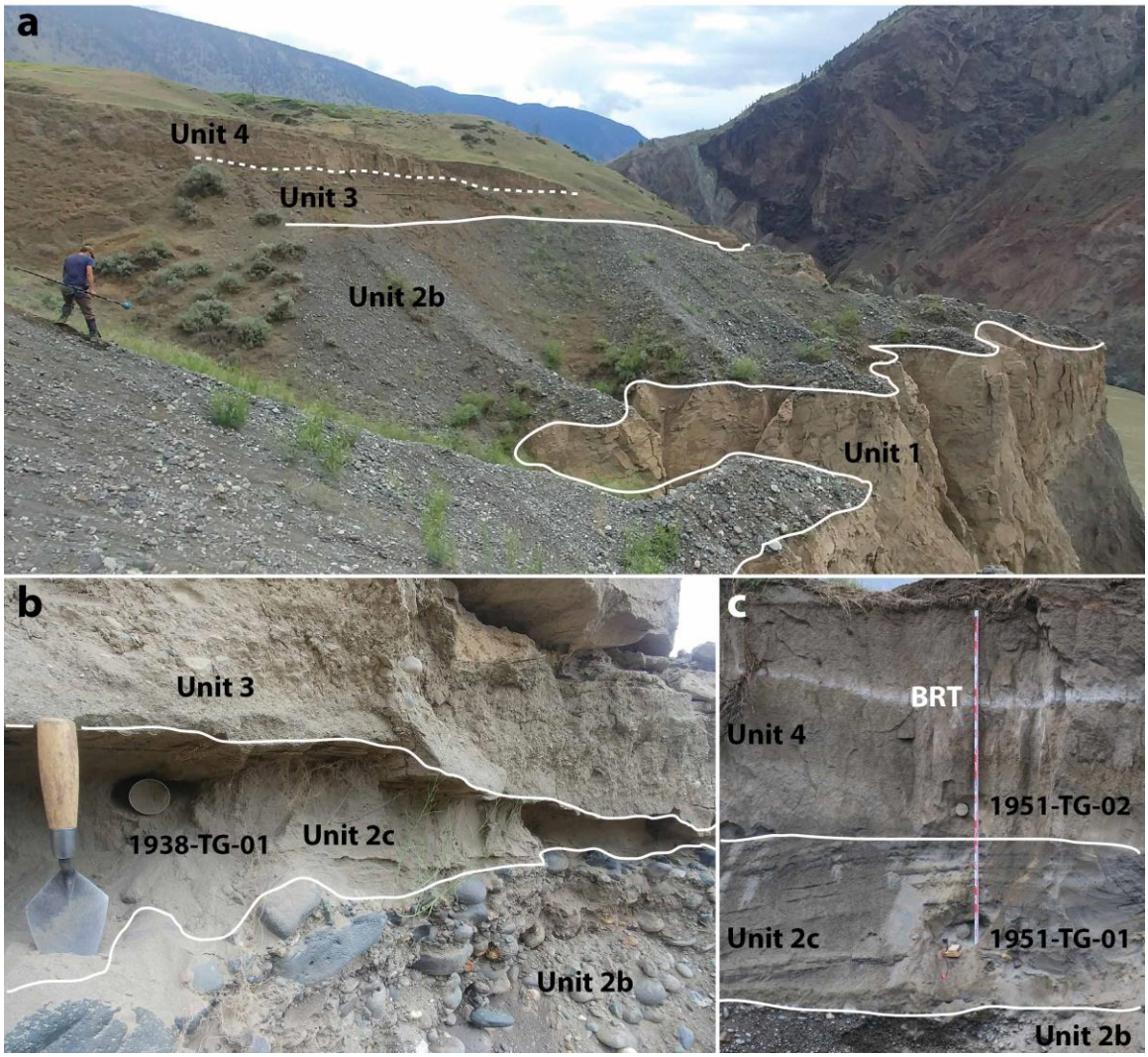

Figure 2.12. a) Fraser River valley fill stratigraphy in the study area typically consists of four palaeoenvironmental units, shown here on a T04 terrace at Big Bar upstream of Chisholm Canyon (location shown in Figure 2.5): unit 1: pre-terrace valley fill; unit 2: ancestral Fraser River sediments (here, unit 2b is 9 m thick); unit 3: paraglacial fan sediment, and; unit 4: aeolian cap. b) Transition from Fraser River sediments (unit 2) to paraglacial fan sediments at site 1938. Optical dating sample 1938-TG-01 was collected from unit 2c. C) Top of terrace at site 1951. Unit 3 is not present at this site. Optical dating samples 1951-TG-01 and 02 were collected from unit 2c and unit 4, respectively. Bridge River Tephra (BRT) (Clague *et al.* 1995) is clearly visible in unit 4.

The geomorphic context of site 1960 aids in the interpretation of unit 2a. At site 1960, the streamlined bedrock landform (Figure 2.6) acted as a resistant obstacle that impeded river flow causing lee side flow separation and deposition Southward dipping gravel clinoforms are consistent with lee side deposition, forming as flow overtopped the

bedrock obstacle and lost energy. The preservation of diamicton intraclasts in unit 2a indicate short transport distances, fast dissipation of water energy, and rapid deposition and burial. Unit 2a is consistent with a short-lived, high discharge event, perhaps even a megaflood based on the observed clinoforms and intraclasts (Carling 2013).

Unit 2b is 1–18 m thick and rests sharply on unit 1 in all cases except site 1960 where it conformably overlies unit 2a gravel. Unit 2b consists mainly of horizontally bedded clast-supported cobble to pebble gravel (Figure 2.12b). Clasts are subrounded to well-rounded with rounded being most dominant. The matrix ranges from medium sand to granules and openwork lenses of pebbles are commonly present. Trough cross-bedding occurs at site 1951. Clast fabrics collected from sites 1954, 1938, 1956, and 1951 indicate palaeoflows parallel to valley axis (Figure 2.5). The majority of clasts are found with *a*-axis transverse to flow (Appendix B), indicating rolling in a fluvial environment. Unit 2b is observed near the top of each terrace in the study except at site 1966.

Unit 2b is interpreted to be ancestral Fraser River floodplain sediment due to the rounded nature of clasts, clast fabrics that are consistent with the flow direction and nature of present-day Fraser River, and the position of unit 2b, stratigraphically above glacial valley fill and near the top of each terrace. It is correlated to unit VII of Lian and Hicock (2001).

Unit 2c is commonly <1m thick. However, at site 1958 it is 3.5 m thick and at site 1966 it is ~6 m thick. Unit 2c rests conformably on unit 2b where observed; at site 1966 no lower contact was observed. Unit 2c consists of bedded granules to fine sand with medium sand being dominant. Structures in unit 2c include ripple cross lamination in medium and fine sand indicating palaeoflows parallel to valley axis and consistent with present-day Fraser River flow direction. Trough cross bedding is present at sites 1954 and 1962 with single grain thick pebble beds armoring coarse sand beds. Interbedding occurs between unit 2c and unit 2b at site 1956.

Unit 2c is interpreted to be more distal floodplain overbank sediment deposited during flood stages of ancestral Fraser River due to its grain size and unit thickness (typically <1 m), and the position of unit 2c overlying the fluvial gravel of unit 2b. The interbedding that occurs between unit 2c and 2b is attributed to periodic flood events

which left behind pockets of sand near flow obstacles or tributary confluences before either a higher flood event or channel migration occurred to deposit a gravel bed over sand. All terrace fluvial optical dating samples were collected from unit 2c and site to site differences in sedimentology are noted in Appendix B (Table B.4).

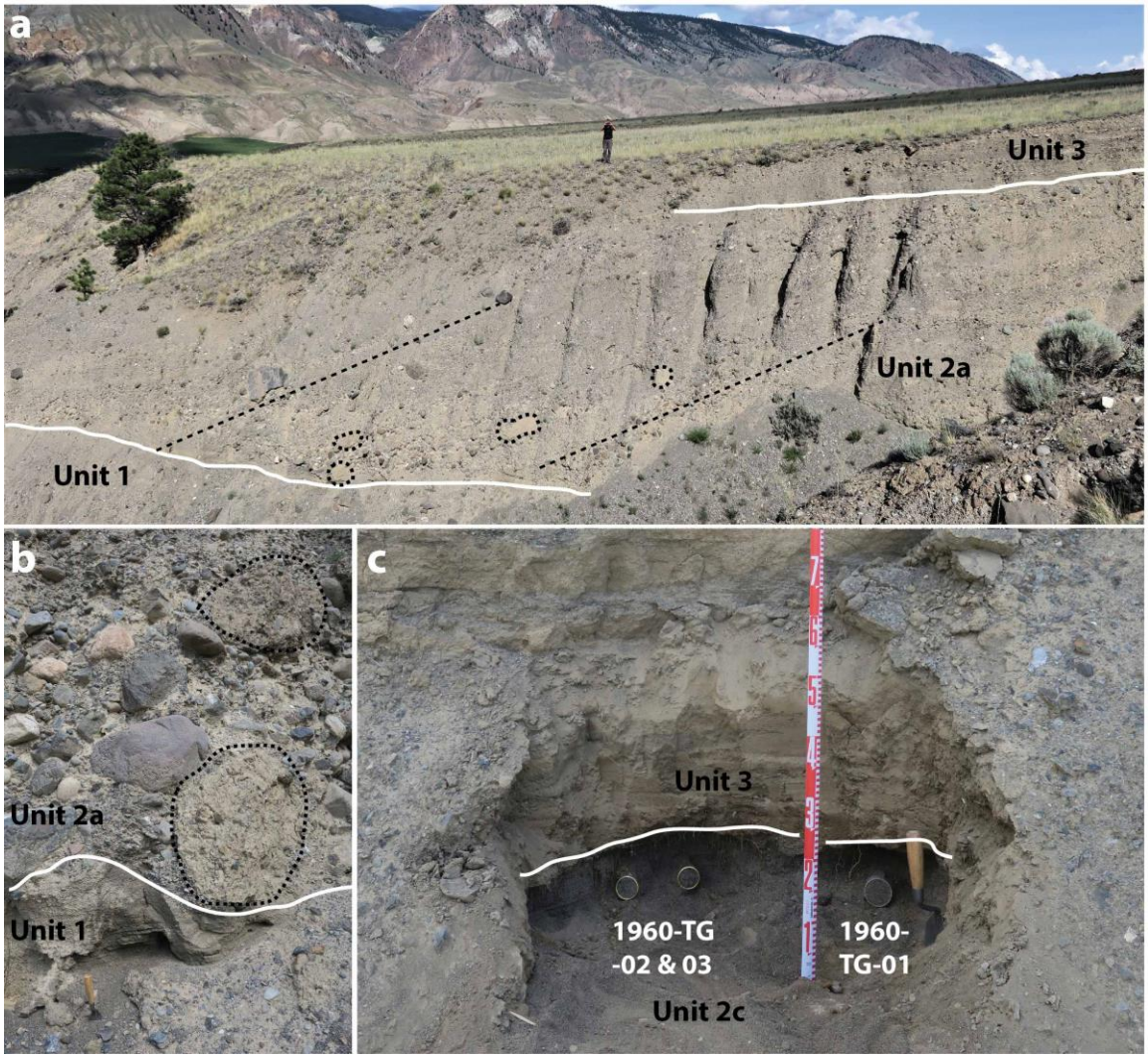

Figure 2.13. Stratigraphy around site 1960. Photos in (a) and (b) are from ~100m south of site 1960 in the same terrace. a) Unit 2a clinoforms (highlighted by black dashed lines) containing diamicton intraclasts (dotted outlines) overlying unit 1. Unit 2a is ~20 m thick here. b) Diamicton intraclasts (dotted outline) in unit 2a. Contact between unit 1 and 2a is sharp and erosive. Trowel handle in bottom left ~10 cm. c) Optical dating samples 1960-TG-01, 02, and 03 were collected from unit 2c. Samples 1960-TG-02 and 03 were collected to ensure enough material was available and not processed as sufficient sand was collected from 1960-TG-01. Stadia rod is numbered in dm.

Site 1966, located on the west side of Fraser River at Big Bar, presents a 6 m thick exposure of unit 2c sand (Figure 2.14). It is at the downstream end of a T11 terrace that stands 11-13 m (based on DEM elevations) above present-day river level (Figure 2.5). Here, 10-30 cm thick rhythmites of fine sand and silt grade inversely into medium sand (Figure 2.14b), then each rhythmite is topped with a thin (5 mm) bed of silt. Contacts between rhythmites range from sharp to diffuse. Ripple cross laminations are visible in medium sand beds with thin brecciated silt beds visible at some contacts (Figure 2.14b). A modern analogue for the thin silt beds was observed in slopewash deposits on an active sand bar within 100 m of site 1966 (Figure 2.15). Four beds of fine sand containing charcoal and rounded clasts with angular breakages up to pebble size occur within the rhythmites (Figure 2.14c). These beds are located 2-4.5 m from the base of the exposure, with the uppermost beds 1.5 m from the surface (Figure 2.11). ^{14}C samples were collected from the lowest two beds, 2 m from the base of the exposure and 4 m from the surface (Figure 2.11, 2.14). All clasts observed were volcanic and typically have one or two rounded sides and several jagged surfaces. The upper 40 cm of the exposure has been bioturbated by modern root activity and contains a weakly developed modern soil.

The rhythmites of unit 2c at site 1966 are interpreted to be sequential overbank sediments deposited during high water stages of present-day Fraser River. Thin silt beds capping medium sand were observed along modern-day sand bars (Figure 2.15) and may be related to slope wash from rain events armoring sand beds prior to subsequent flood events or settling out from overbank ponds. Ripple cross laminations in medium sands indicate slightly higher flow velocities, consistent with shallow water in overbank flood environments. The rounded clasts with angular breakages associated with the charcoal beds are interpreted to be fluvially rounded stones that have been subsequently fire-cracked. The fine sand, charcoal beds, and fire-cracked stones are likely derived from debris flows from the valley sides, associated with wildfire events which destabilized the slopes.

Unit 3: Paraglacial fan sediment

Unit 3 exists at sites 1960, 1954, 1938, 1958, and 1956 (Figure 2.11). It consists of beds of diamicton and clast-supported angular to rounded gravel 1–20 m thick, and forms fan-shaped landforms resting on unit 2. Diamicton is matrix-supported with coarse

sand to silt matrix; clasts are cobble to pebble sized, angular to subrounded, and are generally of more local lithology than clasts in unit 2. Gravel beds are typically poorly sorted with clasts ranging from cobble to pebble size. Beds range in thickness from ~10 cm to up to 2 m, thinning toward valley axis. Lower beds within unit 3 typically contain more rounded clasts, and angularity increases with height above the lower contact. Unit 3 is interbedded with unit 2c at sites 1960, 1958, and 1956.

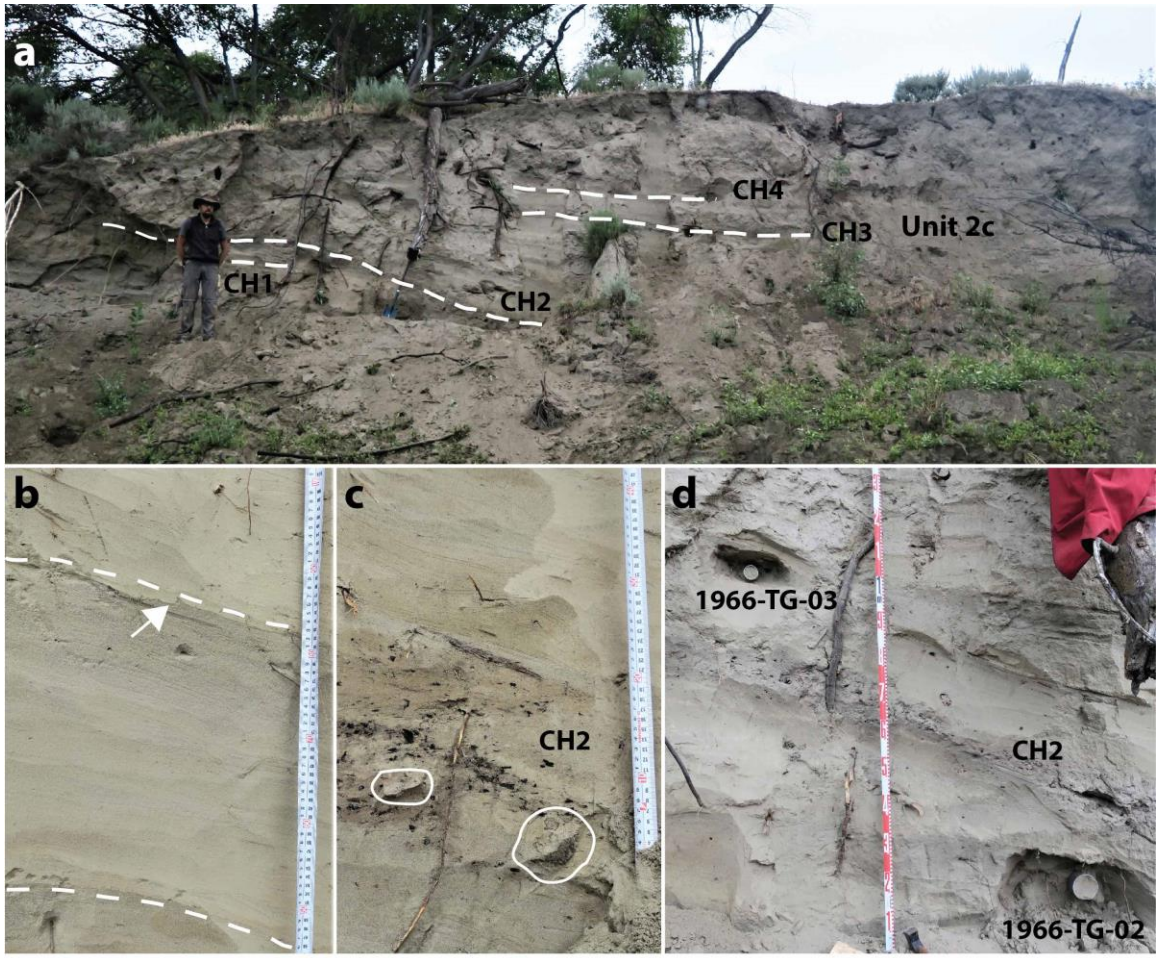

Figure 2.14. Site 1966 stratigraphy. a) Site 1966 is composed of sand-silt rhythmites (unit 2c) associated with present-day (<0.5 ka) flood events. White dashed lines indicate four beds of charcoal and fire-cracked rock within the rhythmite sequence. All charcoal beds (CH1-CH4) were sampled for ^{14}C dating although only CH1 and CH2 were dated for this study. b) Inverse grading of a rhythmite with fine sand and silt grading into medium sand (bounded by dashed lines). A thin discontinuous bed of silt rests on top of medium sand at the top of the rhythmite (arrow). c) Charcoal bed where ^{14}C sample CH2 was collected. Fire cracked rocks are circled. d) Optical dating samples 1966-TG-02 and 03 were collected from unit 2c rhythmites below and above ^{14}C sample CH2, respectively.

Figure 2.15. Modern sand bar showing a thin silt bed overlying medium sand, in this case drying out and becoming discontinuous. This silt bed issued from the mouth of an ephemeral stream active during recent rain events. Similar beds were found in the stratigraphy of site 1966, potentially marking the cessation of periodic flood events.

Unit 3 is interpreted to be paraglacial fan sediment due to the thinning of beds toward the valley axis suggesting that unit 3 was formed from sediments sourced from the valley sides and the prevalence of angular clasts of local lithology suggesting deposition near the source material (Ryder 1971). The poorly sorted nature of the diamicton and gravel beds suggest they were deposited mainly as debris flows with some ephemeral fluvial reworking after Fraser River incision and floodplain abandonment. Unit 3 is correlated to Unit VI in Lian and Hicock (2001). Interbedding of units 2c and 3 suggests periodic Fraser River flood events and slope derived debris flow sedimentation at sites 1960, 1958, and 1956 (Figure 8, #4, Ryder 1971).

Unit 4: Aeolian cap

Unit 4 is up to 6 m thick and caps some of the terrace-top sequences; it was not found at sites 1961,1962, or 1966 (Figure 2.11). It consists of well-sorted nearly massive fine sand to silt with minor granules. It rests on a typically sharp lower contact, though

unit 4 is interbedded with unit 3 at site 1956. At two sites, 1956 and 1951, a 2 cm thick white tephra bed consisting of grains up to ~1 mm in diameter was found near the top of unit 4 (Figure 2.12c).

Unit 4 is interpreted to as aeolian sand and silt due to its massive character, high degree of sorting, and its stratigraphic position overlying units 2 and 3. It is correlated to unit 51-2 in Lian and Huntley (1999). The white tephra bed is assumed to be Bridge River Tephra (BRT), as it was previously identified in the study area at this stratigraphic position by Lian and Huntley (1999). BRT has a known age of 2.36 ka (Clague *et al.* 1995). All aeolian optical dating samples were collected from Unit 4. Interbedding of units 3 and 4 suggests that aeolian deposition occurred contemporaneously with paraglacial fan processes at site 1956.

2.3.3. Dating

Radiocarbon dating

Two charcoal samples from site 1966, CH1 and CH2 (Figure 2.11, 2.14), were dated using AMS ^{14}C techniques which provided ranges with associated probabilities. Sample CH1 (UOC-11654, Figure 2.16a) has an uncalibrated ^{14}C age of 0.323 ± 0.022 ka, and when calibrated has a 95.4% probability of being in the range 0.457– 0.310 ka BP, with peaks in the probability distribution at ~0.425, ~0.380, and ~ 0.320 ka.

Sample CH2 (UOC-11655, Figure 2.16b) has an uncalibrated ^{14}C age of 0.171 ± 0.023 ka, and when calibrated it has a 95% probability of being in the range of 0.288 ka BP to modern. Peaks in the probability distribution occur at ~0.270, ~0.220-0.170, ~0.150 and ~0.020 ka, with 69.0% of the probability distribution between 0.288-0.137 ka. A 20.3% probability is associated with the age range of 0.035 ka to present. Given this age, the upper 4 m of the sequence at site 1966 was deposited sometime in the last 300 years.

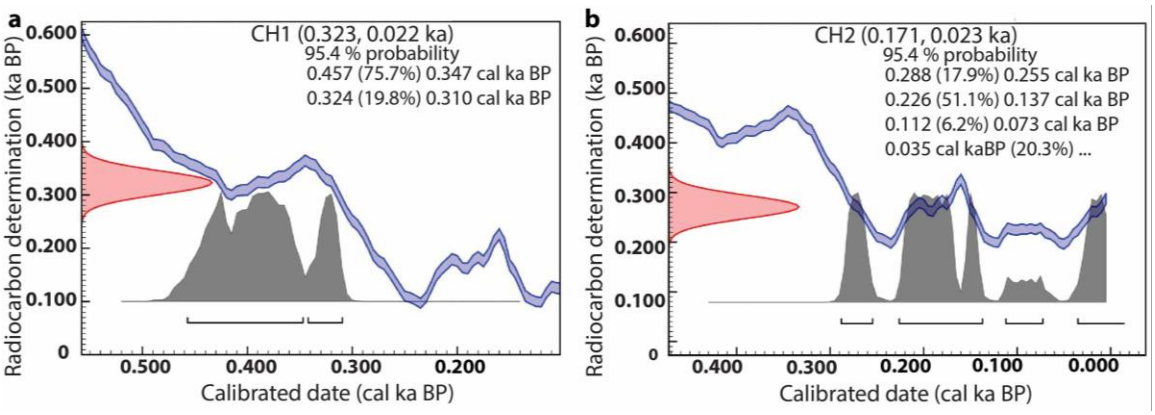

Figure 2.16. Calibration curves for ^{14}C samples CH1 and CH2. Ages were calibrated using OxCal v. 4.4.2 (Bronk Ramsey 2020) and the IntCal 20 calibration curve of Reimer *et al.* (2020). The red distributions denote radiocarbon ages with associated error, which are projected onto the blue calibration curves to produce the gray distributions which denote the probability distributions of the calibrated ages. Square brackets under gray curves denote each probability distribution of a range of ages denoted in text at the top right of each chart.

Optical dating

The SAR protocol was used to obtain equivalent doses for 180 – 250 µm KF sand grains from 13 samples (Table 2.4). Eleven samples were from fluvial sediments (unit 2c) and two were from aeolian caps (unit 4). Overdispersion values ranged from 14 ± 2 to 69 ± 7% and were divided along the conventional 20% mark to justify use of the MAM or the CAM for final equivalent dose calculations. MAM ages were calculated using 15% as the σb value as the best-bleached samples from the study area, namely the two aeolian samples 1951-TG-02 and 1956-TG-03 returned OD values of 14 ± 2 % and 15 ± 2%, respectively.

For all but the youngest optical dating samples (1966-TG-02, 1966-TG-03, and BBL19), aliquots were rejected when the recycling ratio and recuperation values were outside of conventional tolerances of 1.0 ± 0.1 and 5%, respectively (Murray and Wintle 2000; Wintle and Murray 2006). For the two samples, 1966-TG-02 and 1966-TG-03, that were younger than 1 ka, recuperation values up to 15% were allowed, as even a small amount of thermal transfer resulted in the signal from the zero-dose point being more than 5% of the relatively low natural signal. This has the potential to underestimate the D_e (Murray and Wintle 2000), which may underestimate ages. For the modern sample, BBL-19, no restrictions on recuperation values were used and they ranged from 8-39 %,

as expected for a modern sample; recycling ratio limits for this sample remained at within the 1.0 ± 0.1 tolerance.

Equivalent dose values ranged between 22.5 ± 2.4 Gy (1960-TG-01) and 0.36 ± 0.04 Gy (BBL-19). Dose rates were calculated for each sample using radionuclide concentrations, present burial depths, as-collected water content, altitude, and latitude as variables, each of which is summarized in Appendix C. Dose rates ranged between 2.43 ± 0.15 Gy/ka (1956-TG-02) and 3.30 ± 0.16 Gy/ka (1966-TG-03), with the highest dose rates associated with samples collected from site 1966. Fading rates ranged between 2.51 ± 0.64 %/decade (1961-TG-01) and 4.16 ± 0.26 %/decade (1958-TG-01). Optical ages are presented in Table 2.4 and ages are plotted by height above river level in Figure 2.17.

2.4. Discussion

2.4.1. Optical dating age reliability and terrace ages

Optical dating age reliability for the youngest samples was explored using analysis of residual signal. A residual signal is present if sand grains are not completely bleached before burial. Due to the turbidity of the present-day Fraser River, it is likely that the ancestral Fraser River was at least similarly turbid and therefore it is possible samples were not completely bleached prior to burial. To test the level of bleaching in modern-day Fraser River sand, a modern-day sample, BBL19, was collected from a depositional environment like that from which the older samples were collected. The minimum age from BBL19 is 0.155 ± 0.017 ka, which means that optical ages for other samples may be ~150 years younger than reported. For most samples, this is more than an order of magnitude smaller than their ages and lies within analytical uncertainties.

Site 1966 (T11) contains an apparent age reversal within the stratigraphic sequence (Figure 2.11, 2.14d). Sample 1966-TG-02 gave an age of 0.375 ± 0.040 ka and was collected 1.5 m lower than sample 1966-TG-03, which yielded an age of 0.411 ± 0.059 ka (Table 2.4). These ages are, however, within error of one another and thus this discrepancy does not pose a serious issue to the accuracy of the ages in this study.

Table 2.4. Optical ages from this study. Samples are arranged from highest above river level to nearest river level.

Sample	T#	Height above river (m)	n for dating	OD (%)	Model	D_e (Gy)	Dose Rate (Gy/ka)	Uncorrected Age (ka)	g value (%/decade)	n for fading	Corrected Age (ka)
1960-TG-01	T01	179	47/48	69 ± 7	MAM	22.5 ± 2.4	2.72 ± 0.15	8.27 ± 1.00	3.11 ± 0.29	4/12	11.3 ± 1.5
1954-TG-01	T02	161	45/48	66 ± 7	MAM	17.3 ± 1.9	2.58 ± 0.15	6.71 ± 0.85	3.24 ± 0.21	10/12	9.27 ± 1.17
1938-TG-01	T03	123	24/24	16 ± 2	CAM	16.7 ± 0.6	2.65 ± 0.15	6.28 ± 0.42	2.89 ± 0.19	10/12	8.32 ± 0.54
1958-TG-01	T04	102	22/24	19 ± 3	CAM	13.1 ± 0.5	2.57 ± 0.15	5.09 ± 0.37	4.16 ± 0.26	8/12	6.23 ± 0.48
1961-TG-01	T06	75	21/24	24 ± 4	MAM	10.6 ± 1.1	2.48 ± 0.15	4.29 ± 0.52	2.51 ± 0.64	7/12	5.42 ± 0.80
1956-TG-03*	T06	79	23/24	15 ± 2	CAM	6.86 ± 0.22	2.72 ± 0.15	2.53 ± 0.16	3.67 ± 0.41	11/12	3.65 ± 0.31
1956-TG-02	T06	73	24/24	27 ± 4	MAM	11.2 ± 1.0	2.43 ± 0.15	4.59 ± 0.50	3.53 ± 0.48	5/12	6.51 ± 0.87
1962-TG-02	T07	57	24/24	16 ± 2	CAM	9.06 ± 0.31	2.53 ± 0.15	3.58 ± 0.25	2.58 ± 0.35	11/12	4.54 ± 0.40
1951-TG-02*	T09	38	24/24	14 ± 2	CAM	5.70 ± 0.17	2.62 ± 0.15	2.18 ± 0.14	3.63 ± 0.26	8/12	3.11 ± 0.23
1951-TG-01	T09	37	24/24	19 ± 3	CAM	7.91 ± 0.30	2.41 ± 0.15	3.28 ± 0.24	2.77 ± 0.31	7/12	4.21 ± 0.32
1966-TG-03	T11	10	29/48	58 ± 8	MAM	1.07 ± 0.14	3.30 ± 0.16	0.324 ± 0.045	2.95 ± 0.43	7/12	0.411 ± 0.059
1966-TG-02	T11	9	37/48	63 ± 7	MAM	0.88 ± 0.10	2.93 ± 0.15	0.300 ± 0.031	2.79 ± 0.33	5/12	0.375 ± 0.040
BBL19	T12	2	22/48	41 ± 6	MAM	0.36 ± 0.04	2.88 ± 0.15	0.125 ± 0.015	2.87 ± 0.38+	12/24+	0.155 ± 0.017

n for dating/fading: number of aliquots used per number of aliquots tested; OD: Overdispersion; MAM: Minimum age model; CAM: Central Age Model; D_e: Equivalent dose; g value: fading rate

* Aeolian sample (unit 4); all others are fluvial samples (unit 2c)

+ Fading rate calculated using g-values from samples 1966-TG-02 and 1966-TG-03

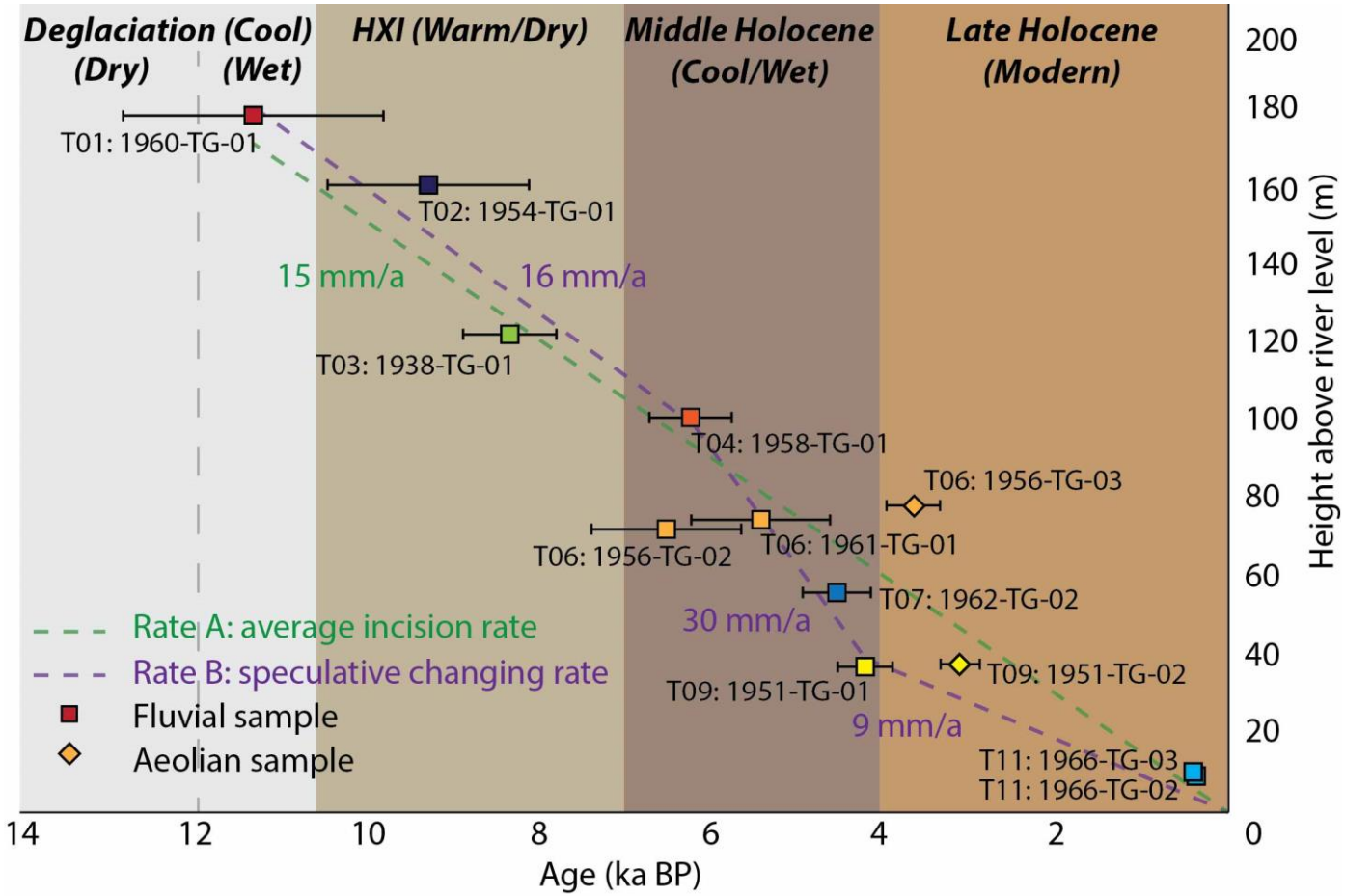

Figure 2.17. Optical ages vs height above river level. Error bars are 1 σ. Also shown are generalized climate intervals from Hebda (1995) with climate >10 ka from Mathewes (1985). Pre-modern climate descriptors are in relation to modern climate. The average incision rate over the postglacial period as well as a speculative changing rate discussed in Section 2.4.3 are provided. Three terrace-building stages, T01-T03, T04-T08, and T09-T12 roughly follow the climate data trends. Refer to section 2.4.3 for discussion. HXI: Holocene xerothermic interval.

Compared to the ^{14}C ages collected from adjacent strata (Figure 2.11, 2.14), the optical ages at site 1966 pose a discrepancy. Sample CH1, collected below optical dating sample 1966-TG-02 (0.375 ± 0.040 ka), has a 95.4% probability age range of 0.457-0.310 cal ka BP, with which there are no issues. Sample CH2, which was collected from a charcoal unit between optical dating samples 1966-TG-02 (0.375 ± 0.040 ka) and 1966-TG-03 (0.411 ± 0.059 ka), has a 95.4% probability age range of 0.288-0 cal ka BP, which is younger than the overlying optical age for 1966-TG-03. However, if the residual optical age of sample BBL19 (0.155 ± 0.017 ka) is subtracted from both optical ages, it brings the corrected optical age of 1966-TG-03 to 0.256 ± 0.076 ka, which is within error of sample CH2, thus explaining any apparent age reversals in the stratigraphy. However, additional modern samples from similar depositional environments should be analyzed to see if the residual age for sample BBL19 is representative.

One other apparent age reversal is found at site 1956 (T06) where sample 1956-TG-02 (6.51 ± 0.87 ka) has an apparently older optical age than 1961-TG-01 (T06, 5.42 ± 0.80 ka) and 1958-TG-01 (T04, 6.23 ± 0.48 ka) which were collected 2.4 m and 28.7 m higher than sample 1956-TG-02, respectively (Figure 2.11). Sample 1956-TG-02 has a higher OD value than either sample 1961-TG-01 or 1958-TG-01 (Table 2.4), which may indicate incomplete bleaching during deposition. This could increase the apparent age of this sample. However, all three of these ages falls within error of each other at less than 1σ, thus the apparent age reversal may not be real. Due to the lower OD values of 1961-TG-01 and 1958-TG-01, however, it is likely that their two ages, 5.42 ± 0.80 and 6.23 ± 0.48 ka, are more reliable for their respective elevations at terraces T04 and T06, respectively.

Aeolian cap ages provide minimum limiting ages of floodplain abandonment for sites 1956 (T06) and 1951 (T09). Aeolian sample 1956-TG-03 was collected from unit 4, 3 m above fluvial sample 1956-TG-02 and 60 cm below BRT (Figure 2.11). The optical age of 1956-TG-03 is 3.65 ± 0.31 ka and is 2.86 ka younger than the fluvial age of 6.51 ± 0.87 ka and is older than the age of BRT, which is ~2.4 ka (Clague *et al.* 1995). Aeolian sample 1951-TG-02 was collected from unit 4, 70 cm above fluvial sample 1951-TG-01 and 70 cm below BRT (Figure 2.11, 2.12c). The aeolian age of 3.11 ± 0.23 ka is 1.10 ka younger than the fluvial age of 4.21 ± 0.32 ka and is older than the BRT age of

~2.4 ka. That these optical ages are slightly older than overlying BRT provides further evidence that the optical dating protocol employed in this study is sufficient for the KF found in the study area. This means that the floodplain at site 1956, 70 m above present-day river level, must have been abandoned by 3.65 ± 0.31 ka ago. Additionally, the aeolian cap at site 1956 (Figure 2.11), indicates that paraglacial fan sedimentation at site 1956 ceased before 3.65 ± 0.31 ka. The floodplain at site 1951, 35 m above present-day river level (T09), must have been abandoned by 3.11 ± 0.23 ka ago.

This study demonstrates that the SAR protocol used here can be used successfully to date all but the youngest (<1 ka) Holocene river sand along Fraser River. However, by increasing the recuperation ratio threshold from 5 to 15%, age estimates for <1 ka samples can also be achieved. As seen by the modern sample BBL-19, further experimentation could be done to provide age estimates within the constraints of recycling ratio and recuperation value thresholds. Future optical dating studies on fluvial sediments in the area should include a hot wash step in the procedure to reduce recuperation (Murray and Wintle 2003; Murray and Wintle 2006). The MAM technique for samples with high (>20%) OD is effective in calculating reliable ages for fluvial samples that likely suffer from incomplete bleaching. Independent ages calculated using ^{14}C for site 1966 confirm that the optical dating ages from 1966-TG-02 and 1966-TG-03 are consistent within error, considering the residual signal as measured with a modern sample.

Optical dating ages from this study provide ages of fluvial activity at each terrace level which thus are maximum ages of fluvial incision and floodplain abandonment. This study therefore provides absolute ages of postglacial fluvial activity at different levels during the incision of Fraser River to its present-day position.

Site 1960: dating the outburst flood of glacial Lake Fraser

Unit 2a sediments found at site 1960 (Figure 2.13) are consistent with other sediments described by Clague *et al.* (2021) along the Fraser River further south of this study area that indicate a fast, short-lived, sediment-laden flow of water from the north that followed the course of the present-day Fraser River. For example, they are consistent with gravel deposited behind anchoring bedrock spurs like those described by Clague *et al.* (2021) but the landform at site 1960 is more likely a leeside bar as

described by Carling (2013) than an expansion bar like that described by Clague *et al.* (2021).

An optical age from sample 1960-TG-01 in T01 terrace, combined with the sedimentology of unit 2a at site 1960 suggests that this high energy leeside bar was likely deposited at 11.3 ± 1.5 ka. Two previous studies employing different dating methods have also inferred that a catastrophic flood event occurred at this time. Blais-Stevens *et al.* (2003) record clay beds within a sedimentary core taken from the Saanich Inlet on Vancouver Island that are indicative of a BC Interior-derived glacial lake outburst flood (GLOF). ^{14}C ages of shell material surrounding a distinct layer of GLOF sediment indicate that this event occurred after 12.3 ± 0.3 cal ka (GSC ^{14}C sample 1034E-6H1, 69, Blais-Stevens *et al.* 2003) and before 11.9 ± 0.5 cal ka (GSC ^{14}C sample 1033B-6H4, 110, Blais-Stevens *et al.* 2003). Clague *et al.* (2021) have also provided a stratigraphic and sedimentological case for the drainage of glacial Lake Fraser southward through Fraser Valley. ^{10}Be ages calculated from nine fluvially-transported boulders interpreted to have been associated with the GLOF event provide a median age of 11.1 ± 0.6 ka (Clague *et al.* 2021). The optical age from this study agrees with the ages proposed in both studies and provides support for the interpretation that the sediments at site 1960 were deposited by with the outburst flood of glacial Lake Fraser.

Site 1966: near-modern flood record

Unit 2c at site 1966 (T11, Figure 2.11, 2.14) provides insight into periodic flood events occurring in modern (<0.5 ka) times. Optical and ^{14}C ages agree that this site has been active within the last 0.5 ka. The sand rhythmites suggest similar flood events occurred periodically. The top of the terrace in which this exposure is located is 11-13 m above present-day river level. When the terrace height is compared to estimated maximum river levels and flood frequencies (Appendix A) it shows that the river will overtop this landform every 25-50 years, or 2-4 times per century. This is consistent with the ~11 flood sand sequences overlying optical dating and radiocarbon samples (Figure 2.11), which were deposited in the last 300 years. This also shows that at Big Bar, terraces at 10 m above Fraser River low water levels are still overtopped at a decadal scale.

Given the decadal overtopping of T11 terraces at site 1966, it must be considered that other, higher terraces were regularly overtopped by flood waters after

initial incision and thus not immediately abandoned. This is unlikely for several reasons. First, as Fraser River is now flowing on bedrock, flood stages must increase river depth rather than increase bed erosion which in turn causes river height at flood stage to be more extreme in the present day. This is further exacerbated by the narrow course that Fraser River now runs in, which likely causes drastically increased river heights during flood stage compared to the heights associated with floods when Fraser River ran in a wider floodplain even at T08-T10 phases. There are no substantial rhythmic facies of sand suggesting periodic overtopping of terrace surfaces in any higher terraces in the study area. For these reasons, it is likely that fluvial sand deposits capping terraces above T11 were indeed deposited close to the time of incision and abandonment of each associated floodplain, thus T01-T09 fluvial sand ages, although maxima, likely are reasonable estimates for the timing of floodplain incision and abandonment.

2.4.2. Terrace formation and timing of incision

Terrace formation

T01 terraces (180 ± 10 m above river level) are paired and only observed in the Watson Bar reach of the study area (Table 2.3, Figures 2.7, 2.8). T01 contains unit 2a sediments at site 1960 (Figure 2.11, 2.14), which record the GLOF of glacial Lake Fraser at 11.3 ± 1.5 ka ago. The paired nature of the T01 terrace stage is indicative of an event that spanned the valley, depositing sediment quickly before beginning an incision phase.

T02 (160 ± 5 m above present-day river level) terraces are unpaired and only definitively observed in the Big Bar reach (Table 2.3, Figures 2.7, 2.8). T03 (120 ± 5 m above present-day river level) terraces may be correlated downstream and cross-valley (Table 2.3), but correlations are uncertain due to thick fan sediments and poor access precluded dGPS surveying of potential Watson Bar T03 terraces. The unpaired nature of these terrace stages suggests that they may have been formed during a period of sustained incision wherein the main trunk of ancestral Fraser River switched back and forth between valley sides, abandoning its floodplain as it migrated laterally. Paraglacial fan sediment (unit 3, Figure 2.11) is present at both site 1954 and 1938, suggesting that paraglacial fan activity from tributary streams may have had some impact on lateral migration of Fraser River. The maximum ages for T02 and T03 terrace formation are 9.27 ± 1.17 ka and 8.32 ± 0.54 ka, respectively (Table 2.4).

T04 (100 ± 5 m above present-day river level) to T08 (45 ± 5 m above present-day river level) terraces are all found in the Watson Bar reach, while T04, T05, and T08 are also found in the Big Bar reach. They are commonly paired with the exceptions of terraces T05 and T07. Due to their prevalence around Watson Bar, they may have been influenced by increased sediment input from Ward Creek and Watson Bar creek, encouraging rapid aggradation. The interbedding of unit 3 paraglacial fan sediment with unit 2 fluvial sediments at sites 1958 and 1956 further show that paraglacial sedimentation influenced Fraser River activity on terraces T04 and T06. Additionally, the paraglacial fan issuing from Indian Creek on the east side of the valley would provide a sediment source for downstream aggradation, evidenced by the truncation of this fan above terrace T04 (Figure 2.5). The maximum ages for terrace abandonment for this group are 6.23 ± 0.48 ka (1958-TG-01) for T04, 5.42 ± 0.80 ka (1961-TG-01) and 6.51 ± 0.87 ka (1956-TG-02) for T06, although T06 abandonment must be more recent than T04 as T06 terraces are positioned lower than and adjacent to T04 terraces, so 5.42 ± 0.80 ka is a more likely T06 age, and 4.54 ± 0.32 ka (1962-TG-02) for T07.

Alternatively, the T04-T08 terraces at Watson Bar may be associated with downstream landslide activity. Church and Ryder (1986) suggest that some Fraser River floodplains around Lillooet were developed during landslide damming events at downstream Texas Creek, which was further corroborated by Ryder *et al*. (1990). At least 5 landslide scars were identified within ~20 km downstream of Watson Bar, including one at High Bar Canyon, ~5 km downstream of Watson Bar (Figure 2.10). The surface of the toe of the High Bar Canyon landslide is at ~100 m above present-day river level, consistent with the elevation of T04 terraces at Watson Bar. As landslides can quickly raise local base level for a short period of time, it is possible that this event and/or other landslides downstream of Watson Bar caused backwater effects at Watson Bar and significant floodplain aggradation before a breach in the dam would have resulted in rapid incision, creating paired terraces.

T09 (35 ± 2 m above present-day river level) to T12 (5 ± 2 m above present-day river level) terraces are mainly paired other than T12 terraces, the latter being unpaired and found in both the Big Bar and Watson Bar reaches of the study area. An exception is terrace T09, present only in the Big Bar reach of the study area and the highest terrace in this group. T09 was an active floodplain as recently as 4.21 ± 0.32 ka (1951-TG-01), with unit 2c fluvial sands directly overlain by unit 4 aeolian cap sediments that

provide an age of 3.11 ± 0.23 ka (1951-TG-02). This suggests that between ~3-4 ka ago, fluvial activity ceased on T09 terraces ~35 m above present-day river level and the river incised to another, lower floodplain. T09 terraces are paired upstream of the Big Bar Creek confluence and include an incised fan at the confluence as well. The T09 floodplain formation stage may have been caused by increased sedimentation from Big Bar Creek causing backwater effects, like that inferred for the Watson Bar T04-T08 terrace group.

Past placer mining activity limits observations of undisturbed fluvial sediments between T09 and T11 terraces so further explanation of terrace formation mechanisms for the lower terraces are not attempted. T11 is still active at 25-50 year flood stages, while T12 terrace may be active during most freshets.

Postglacial incision rate

Fluvial terrace ages are positively correlated with height above river level (Figure 2.17) and show a pattern of sustained incision through the postglacial period. After the glacial Lake Fraser GLOF along the Fraser River valley at 11.3 ± 1.5 ka, Fraser River incised through at least 180 m of glacial valley fill to reach its present-day elevation. The average incision rate over this time is 15 mm/a (Figure 2.17, rate A). This incision rate is comparable to those estimated downstream in Lillooet, which range from 9-26 mm/^{14}C a (Ryder and Church 1986). Ryder and Church (1986) suggested, however, that there may be different rates of incision at Lillooet throughout the postglacial period. We explore this possibility for Big Bar and Watson Bar below, hypothesizing that postglacial climate variation was a key driver for Fraser River incision.

2.4.3. Climate correlation

Terrace formation is a complex interplay between fluvial aggradation and incision involving shifts in stream power, base level, and sediment supply which are, in turn, driven by a variety of factors including climate, tectonics, isostasy, and autocyclicity. It is impossible to completely disentangle these factors from one another, but with the ages obtained in this study from optical dating and what is known about the climate and geomorphology of the area, speculations can be made about Fraser River terrace formation and its correlation to postglacial climate shifts. Below, we distill terrace formation to two variables (sediment input and stream power) and correlate terrace ages

to major shifts in paraglacial sedimentation (Church and Ryder 1972, Church and Slaymaker 1989) and postglacial climate that have been elucidated from the palaeoecological record for regions of BC upstream and adjacent to the study area.

Glacioisostatic adjustment likely did not play a changing role in early Fraser River terrace formation even though the interior landscape was depressed by up to 400 m during glaciation (Clague and James 2002). Clague and James (2002) state that glacioisostatic adjustment (uplift) in the BC interior occurred over a relatively short period of time (<2 ka) as the ice sheet was thinning. The timing of adjustment is corroborated by relative sea level curves along the BC coast (Shugar et al. 2014), that show most glacioisostatic adjustment occurring over ~1 ka around 14 – 13 ka ago. Ice had also significantly thinned in the BC interior by ~14 ka (Margold et al. 2014; Menounos et al. 2017), at which point glacioisostatic adjustment would have already been in progress. With the interior being nearly ice-free by ~12 ka (Clague 2017), glacioisostatic adjustment would have been complete at or near this time. So, for the purposes of this discussion we assume that glacioisostatically induced river slope changes are not a significant changing variable impacting terrace formation.

An average incision rate over the postglacial period may not fully explain the incision history of Fraser River, thus we speculate that there may have been changes in the incision rate over time which may be explained, at least partially, by postglacial climatic variation. The first incision phase captured by our data (T01-T03) starts at 11.3 ± 1.5 ka (T01, 180 ± 10 m above present-day river level) after the GLOF of glacial Lake Fraser and ends after 8.32 ± 0.54 ka (T03, 120 ± 5 m above present-day river level). This incision phase coincides with two climate phases that may have resulted in different energy and sediment supply conditions, yet a similar net incision rate of 16 mm/a (Figure 2.17, rate B). The following explanation is based on three optical dating ages and additional data is required to more confidently constrain and/or differentiate incision rates in this period. The T01-T03 phase begins during the late deglacial cool and wet period (~12.0 to 10.5 cal ka, Mathewes 1985; Figures 2.2, 2.17). High precipitation likely resulted in high flow power and a competent river able to erode and transport a substantial amount of sediment. However, the late deglacial was also a time of high paraglacial sedimentation from the uplands into the Fraser River valley (Church and Ryder 1972; Church and Slaymaker 1989). This increased sediment supply and load likely moderated fluvial incision rates through the late deglacial period.

The second part of the first incision phase coincides with the HXI (10.5 to 7.0 cal ka, Figure 2.17) (Mathewes 1985; Hebda 1995), a warm, dry climate. Less precipitation during the HXI likely reduced flow power, and although warm temperatures likely increased alpine glacier melt, this may have been insufficient to offset the reduction in precipitation. Greater forest fire activity (Mathewes 1985; Hallett et al. 2003) could have destabilized slopes and periodically increased sediment inputs, although no charcoal was found in T01-T03 floodplain sediments in the study area. A moderate incision rate (16 mm/a, Figure 2.17, rate B) throughout the HXI may be attributed to reduced flow power compared to the late deglacial period. Unpaired terraces T02 and potentially T03 (pairing is unverified for T03) are indicative of moderate but sustained lateral incision (Bull 1990) due to less valley constraint and a wider floodplain.

The second incision phase (T04-T08) begins at 6.23 ± 0.48 ka (T04, 100 ± 5 m above present-day river level) and ends after 4.54 ± 0.32 ka (T07, 55 ± 2 m above present-day river level), coinciding with the cooler than HXI and wetter than present day middle Holocene (7-4 ka, Hebda 1995; Figure 2.17). This phase, typified by prominent terraces at Watson Bar, is a time of relatively fast incision at a rate of 30 mm/a (Figure 2.17, rate B). This rate is similar to that reported for the last 1.2 ka for Fraser River at Lillooet (22-26 mm/a, Ryder and Church 1986). It is likely that during the middle Holocene, upland paraglacial sedimentation was dwindling (Church and Ryder 1972) and valley fill reworking or secondary remobilization was becoming dominant (Church and Slaymaker 1989), which would account for increased incision as upland paraglacial sediment inputs dwindled and flow power increased. However, local floodplain aggradation also occurred during this rapid incision phase due to local base level changes (cf. Ryder et al. 1990). Landslides downstream of Watson Bar, like those at High Bar Canyon (Figure 2.10), likely caused localized fluvial aggradation, which, when the landslide dam was breached, resulted in rapid fluvial incision and paired terrace (T04, T06, T07, T08, Figure 2.7) formation (Bull 1990). Prograding paraglacial fans may have similarly acted as temporary hydraulic dams. The wetter conditions and high incision rates during this phase created prime conditions for mass wasting events. This is corroborated by the increase in earthflow activity in BC during the middle Holocene (Bovis and Jones 1992).

The final incision phase (T09-T12) spans from 4.21 ± 0.32 ka (T09, 35 ± 2 m above present-day river level) to present. The incision rate during this phase is

apparently much lower at 9 mm/a (Figure 2.17, rate B) and coincides with Fraser River's incision to bedrock. Thus the 9 mm/a rate likely underestimates the incision rate prior to bedrock contact. T09 ages at site 1951 provide a bracketed terrace abandonment age between 4.21 ± 0.32 ka and 3.11 ± 0.23 ka. The occurrence of paired T09 terraces upstream of Big Bar Creek (Figure 2.5) could be explained by backwater effects resulting from increased sedimentation from Big Bar Creek at the end of the middle Holocene, causing temporary floodplain aggradation before the river quickly incised through valley fill sediments to reach bedrock; similar processes to those invoked for the middle Holocene. More ages during the last 4 ka (and thus the last 35 m of local Fraser River valley fill incision) are needed to constrain the timing of incision to bedrock and any changes in incision rates over this period. This could be conducted using TCN dating on bedrock surfaces near present-day river level or optical dating of fluvial sand on terraces 15-30 m above present-day river level if suitable sand can be found.

Optical ages at site 1966 show that the floodplain ~10 m above present-day river level was active around 0.411 ± 0.059 ka. Our CH2 ^{14}C sample has an age probability as low as zero (modern), suggesting that the T11 terraces may still be active at present, which is corroborated by flood frequency analysis showing that T11 terraces are inundated perhaps as regularly as 2-4 times per century (Appendix A). Site 1966 ages are also associated with charcoal layers, suggesting that fires may have contributed, and may still contribute, to slope destabilization and sediment supply during the last ~0.5 ka, a process reported to have also occurred during postglacial time in southwestern BC (Lian and Hickin 1996). Both flood (Curry et al. 2019) and fire frequency (Wotton et al. 2010) may be affected by further climate warming.

Incision rates discussed in this section are based on a small number of optical dating ages from terraces found over a short reach of Fraser River. Incision rates in the middle Holocene are best constrained by our optical ages. More ages are needed from around the study area to better constrain incision rates and bedrock contact in the late deglacial, HXI and late Holocene, and at other sites in the Fraser River drainage basin to better understand the role of regional and local drivers of terrace formation in this system.

2.5. Conclusions

1. This is the first study to provide absolute ages for post-glacial incision and terrace formation of Fraser River, a major river draining regions covered by the Cordilleran Ice Sheet. This information can be used as a starting point for more detailed studies of the character and timing of incision and terrace formation along the Fraser River and its tributaries.

2. Optical ages agree with age information from other studies on the timing of the catastrophic drainage of glacial Lake Fraser. With the results of this study, there are now three studies that agree on the timing of this event; one can now be more confident that the flood occurred around 11.3 ka ago, but the identification and optical dating of more gLF outburst flood deposits beyond the study area would help reinforce it.

3. The average postglacial incision rate of Fraser River at Big Bar and Watson Bar reaches, from 440 m asl to its present position on bedrock at Watson Bar of 280 m asl is 15 mm/a. It is likely, however, that the incision rate varied through postglacial time, and the data presented here suggest that this was the case. This study, however, can only speculate on what this variation may have been, given the sparseness of data points (optical ages). Additional dating studies could better resolve variations in incision rate, especially in the early Holocene and in the late Holocene when Fraser River incised to bedrock.

4. Climate phases that have been recognized from previous palaeoecology studies could explain apparent changes in the timing of fluvial incision rates and terrace formation phases. For example, during the middle Holocene (T04-T08 phase;~8-4 ka), a relatively high (30 mm/a) average incision rate occurred due to increased flow power during this wetter climatic period and the transition from high rates of upland paraglacial sedimentation to the reworking of valley fill during secondary remobilization of paraglacial sediments. Landslide dams and paraglacial fan sedimentation caused localized floodplain aggradation and resulted in paired terrace formation around Watson Bar. . Fraser River incised to bedrock sometime in the last 4

ka and presently flows on bedrock and overtops terraces ~10 m above river level 2-4 times per century.

Chapter 3.

Concluding remarks

The aim of this thesis was to (i) provide limiting ages for postglacial terrace formation in Fraser River valley between Big Bar and Watson Bar (Figure 1.1), (ii) determine the rate of incision of Fraser River through its glacial valley fill, and (iii) look for correlation between the timing of terrace formation and existing information on the paraglacial cycle, postglacial climate change and changes in local base level. Each objective and its relative success are discussed below, ending with suggestions for future work.

3.1. Dating of Fraser River terraces

The objective of this thesis was to provide limiting ages for Fraser River terrace formation. Thirteen optical ages were determined from ten different sites, providing a record of Fraser River activity spanning the last ~11.3 ka. Fluvial sand resting on terraces (unit 2c) was dated to provide maximum ages of fluvial incision and terrace abandonment. Unit 4 aeolian caps on terraces at two sites (1956 and 1951) were dated to bracket the timing of terrace abandonment. Further, fluvial sediments at two sites (1960 and 1966) and aeolian sediments at two sites (1951 and 1956) had independent age controls to provide support for the accuracy of the optical ages. Site 1960 provides an optical dating age of 11.3 ± 1.5 ka to support radiocarbon and cosmogenic ages from other locations that date the GLOF of glacial Lake Fraser during the early postglacial period. Site 1966 uses optical dating and radiocarbon ages to constrain the timing of recent (<0.5 ka) Fraser River flood events on a terrace ~10 m above present-day river level.

3.2. Postglacial Fraser River incision rates

Using optical dating ages, postglacial Fraser River incision rates were explored. An average incision rate of 15.0 mm/a was calculated, which spans the study's timeframe of 11.3 ± 1.5 ka to present. During this time, Fraser River incised through

~180 m of glacial and paraglacial valley fill to reach bedrock. This rate fits well with other incision rates that were derived at Lillooet (Ryder and Church 1986).

3.3. Correlating incision rates to postglacial climate

Stepping past an average incision rate, a speculative model of varied incision rates was introduced to explain how Fraser River terrace formation may have been influenced by postglacial climate variation interacting with the paraglacial cycle. During the T01-T03 stage, roughly associated with the late deglacial period and HXI (12 – 7 ka), climate changed from moist between 12.0 and 10.5 ka, then dried through the HXI from 10.5 to 7.0 ka, increasing and decreasing Fraser River discharge and thus stream power, respectively. Upland paraglacial sedimentation was likely high throughout of the T01-T03 stage, countering and moderating increased stream power from high precipitation in the late deglacial period and increased glacial melt during the HXI. The transition to valley fill reworking and secondary mobilization of paraglacial sediment (Church and Slaymaker 1989) likely occurred during the middle Holocene, 7 – 4 ka ago, which is the best-constrained period in this study. Additionally, the cool and wet mid-Holocene likely promoted both increased sedimentation from paraglacial fans and high rates of incision from increased discharge, while valley-filling landslides may have occurred downstream of Watson Bar, resulting in floodplain aggradation and rapid incision. Rapid incision likely continued into the late Holocene, 4 ka to present, until Fraser River incised to bedrock, although there is a paucity of ages from this study to constrain when this occurred. The late Holocene marks a time of apparent slow incision which is likely due to Fraser River now running on bedrock through Big Bar and Watson Bar, inhibiting high incision rates.

3.4. Suggestions for future work

This work forms the basis for a more detailed dating campaign in the study area. Future studies should attempt to find additional material suitable for dating at similar terrace elevations to provide a more robust dataset for calculating incision rates and for constraining varying rates of incision that were speculated on in this study. Furthermore, this study should be extended to other regions along Fraser River and its tributaries to assess the degree of correlation between terrace ages from this area and those in other

areas. This would help our understanding of how major rivers in BC adjusted following the demise of the Cordilleran Ice Sheet.

Future optical dating work could explore the use of smaller aliquots and even single grains in order to utilize more robust statistical models (i.e., finite mixture model, etc.) to assess the level of bleaching that had occurred in ancient Fraser River sediments, and to look for age populations. Additionally, very young (<1 ka) samples would likely benefit from a hot wash being incorporated into the optical dating protocol to reduce recuperation values. Further work on dating the youngest terraces, such as those that are periodically overtopped during extreme floods (e.g., site 1966 in this study), along Fraser River and its tributaries would gain insight into how sediment is stored and moved out of the system and perhaps extend flood frequency graphs beyond historic data. Finally, this study did not constrain the timing of Fraser River reaching bedrock in the study area, and thus future dating studies could incorporate TCN on bedrock near valley bottom to elucidate this age and thus discern when valley fill was fully incised.

References

Allmendinger, R.W., Cardozo, N., and Fisher, D.M. 2011. Structural Geology Algorithms: Vectors and Tensors. In 1st edition. Cambridge University Press, Cambridge.

Auclair, M., Lamothe, M., and Huot, S. 2003. Measurement of anomalous fading for feldspar IRSL using SAR. Radiation Measurements, **37**: 487–492. doi:10.1016/S1350-4487(03)00018-0.

Ballantyne, C.K. 2002. Paraglacial geomorphology. Quaternary Science Reviews, **21**: 1935–2017.

Berger, G.W. 1988. Dating Quaternary events by luminescence. In Quaternary Sediments. Geological Society of America Special Paper 227, Boulder, Colorado. pp. 13–50.

Blais-Stevens, A., Clague, J.J., Mathewes, R.W., Hebda, R.J., and Bornhold, B.D. 2003. Record of large, Late Pleistocene outburst floods preserved in Saanich Inlet sediments, Vancouver Island, Canada. Quaternary Science Reviews, **22**: 2327–2334. doi:10.1016/S0277-3791(03)00212-9.

Blong, R.J., and Gillespie, R. 1978. Fluvially transported charcoal gives erroneous 14C ages for recent deposits. Nature, **271**: 739–741. doi:10.1038/271739a0.

Blum, M.D., and Törnqvist, T.E. 2000. Fluvial responses to climate and sea-level change: A review and look forward. Sedimentology, **47**: 2–48. doi:10.1046/j.1365-3091.2000.00008.x.

Bovis, M.J., and Jones, P. 1992. Holocene history of earthflow mass movements in south-central British Columbia: the influence of hydroclimatic changes. Canadian Journal of Earth Sciences, **29**: 1746–1755. doi:10.1139/e92-137.

Brennan, B.J. 2003. Beta doses to spherical grains. Radiation Measurements, **37**: 299–303. doi:10.1016/S1350-4487(03)00011-8.

Brennand, T.A., Lian, O.B., and Perkins, A.J. 2014. The life and times of the Cordilleran Ice Sheet around the southern Fraser Plateau, British Columbia. In GSA Field Guide 38: Trials and Tribulations of Life on an Active Subduction Zone: Field Trips in and around Vancouver, Canada. Geological Society of America. pp. 101–124. doi:10.1130/2014.0038(06).

Bronk Ramsey, C. 2009. Bayesian analysis of radiocarbon dates. Radiocarbon, **51**: 337–360. doi:10.1017/S0033822200033865.

Bronk Ramsey, C. 2020. OxCal v. 4.4.2. Oxford, UK.

Bull, W.B. 1990. Stream-terrace genesis: implications for soil development. Geomorphology, **3**: 351–367. doi:10.1016/0169-555X(90)90011-E.

Bulur, E. 1996. An alternative technique for optically stimulated luminescence (OSL) experiment. Radiation Measurements, **26**: 701–709. doi:10.1016/S1350-4487(97)82884-3.

Cardozo, N., and Allmendinger, R.W. 2013. Spherical projections with OSXStereonet. Computers & Geosciences, **51**: 193–205. doi:10.1016/j.cageo.2012.07.021.

Carling, P.A. 2013. Freshwater megaflood sedimentation: What can we learn about generic processes? Earth-Science Reviews, **125**: 87–113. doi:10.1016/j.earscirev.2013.06.002.

Church, M., and Ryder, J.M. 1972. Paraglacial sedimentation: A consideration of fluvial processes conditioned by glaciation. Geological Society of America Bulletin, **83**: 3059–3072.

Church, M., and Slaymaker, O. 1989. Disequilibrium of Holocene sediment yield in glaciated British Columbia. Nature, **337**: 452–454. doi:10.1038/337452a0.

Clague, J.J. 1981. Late Quaternary geology and geochronology of British Columbia: Part 2: summary and discussion of radiocarbon-dated Quaternary history. Geological Survey of Canada, Ottawa, ON.

Clague, J.J. 2017. Deglaciation of the Cordillera of Western Canada at the end of the Pleistocene. Cuadernos de Investigación Geográfica, **43**: 449–466. doi:10.18172/cig.3232.

Clague, J.J., Evans, S.G., Rampton, V.N., and Woodsworth, G.J. 1995. Improved age estimates for the White River and Bridge River tephras, western Canada. Canadian Journal of Earth Sciences, **32**: 1172–1179. doi:10.1139/e95-096.

Clague, J.J., and James, T.S. 2002. History and isostatic effects of the last ice sheet in southern British Columbia. Quaternary Science Reviews, **21**: 71–87. doi:10.1016/S0277-3791(01)00070-1.

Clague, J.J., Luternauer, J.L., and Hebda, R.J. 1983. Sedimentary environments and postglacial history of the Fraser Delta and lower Fraser Valley, British Columbia. Canadian Journal of Earth Sciences, **20**: 1314–1326. doi:10.1139/e83-116.

Clague, J.J., Roberts, N.J., Miller, B., Menounos, B., and Goehring, B. 2021. A huge flood in the Fraser River valley, British Columbia, near the Pleistocene Termination. Geomorphology, **374**: 1–17. doi:10.1016/j.geomorph.2020.107473.

Colarossi, D., Duller, G.A.T., Roberts, H.M., Tooth, S., and Lyons, R. 2015. Comparison of paired quartz OSL and feldspar post-IR IRSL dose distributions in poorly bleached fluvial sediments from South Africa. Quaternary Geochronology, **30**: 233–238. doi:10.1016/j.quageo.2015.02.015.

Crann, C.A., Murseli, S., St-Jean, G., Zhao, X., Clark, I.D., and Kieser, W.E. 2017. First status report on radiocarbon sample preparation techniques at the A.E. Lalonde AMS Laboratory (Ottawa, Canada). Radiocarbon, **59**: 695–704. doi:10.1017/RDC.2016.55.

Cunningham, A., Wallinga, J., and Minderhoud, P. 2011. Expectations of scatter in equivalent-dose distributions when using multi-grain aliquots for OSL dating. Geochronometria, **38**: 424–431. doi:10.2478/s13386-011-0048-z.

Curry, C.L., Islam, S.U., Zwiers, F.W., and Déry, S.J. 2019. Atmospheric rivers increase future flood risk in Western Canada's largest Pacific river. Geophysical Research Letters, **46**: 1651–1661. doi:10.1029/2018GL080720.

Dietze, M., Kreutzer, S., Burow, C., Fuchs, M.C., Fischer, M., and Schmidt, C. 2016. The abanico plot: Visualising chronometric data with individual standard errors. Quaternary Geochronology, **31**: 12–18. doi:10.1016/j.quageo.2015.09.003.

Durcan, J.A., King, G.E., and Duller, G.A.T. 2015. DRAC: Dose Rate and Age Calculator for trapped charge dating. Quaternary Geochronology, **28**: 54–61. doi:10.1016/j.quageo.2015.03.012.

Egan, J., Staff, R., and Blackford, J. 2015. A high-precision age estimate of the Holocene Plinian eruption of Mount Mazama, Oregon, USA. The Holocene, **25**: 1054–1067.

Evans, D.J.A., and Benn, D.I. 2021. A Practical Guide to the Study of Glacial Sediments, Second Edition. Quaternary Research Association, London.

Eyles, N., and Clague, J.J. 2007. Glaciolacustrine sedimentation during advance and retreat of the Cordilleran ice sheet in central British Colombia. Géographie physique et Quaternaire, **45**: 317–331. doi:10.7202/032878ar.

Faulkner, D.J., Larson, P.H., Jol, H.M., Running, G.L., Loope, H.M., and Goble, R.J. 2016. Autogenic incision and terrace formation resulting from abrupt late-glacial base-level fall, lower Chippewa River, Wisconsin, USA. Geomorphology, **266**: 75–95. doi:10.1016/j.geomorph.2016.04.016.

Fulton, R.J., and Walcott, R.I. 1975. Lithospheric flexure as shown by deformation of glacial lake shorelines in southern British Columbia. In Quantitative Studies in the Geological Sciences, Memoir 142. Geological Society of America. pp. 163–173.

Galbraith, R.F., and Roberts, R.G. 2012. Statistical aspects of equivalent dose and error calculation and display in OSL dating: An overview and some recommendations. Quaternary Geochronology, **11**: 1–27. doi:10.1016/j.quageo.2012.04.020.

Galbraith, R.F., Roberts, R.G., Laslett, G.M., Yoshida, H., and Olley, J.M. 1999. Optical dating of single and multiple grains of quartz from Jinmium rock shelter, Northern Australia: Part I, experimental design and statistical models. Archaeometry, **41**: 339–364. doi:10.1111/j.1475-4754.1999.tb00987.x.

Galbraith, R.F., Roberts, R.G., and Yoshida, H. 2005. Error variation in OSL palaeodose estimates from single aliquots of quartz: A factorial experiment. Radiation Measurements, **39**: 289–307. doi:10.1016/j.radmeas.2004.03.023.

Province of British Columbia. 2021. Big Bar Landslide Incident. Province of British Columbia. Available from https://www2.gov.bc.ca/gov/content/environment/plants-animals-ecosystems/fish/aquatic-habitat-management/fish-passage/big-bar-landslide-incident [accessed 30 July 2021].

Guérin, G., Mercier, N., and Adamiec, G. 2011. Dose-rate conversion factors: update. Ancient TL, **29**: 5–8.

Hallett, D.J., Lepofsky, D.S., Mathewes, R.W., and Lertzman, K.P. 2003. 11 000 years of fire history and climate in the mountain hemlock rain forests of southwestern British Columbia based on sedimentary charcoal. Canadian Journal of Forest Research, **33**: 292–312. doi:10.1139/x02-177.

Hebda, R.J. 1995. British Columbia vegetation and climate history with focus on 6 ka BP. Géographie physique et Quaternaire, **49**: 55–79. doi:10.7202/033030ar.

Huntley, D.H., and Broster, B.E. 1994. Glacial Lake Camelsfoot: a Late Wisconsinan advance stage proglacial lake in the Fraser River valley, Gang Ranch area, British Columbia. Canadian Journal of Earth Sciences, **31**: 798–807. doi:10.1139/e94-073.

Huntley, D.J., and Baril, M.R. 1997. The K content of the K-feldspars being measured in optical dating or in thermoluminescence dating. Ancient TL, **15**: 11–13.

Huntley, D.J., and Hancock, R.G.V. 2001. The Rb contents of the K-feldspar grains being measured in optical dating. Ancient TL, **19**: 43–46.

Huntley, D.J., and Lamothe, M. 2001. Ubiquity of anomalous fading in K-feldspars and the measurement and correction for it in optical dating. Canadian Journal of Earth Sciences, **38**: 1093-1106.

Iseya, F., and Ikeda, H. 1987. Pulsations in bedload transport rates induced by a longitudinal sediment sorting: A flume study using sand and gravel mixtures. Geografiska Annaler, **69 A**: 15–27.

Jain, M., Buylaert, J.P., Thomsen, K.J., and Murray, A.S. 2015. Further investigations on 'non-fading' in K-Feldspar. Quaternary International, **362**: 3–7. doi:10.1016/j.quaint.2014.11.018.

Johnsen, T.F., and Brennand, T.A. 2004. Late-glacial lakes in the Thompson Basin, British Columbia: paleogeography and evolution. **41**: 1367–1383.

Kovanen, D., and Slaymaker, O. 2015. The paraglacial geomorphology of the Fraser Lowland, southwest British Columbia and northwest Washington. Geomorphology, **232**: 78–93. doi:10.1016/j.geomorph.2014.12.021.

Kreutzer, S. 2020. calc_FadingCorr(): Apply a fading correction according to Huntley & Lamothe (2001) for a given g-value and a given tc. Available from https://CRAN.R-project.org/package=Luminescence.

Kreutzer, S., Burow, C., Dietze, M., Fuchs, M., Schmidt, C., Fischer, M., and Friedrich, J. 2020. Luminescence: Comprehensive Luminescence Dating Data Analysis. R package version 0.9.7. Available from https://CRAN.R-project.org/package=Luminescence.

Lian, O.B., and Clague, J.J. 2009. Recent developments in the understanding of the timing of postglacial fluvial incision, Fraser River valley, southcentral British Columbia. In Canadian Quaternary Association Meeting Program and Abstracts. p. 122.

Lian, O.B., and Hickin, E.J. 1996. Early postglacial sedimentation of lower Seymour Valley, southwestern British Columbia. Géographie physique et Quaternaire, **50**: 95–102. doi:10.7202/033078ar.

Lian, O.B., and Hicock, S.R. 2001. Lithostratigraphy and limiting optical ages of the Pleistocene fill in Fraser River valley near Clinton, south-central British Columbia. Canadian Journal of Earth Sciences, **38**: 839–850.

Lian, O.B., Hu, J., Huntley, D.J., and Hicock, S.R. 1995. Optical dating studies of Quaternary organic-rich sediments from southwestern British Columbia and northwestern Washington State. Canadian Journal of Earth Sciences, **32**: 1194–1207. doi:10.1139/e95-098.

Lian, O.B., and Huntley, D.J. 1999. Optical dating studies of postglacial aeolian deposits from the south-central interior of British Columbia, Canada. Quaternary Science Reviews, **18**: 1453–1466. doi:10.1016/S0277-3791(98)00085-7.

Lian, O.B., and Roberts, R.G. 2006. Dating the Quaternary: progress in luminescence dating of sediments. Quaternary Science Reviews, **25**: 2449–2468. doi:10.1016/j.quascirev.2005.11.013.

Lindholm, R. 1987. A Practical Approach to Sedimentology. Allen & Unwin, Winchester, MA.

Margold, M., Stroeven, A.P., Clague, J.J., and Heyman, J. 2014. Timing of terminal Pleistocene deglaciation at high elevations in southern and central British Columbia constrained by 10Be exposure dating. Quaternary Science Reviews, **99**: 193–202. doi:10.1016/j.quascirev.2014.06.027.

Mathewes, R.W. 1985. Paleobotanical evidence for climatic change in southern British Columbia during late-glacial and Holocene time. Syllogeus, **55**: 397–422.

Mathewes, R.W., and Heusser, L.E. 1981. A 12 000 year palynological record of temperature and precipitation trends in southwestern British Columbia. Canadian Journal of Botany, **59**: 707–710. doi:10.1139/b81-100.

Mathewes, R.W., and King, M. 1989. Holocene vegetation, climate, and lake-level changes in the Interior Douglas-fir Biogeoclimatic Zone, British Columbia. Canadian Journal of Earth Sciences, **26**: 1811–1825. doi:10.1139/e89-154.

Mathews, W.H., and Rouse, G.E. 1984. The Gang Ranch – Big Bar area, south-central British Columbia: stratigraphy, geochronology, and palynology of the Tertiary beds and their relationship to the Fraser Fault. Canadian Journal of Earth Sciences, **21**: 1132–1144. doi:10.1139/e84-118.

Menounos, B., Osborn, G., Clague, J.J., and Luckman, B.H. 2009. Latest Pleistocene and Holocene glacier fluctuations in western Canada. Quaternary Science Reviews, **28**: 2049–2074. doi:10.1016/j.quascirev.2008.10.018.

Menounos, B., Goehring, B.M., Osborn, G., Margold, M., Ward, B., Bond, J., Clarke, G.K.C., Clague, J.J., Lakeman, T., Koch, J., Caffee, M.W., Gosse, J., Stroeven, A.P., Seguinot, J., and Heyman, J. 2017. Cordilleran Ice Sheet mass loss preceded climate reversals near the Pleistocene Termination. Science, **358**: 781–784. doi:10.1126/science.aan3001.

Murray, A.S., and Wintle, A.G. 2000. Luminescence dating of quartz using an improved single-aliquot regenerative-dose protocol. Radiation Measurements, **32**: 57–73. doi:10.1016/S1350-4487(99)00253-X.

Murray, A.S., and Wintle, A.G. 2003. The single aliquot regenerative dose protocol: potential for improvements in reliability. Radiation Measurements, **37**: 377–381. doi:10.1016/S1350-4487(03)00053-2.

Murseli, S., Middlestead, P., St-Jean, G., Zhao, X., Jean, C., Crann, C.A., Kieser, W.E., and Clark, I.D. 2019. The preparation of water (DIC, DOC) and gas (CO2, CH4) samples for radiocarbon analysis at AEL-AMS, Ottawa, Canada. Radiocarbon, **61**: 1563–1571. doi:10.1017/RDC.2019.14.

Muto, T., and Steel, R.J. 2004. Autogenic response of fluvial deltas to steady sea-level fall: Implications from flume-tank experiments. Geology, **32**: 401–404. doi:10.1130/G20269.1.

Neudorf, C.M., Lian, O.B., Walker, I.J., Shugar, D.H., Eamer, J.B.R., and Griffin, L.C.M. 2015. Toward a luminescence chronology for coastal dune and beach deposits on Calvert Island, British Columbia central coast, Canada. Quaternary Geochronology, **30**: 275–281. doi:10.1016/j.quageo.2014.12.004.

Perkins, A.J., and Brennand, T.A. 2015. Refining the pattern and style of Cordilleran Ice Sheet retreat: palaeogeography, evolution and implications of lateglacial ice-dammed lake systems on the southern Fraser Plateau, British Columbia, Canada: Cordilleran Ice Sheet retreat, British Columbia, Canada. Boreas, **44**: 319–342. doi:10.1111/bor.12100.

Prescott, J.R., and Hutton, J.T. 1994. Cosmic ray contributions to dose rates for luminescence and ESR dating: Large depths and long-term time variations. Radiation Measurements, **23**: 497–500.

Reimer, P.J., Austin, W.E.N., Bard, E., Bayliss, A., Blackwell, P.G., Bronk Ramsey, C., Butzin, M., Cheng, H., Edwards, R.L., Friedrich, M., Grootes, P.M., Guilderson, T.P., Hajdas, I., Heaton, T.J., Hogg, A.G., Hughen, K.A., Kromer, B., Manning, S.W., Muscheler, R., Palmer, J.G., Pearson, C., van der Plicht, J., Reimer, R.W., Richards, D.A., Scott, E.M., Southon, J.R., Turney, C.S.M., Wacker, L., Adolphi, F., Büntgen, U., Capano, M., Fahrni, S.M., Fogtmann-Schulz, A., Friedrich, R., Köhler, P., Kudsk, S., Miyake, F., Olsen, J., Reinig, F., Sakamoto, M., Sookdeo, A., and Talamo, S. 2020. The IntCal20 Northern Hemisphere Radiocarbon Age Calibration Curve (0–55 cal kBP). Radiocarbon, **62**: 725–757. doi:10.1017/RDC.2020.41.

Ryder, J.M. 1971. The stratigraphy and morphology of para-glacial alluvial fans in south-central British Columbia. Canadian Journal of Earth Sciences, **8**: 279–298. doi:10.1139/e71-027.

Ryder, J.M., Bovis, M.J., and Church, M. 1990. Rock avalanches at Texas Creek, British Columbia. Canadian Journal of Earth Sciences, **27**: 1316–1329. doi:10.1139/e90-142.

Ryder, J.M., and Church, M. 1986. The Lillooet terraces of Fraser River: a palaeoenvironmental enquiry. Canadian Journal of Earth Sciences, **23**: 869–884. doi:10.1139/e86-089.

Shugar, D.H., Walker, I.J., Lian, O.B., Eamer, J.B.R., Neudorf, C., McLaren, D., and Fedje, D. 2014. Post-glacial sea-level change along the Pacific coast of North America. Quaternary Science Reviews, **97**: 170–192. doi:10.1016/j.quascirev.2014.05.022.

Singarayer, J.S., and Bailey, R.M. 2003. Further investigations of the quartz optically stimulated luminescence components using linear modulation. Radiation Measurements, **37**: 451–458. doi:10.1016/S1350-4487(03)00062-3.

Thomsen, K.J., Murray, A.S., Jain, M., and Bøtter-Jensen, L. 2008. Laboratory fading rates of various luminescence signals from feldspar-rich sediment extracts. Radiation Measurements, **43**: 1474–1486. doi:10.1016/j.radmeas.2008.06.002.

Wallinga, J., Murray, A., and Wintle, A. 2000. The single-aliquot regenerative-dose (SAR) protocol applied to coarse-grain feldspar. Radiation Measurements, **32**: 529–533. doi:10.1016/S1350-4487(00)00091-3.

Wintle, A.G. 1973. Anomalous fading of thermo-luminescence in mineral samples. Nature, **245**: 143–144. doi:10.1038/245143a0.

Wintle, A.G. 1997. Luminescence dating: laboratory procedures and protocols. Radiation Measurements, **27**: 769–817. doi:10.1016/S1350-4487(97)00220-5.

Wintle, A.G., and Murray, A.S. 2006. A review of quartz optically stimulated luminescence characteristics and their relevance in single-aliquot regeneration dating protocols. Radiation Measurements, **41**: 369–391. doi:10.1016/j.radmeas.2005.11.001.

Wotton, B.M., Nock, C.A., and Flannigan, M.D. 2010. Forest fire occurrence and climate change in Canada. International Journal of Wildland Fire, **19**: 253–271. doi:10.1071/WF09002.

Zhang, Z., Stadnyk, T.A., and Burn, D.H. 2020. Identification of a preferred statistical distribution for at-site flood frequency analysis in Canada. Canadian Water Resources Journal / Revue canadienne des ressources hydriques, **45**: 43–58. doi:10.1080/07011784.2019.1691942.

Appendix A.

River level and flood frequency analysis

Data used for river level and flood frequency was downloaded from the Water Survey of Canada for Fraser River at Big Bar (station 08MD013) and Fraser River at Texas Creek (station 08MF040). Gauge station data was used to determine peak annual flows and flood frequencies for Fraser River at Big Bar. Big Bar daily discharge data was available from 1935 - 1973 and July 2019 - May 2021, while Texas Creek discharge data was available from 1951 – May 2021. Big Bar discharge data were derived from Texas Creek discharge data for the missing years between 1973 and 2019 using equations derived from linear correlation of the overlapping date ranges (Appendix A.1). When this was checked against the Big Bar data from 1951 - 1972, peak flows appeared to be underestimated in the derived data (Appendix A.2). Peak annual flows were thus extracted from each dataset and Big Bar peak annual flow values were derived from Texas Creek peak annual flows for the missing years (Appendix A.3), which provide a better fit though some overestimation and underestimation persists. Flood frequencies were calculated using the date range from 1935 - 2020, with peak annual flows derived from Texas Creek discharge data between 1973 and 2019. Both log Pearson III (LP3) and Generalized Extreme Values (GEV) probability distributions are commonly used in flood frequency analysis (Zhang *et al.* 2020), so both distributions are presented (Appendix A.4, A.5), though GEV is the preferred distribution to use in Canada (Zhang *et al.* 2020). Finally, maximum annual river stage was estimated using the historical and derived discharge data since 1935 using correlation between discharge and stage at Big Bar from the period when both measures were available, from July 2019 – May 2021 (Appendix A.6).

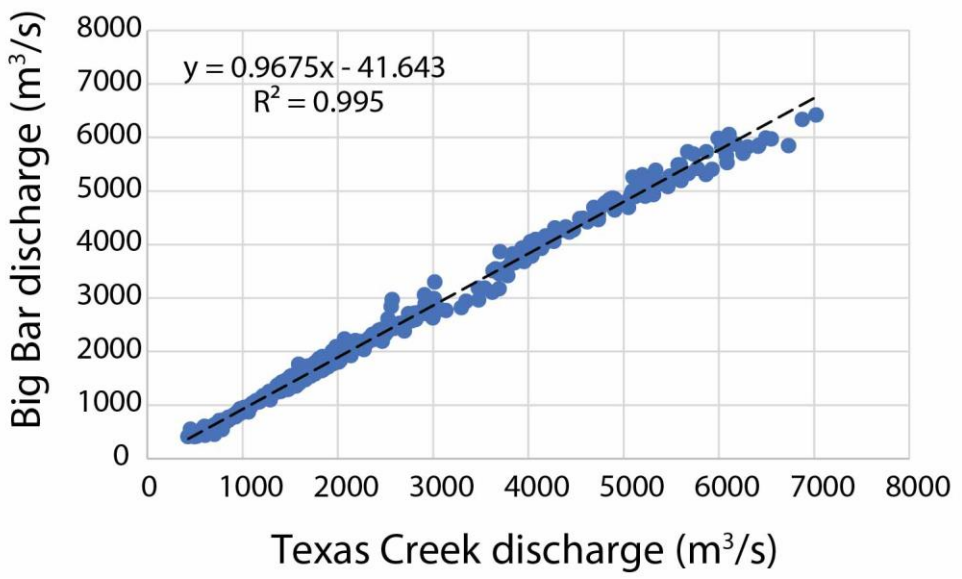

Figure A.1 Correlation between Fraser River discharge values at Big Bar and Texas Creek stations. Data taken from 1951-1972 and 2019-2020 when both stations had data available. Correlation equation was used to estimate discharge for missing flow data at Big Bar from 1972-2019 (Appendix A.2).

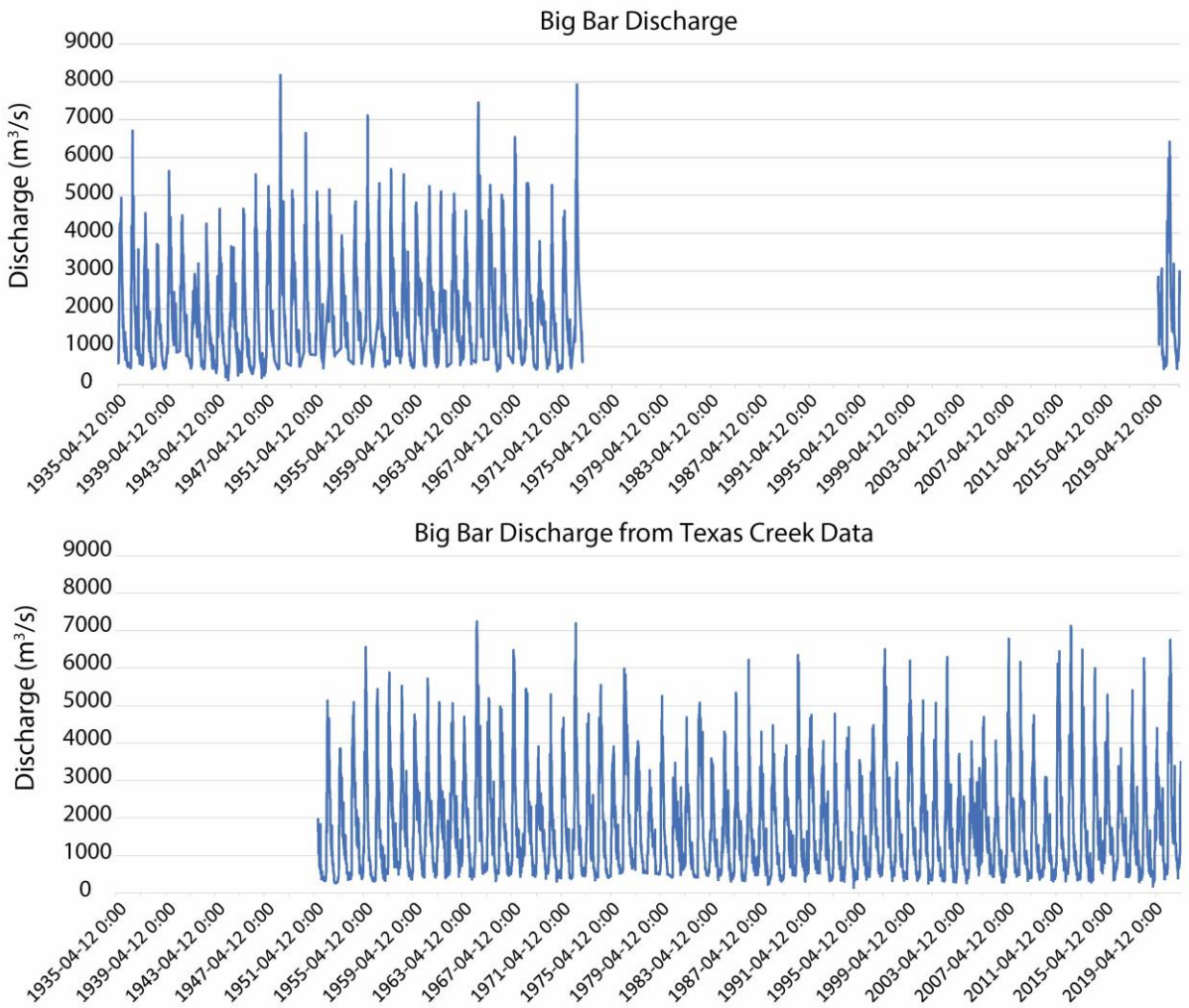

Figure A.2. Big Bar historical discharge (top) versus derived Big Bar discharge from Texas Creek data (bottom). Correlation equation from Appendix A.1 consistently underestimates peak flow values 1951-1972.

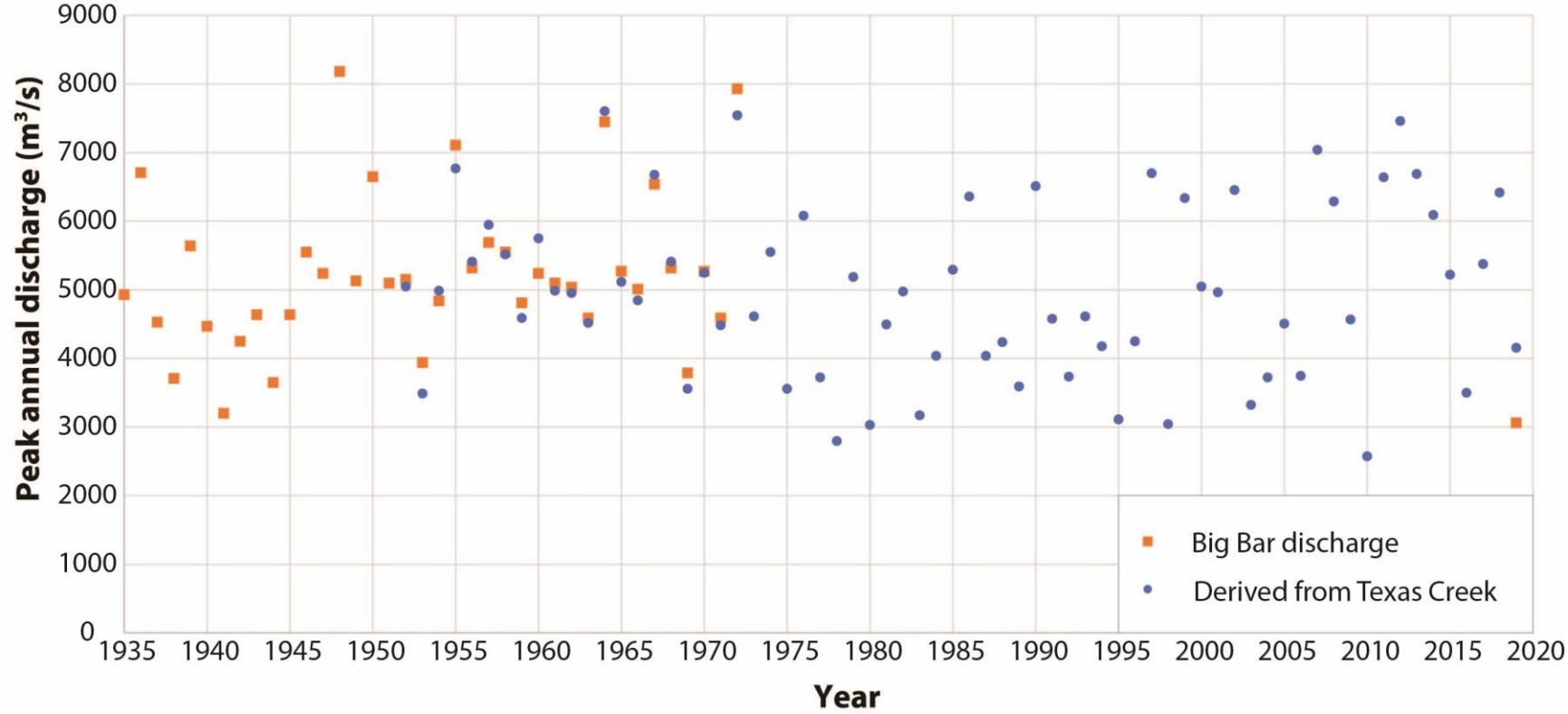

Figure A.3. Peak annual discharge for Fraser River at Big Bar station. Orange boxes are from historical data and blue dots are from correlation equation derived solely from peak annual discharge values.

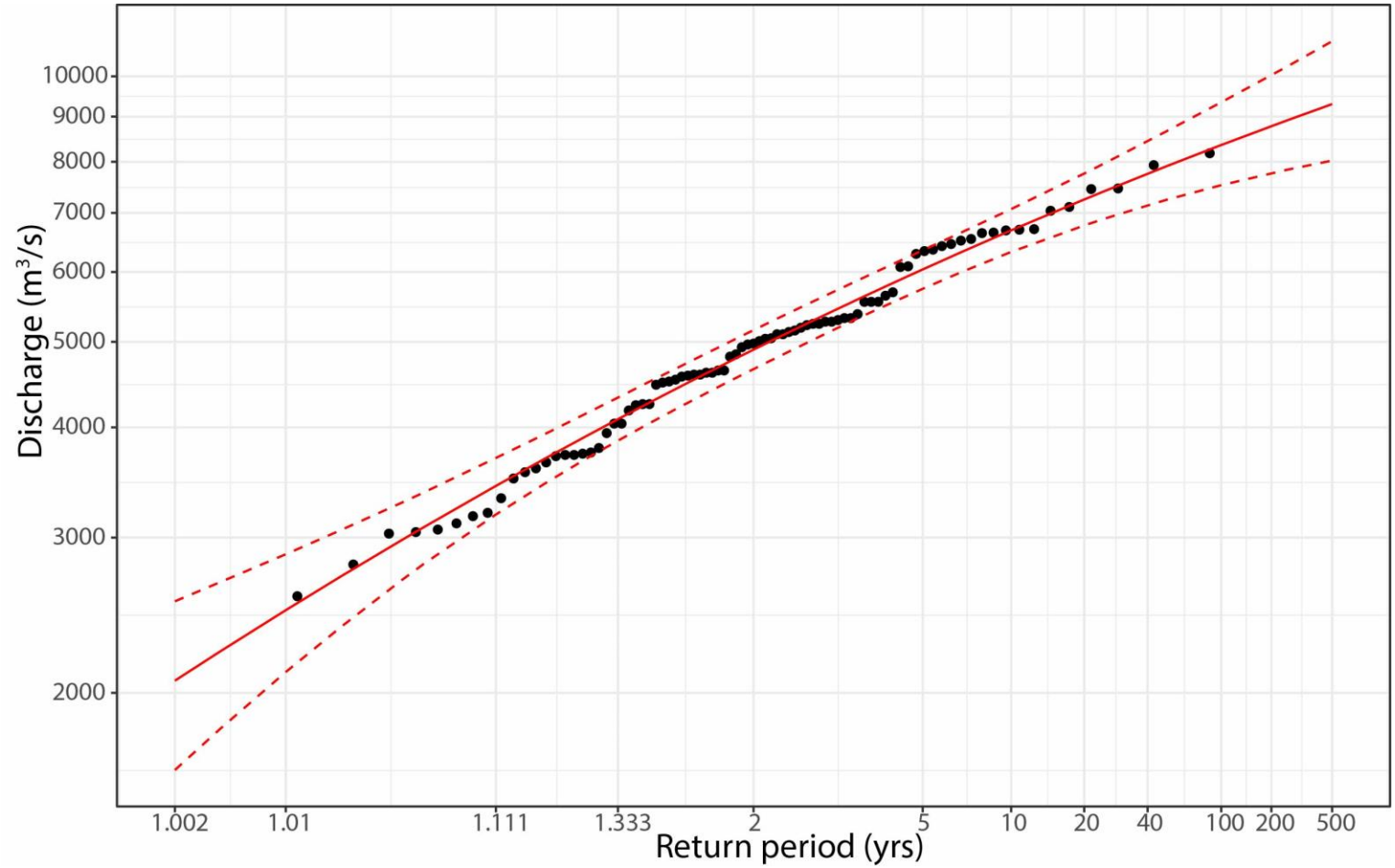

Figure A.4. Flood frequency for Fraser River at Big Bar station using log Pearson III (LP3) probability distribution.

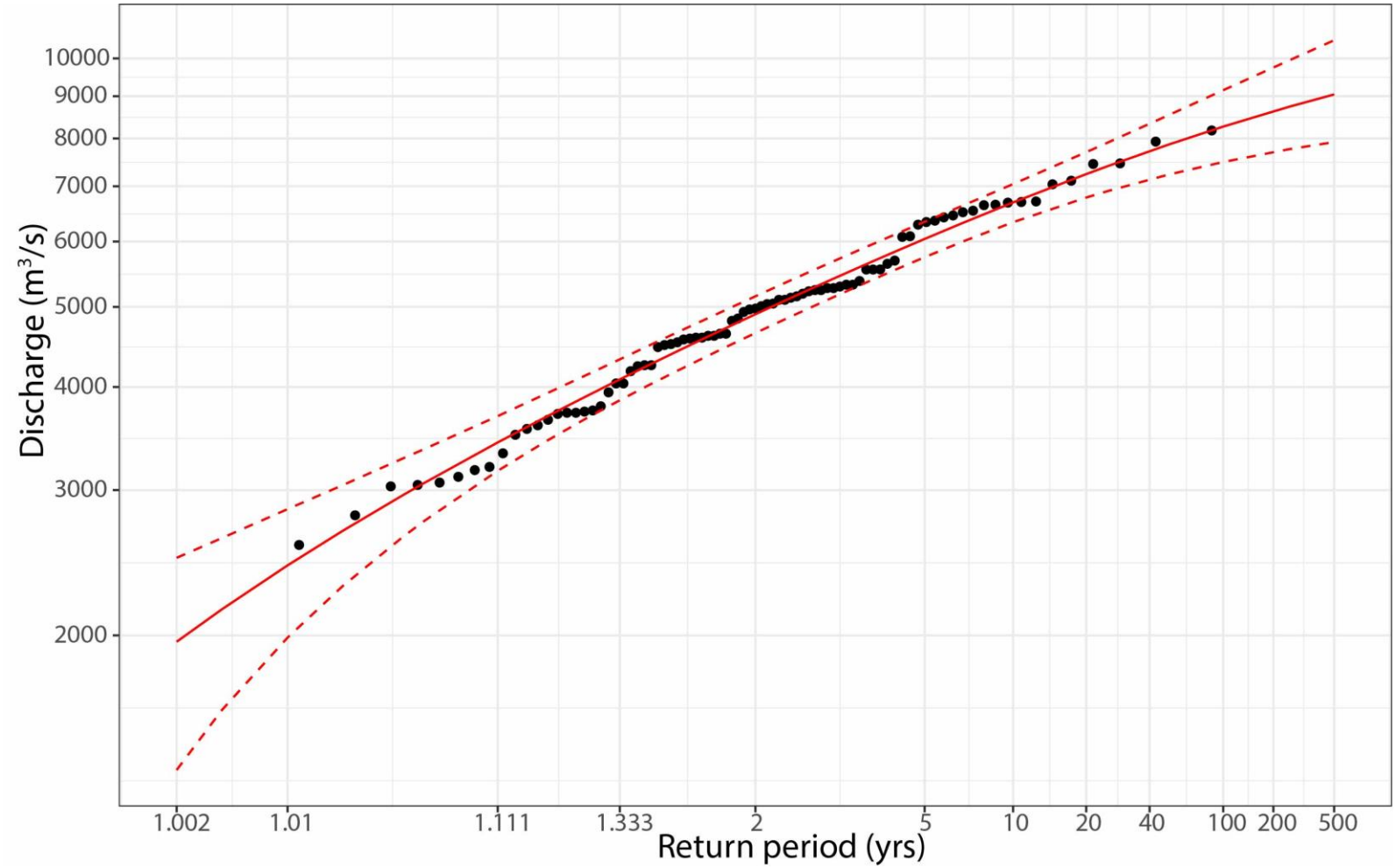

Figure A.5. Flood frequency for Fraser River at Big Bar station using Generalized Extreme Value (GEV) probability distribution.

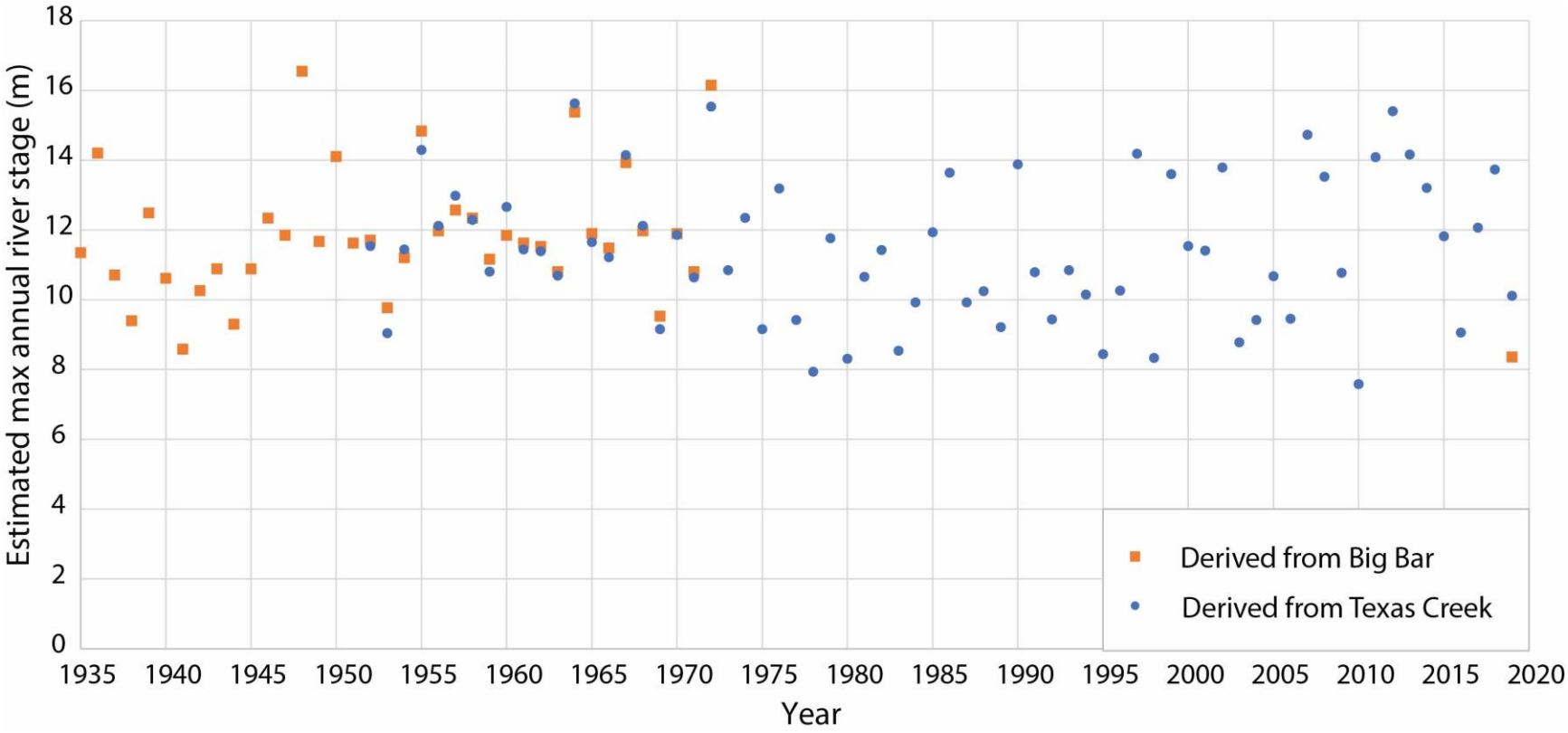

Figure A.6. Estimated maximum annual river stage for Fraser River at Big Bar gauging station. Winter low-water levels are around 4 m, so annual range is ~4-13 m. As of May 2021, the Big Bar station datum is an assumed datum with no publicly-available benchmark.

Appendix B.

Palaeoflow data

Palaeoflow data was measured on cobbles in a 1 m^2 area of an exposure within unit 2b. Columns are arranged as follows:

- Dip: Dip angle of the *ab*-plane
- Trend: Azimuth of the *ab*-plane dip (measured with a compass oriented to true north)
- Corrected: Trend azimuth corrected to magnetic declination
- POT: Orientation of the *a*-axis based on perceived flow direction: P = parallel; O = oblique; T = transverse
- Angularity: WR = well rounded; R = rounded; SR = sub-rounded; SA = sub-angular; A = angular
- Lithology: V = volcanic; V' = veined volcanic (local lithology); P = plutonic; M = metamorphic; S = sedimentary
- *a*, *b*, *c* = Length (mm) of each clast's *a*, *b*, and *c* axes

Table B.1. Clast fabric for site 1938

Clast #	Dip	Trend	Corrected	POT	Angularity	Lithology	*a*	*b*	*c*
1	25	275	291	P	WR	V	130	110	28
2	24	275	291	P	WR	V	165	110	35
3	24	240	256	O	R	V	110	95	35
4	30	280	296	O	SR	V	145	130	40
5	32	235	251	O	R	V	230	150	70
6	15	90	106	T	R	P	160	120	60
7	15	350	6	T	R	V	150	110	40
8	28	285	301	T	SR	V	130	90	27
9	33	290	306	P	SR	P	100	70	30
10	2	40	56	O	WR	V	100	95	45
11	25	200	216	T	SR	V	195	135	90
12	16	285	301	T	R	V	150	130	60
13	26	200	216	T	R	V	165	110	70
14	35	245	261	P	SR	P	135	80	35
15	23	220	236	O	SR	V	160	110	25
16	26	210	226	P	R	V	250	140	70
17	30	220	236	O	SR	M	190	150	90
18	32	200	216	P	SR	V	140	95	50
19	41	285	301	O	SR	V	235	125	45
20	17	300	316	T	R	V	155	105	30

Table B.2. Clast fabric for site 1951

Clast #	Dip	Trend	Corrected	POT	Angularity	Lithology	*a*	*b*	*c*
1	19	355	11	O	R	P	70	60	40
2	60	310	326	T	SR	V'	115	60	45
3	32	315	331	T	R	V	190	100	50
4	26	335	351	T	R	M	90	60	40
5	27	355	11	P	SR	V'	140	100	40
6	45	295	311	T	R	M	130	80	40
7	10	345	1	O	R	S	180	170	80
8	3	335	351	T	SR	V	140	120	50
9	5	295	311	O	SR	V	170	160	85
10	10	325	341	T	SR	M	220	150	100
11	21	290	306	O	SR	P	130	100	55
12	14	340	356	T	R	V	140	110	60
13	10	325	341	T	WR	M	150	140	70
14	40	260	276	O	SR	V'	90	90	40
15	32	345	1	T	SR	V'	160	125	50
16	21	350	6	P	R	P	115	95	55
17	28	290	306	P	R	M	175	140	90
18	25	330	346	O	WR	V	115	105	40
19	34	305	321	T	WR	V	100	80	45
20	15	315	331	P	SR	M	165	120	65
21	32	295	311	T	R	V	135	110	60
22	15	320	336	O	SR	V'	150	100	35
23	34	310	326	T	SR	V	125	50	45
24	14	315	331	O	SR	V	80	70	40
25	37	295	311	O	SR	V'	80	70	20
26	27	325	341	O	WR	M	70	60	25
27	30	275	291	T	SR	V'	140	120	60
28	22	270	286	O	SR	V	130	75	60
29	46	250	266	T	R	V	105	80	50
30	32	260	276	T	SR	V	190	150	100

Table B.3. Clast fabric for site 1954

Clast #	Dip	Trend	Corrected	POT	Angularity	Lithology	*a*	*b*	*c*
1	4	110	126	P	WR	V	100	75	25
2	39	215	231	T	SR	V	220	135	85
3	15	295	311	T	WR	V	100	80	20
4	38	305	321	O	WR	V	140	120	60
5	19	240	256	T	WR	V	110	80	40
6	75	345	1	T	WR	V	130	100	30
7	3	325	341	P	SR	V	120	95	50
8	14	305	321	O	R	V	85	80	50
9	19	275	291	T	SR	V	180	120	80
10	9	165	181	P	WR	V	120	75	20
11	24	135	151	T	R	M	110	85	30
12	42	185	201	P	WR	V	100	90	40
13	58	230	246	T	SR	V	140	110	60
14	39	275	291	T	SR	V	230	145	60
15	35	195	211	T	SR	V	135	80	50
16	11	335	351	P	WR	P	110	85	15
17	21	295	311	T	SR	V	165	130	90
18	25	205	221	T	R	V	160	120	40
19	36	210	226	T	SR	V'	70	130	40
20	19	260	276	T	R	V	130	100	50
21	36	210	226	T	SR	V'	180	110	70
22	17	325	341	T	SR	V'	140	120	60
23	27	285	301	O	SR	V	160	140	70
24	24	210	226	O	SA	V	160	160	30
25	22	345	1	P	WR	V	120	90	30
26	45	280	296	T	R	M	110	70	40
27	13	30	46	O	SR	V	140	140	30
28	29	290	306	T	R	V	270	130	70
29	35	310	326	T	R	M	200	110	80
30	56	225	241	T	SR	V'	200	140	100

Table B.4. Clast fabric for site 1956

Clast #	Dip	Trend	Corrected	POT	Angularity	Lithology	*a*	*b*	*c*
1	14	310	326	P	R	V	160	115	40
2	29	320	336	O	WR	V	215	120	30
3	40	335	351	T	SR	V	115	90	65
4	36	255	271	T	WR	V	130	100	45
5	32	205	221	O	SR	M	125	120	115
6	45	200	216	O	R	V	130	145	50
7	31	320	336	T	WR	V	165	130	50
8	24	340	356	P	R	V	135	75	35
9	16	325	341	T	WR	V	215	160	70
10	26	340	356	T	WR	V	180	145	55
11	24	80	96	O	SR	V	165	160	35
12	25	290	306	O	R	V	160	140	60
13	56	350	6	T	SR	V	175	135	35
14	40	0	16	O	WR	V	130	115	20
15	6	285	301	T	WR	V	160	135	30
16	22	305	321	T	WR	V	130	100	35
17	12	345	1	T	WR	V	135	105	40
18	34	35	51	P	R	P	322	125	75
19	29	330	346	T	WR	V	160	115	35
20	18	300	316	T	SR	V	250	180	40
21	20	265	281	T	WR	V	190	135	30
22	29	300	316	T	R	V	120	95	45
23	26	360	16	T	R	V	130	110	55
24	30	310	326	O	R	V	125	130	60
25	26	290	306	P	SR	V	165	100	85
26	37	5	21	T	WR	V	130	95	40
27	22	275	291	T	R	V	155	115	80
28	14	10	26	P	SA	V	155	130	60
29	32	335	351	T	WR	V	195	170	55
30	25	305	321	T	SR	V	170	130	75

Appendix C.

Additional optical dating data

Table C.1. Dose recovery test results.

Sample	Aliquots used	Mask size (mm)	Given dose (Gy)	De (Gy)	OD (%)	Dose Recovery Ratio
1951-TG-01	24/24	3	8.08 ± 0.15	8.51 ± 0.07	1.11 ± 1.63	1.05 ± 0.01
1966-TG-02	14/24	1	0.962 ± 0.018	1.22 ± 0.05	9.93 ± 3.59	1.27 ± 0.04
1966-TG-02	24/24	3	0.962 ± 0.018	1.29 ± 0.03	10.47 ± 1.84	1.35 ± 0.02
1966-TG-02	24/24	3	8.02 ± 0.15	8.19 ± 0.05	<0.01	1.02 ± 0.01
1960-TG-01	23/24	1	20.0 ± 0.4	20.0 ± 0.2	0.46 ± 4.58	1.00 ± 0.01
1956-TG-02	23/24	3	13.6 ± 0.3	13.7 ± 0.1	<0.01	1.01 ± 0.01
1958-TG-01	23/24	3	12.8 ± 0.2	13.1 ± 0.1	<0.01	1.02 ± 0.01

De = equivalent dose; OD = overdispersion.

Table C.2. Radionuclide concentrations for optical dating samples. Concentrations were provided by Bureau Veritas Laboratories using neutron activation analysis (NAA) techniques.

Sample	U (ppm)	Th (ppm)	K (%)	Rb (ppm)
1938-TG-01	1.47 ± 0.14	5.93 ± 0.32	1.13 ± 0.07	31.0 ± 5.6
1951-TG-01	0.82 ± 0.11	3.22 ± 0.18	1.10 ± 0.07	35.0 ± 5.6
1951-TG-02	1.11 ± 0.15	4.86 ± 0.27	1.17 ± 0.04	35.0 ± 5.7
1954-TG-01	1.00 ± 0.13	2.77 ± 0.17	1.31 ± 0.08	36.0 ± 5.5
1956-TG-02	1.03 ± 0.15	4.22 ± 0.24	1.15 ± 0.08	41.0 ± 6.4
1956-TG-03	1.38 ± 0.15	5.55 ± 0.30	1.12 ± 0.07	34.0 ± 5.4
1958-TG-01	1.31 ± 0.15	6.06 ± 0.32	1.05 ± 0.07	33.0 ± 5.5
1960-TG-01	1.29 ± 0.15	3.32 ± 0.19	1.33 ± 0.08	37.0 ± 5.5
1961-TG-01	1.05 ± 0.13	2.64 ± 0.16	1.14 ± 0.07	39.0 ± 5.7
1962-TG-02	1.39 ± 0.14	4.04 ± 0.22	1.02 ± 0.07	35.0 ± 5.3
1966-TG-02	1.78 ± 0.16	7.48 ± 0.39	1.21 ± 0.07	32.0 ± 5.0
1966-TG-03	1.81 ± 0.17	8.66 ± 0.45	1.52 ± 0.09	51.0 ± 5.5
BBL19	1.76 ± 0.14	6.38 ± 1.20	1.34 ± 1.06	33.1 ± 2.8

Table C.3. Optical dating sample notes. Sand thicknesses and depth of sample collection are provided to assess the distance from bounding strata which may affect dosimetry.

Sample	Sediment Type (Unit #)	Unit thickness (cm)	Depth in unit of sample (cm)	Description
1960-TG-01	Fluvial (2c)	15	10	medium sand to granules overlying cobble lag: many heavy minerals
1954-TG-01	Fluvial (2c)	50	15	trough cross-bedded medium to coarse sand, single grain thick pebble beds throughout
1938-TG-01	Fluvial (2c)	30	5	medium sand overlying cobble gravel
1958-TG-01	Fluvial (2c)	350	100	well-sorted beds of silty fine sand to granules; ripple cross laminations present in fine to medium sand beds
1961-TG-01	Fluvial (2c)	50	20	trough cross-bedded medium sand to granules with single grain thick pebble beds
1956-TG-03	Aeolian (4)	120	100	massive deposition with tephra layer overlying optical dating sample location
1956-TG-02	Fluvial (2c)	20	10	ripple cross-laminated fine to medium sand; bed found at interbedding interface with Unit 3
1962-TG-02	Fluvial (2c)	50	35	medium sand with flames and ripple cross laminae
1951-TG-02	Aeolian (4)	120	100	massive deposition with tephra layer overlying optical dating sample location
1951-TG-01	Fluvial (2c)	100	50	well-sorted beds of fine to coarse sand; ripple cross laminations present
1966-TG-03	Fluvial (2c)	30	15	medium sand in a downward-fining sequence of medium sand to silty fine sand
1966-TG-02	Fluvial (2c)	85	40	medium sand in a downward-fining sequence of medium sand to silty fine sand
BBL19	Fluvial (2c)	>100	50	sand bar at surface of present day river bank

Table C.4. Additional information required for optical dating dose rate calculations.

Sample	As-Collected Water Content	Saturated Water Content	Depth (m)	Elevation (m asl)	Latitude (°N)	Longitude (°W)
1938-TG-01	0.0177 ± 0.0018	0.337 ± 0.034	10 ± 1	389	51	122
1951-TG-01	0.0118 ± 0.0012	0.296 ± 0.030	1.9 ± 0.1	324	51	122
1951-TG-02	0.0352 ± 0.0035	0.354 ± 0.035	1.2 ± 0.1	324	51	122
1954-TG-01	0.0126 ± 0.0013	0.248 ± 0.025	4 ± 0.1	442	51	122
1956-TG-02	0.0673 ± 0.0067	0.317 ± 0.032	4 ± 0.1	353	51	122
1956-TG-03	0.0158 ± 0.0016	0.315 ± 0.032	1.2 ± 0.1	353	51	122
1958-TG-01	0.0262 ± 0.0026	0.307 ± 0.031	6 ± 0.1	380	51	122
1960-TG-01	0.0163 ± 0.0016	0.292 ± 0.029	2.5 ± 0.1	451	51	122
1961-TG-01	0.0262 ± 0.0026	0.249 ± 0.025	0.6 ± 0.1	331	51	122
1962-TG-02	0.0160 ± 0.0016	0.288 ± 0.029	0.8 ± 0.1	321	51	122
1966-TG-02	0.0291 ± 0.0029	0.344 ± 0.034	4 ± 0.1	296	51	122
1966-TG-03	0.0410 ± 0.0041	0.406 ± 0.041	2.5 ± 0.1	296	51	122
BBL19	0.105 ± 0.011	0.367 ± 0.037	0.65 ± 0.1	290	51	122

Optical dating summary figures

Luminescence decay and dose-response curves, abanico plots, and anomalous fading decay plots for representative aliquots for the samples dated. For each sample, (a) provides a plot of a luminescence decay (shinedown) curve of the natural signal. Vertical lines indicate which portion of the shinedown curve was used for the signal (red lines) and background (green lines) measurements; the inset is a dose-response curve with the natural signal's brightness interpolated on the dose-response curve to determine an equivalent dose off the x-axis. b) An abanico plot showing all accepted aliquots for the sample. Abanico plots (Dietze et al. 2016) include a radial plot on the left and a kernel density curve on the right. Points are plotted based on their value and analytical error, with lower error (more precise) points plotting further to the right on the radial plot. Radial plots are read by drawing a line from the origin at the left through each point and onto the axis to the left of the kernel density curve. Two sigma error values can be measured on the graph by drawing a straight line from each of the “2” and “-2” dashes on the standardized estimate axis, through the point, and onto the axis to the left of the kernel density curve. The kernel density curve provides a visual representation of the spread of data CAM D_e = equivalent dose of the sample using the Central Age Model; MAM D_e = equivalent dose of the sample using the Minimum Age Model (when applicable); OD = overdispersion. c) A representative fading plot from one aliquot of the sample. Delay time on the logarithmic x-axis denotes the time between laboratory irradiation and stimulation, with longer delay times resulting in less luminescence being measured because of anomalous fading.

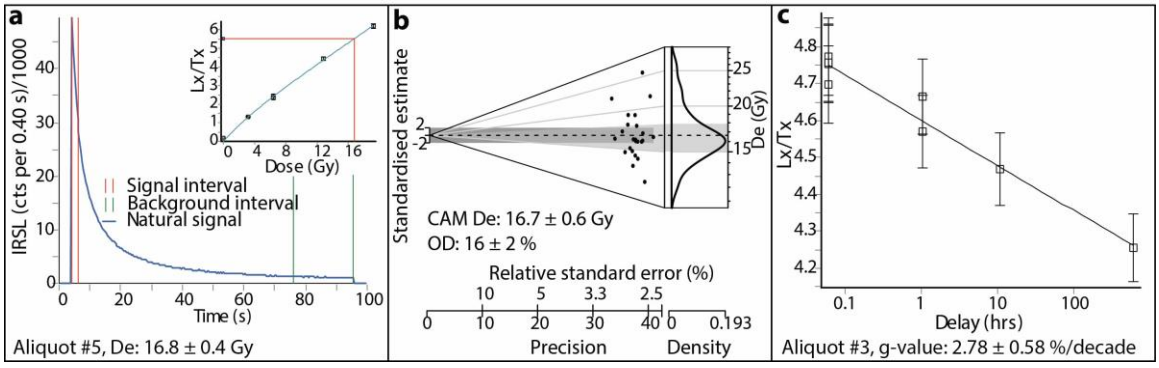

Figure C.1. 1938-TG-01

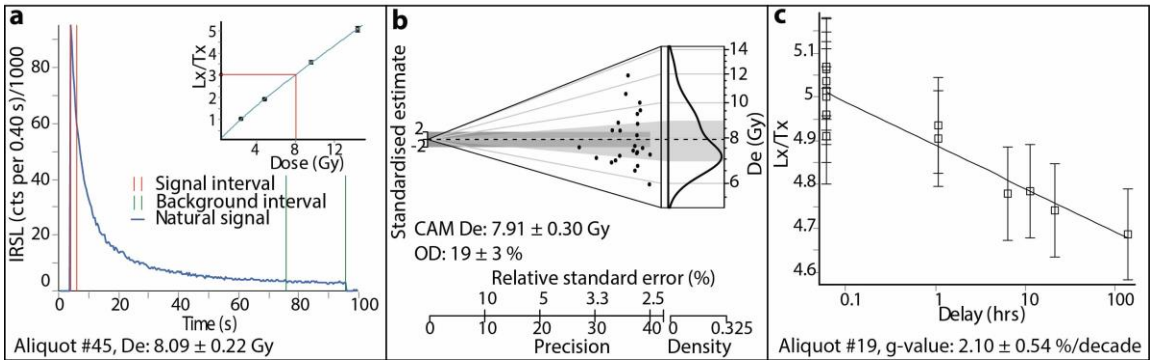

Figure C.2. 1951-TG-01

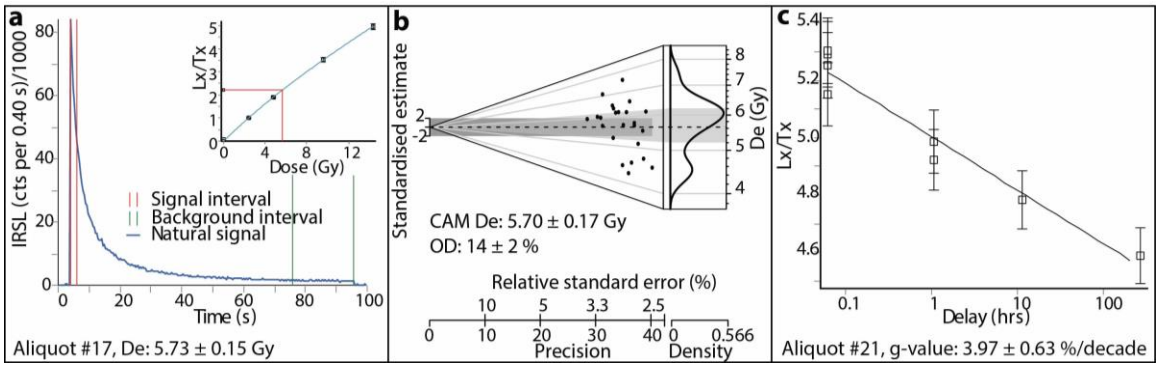

Figure C.3. 1951-TG-02

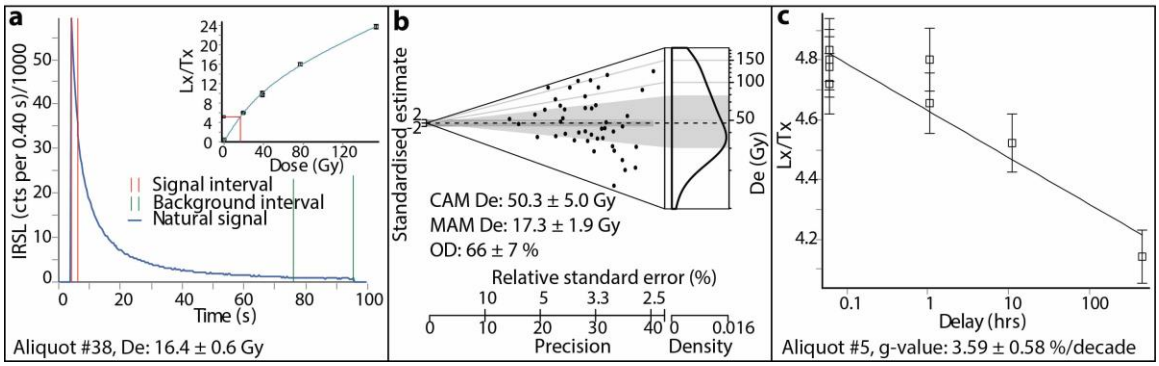

Figure C.4. 1954-TG-01

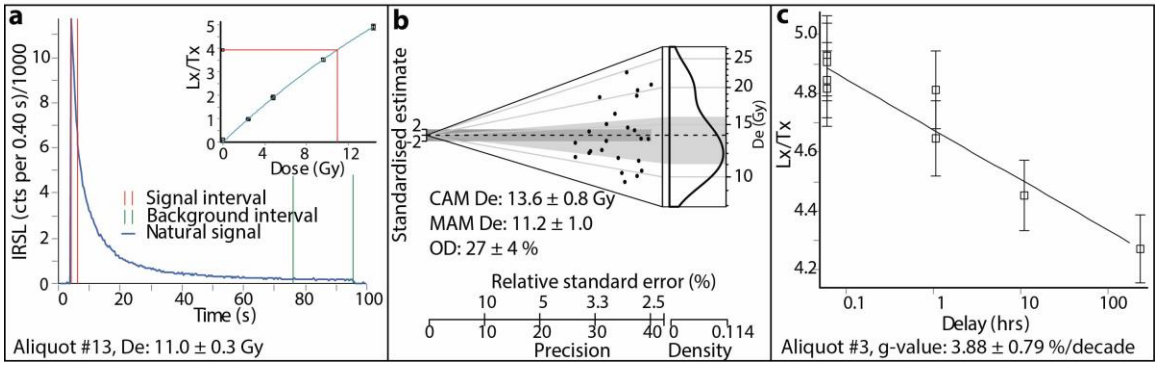

Figure C.5. 1956-TG-02

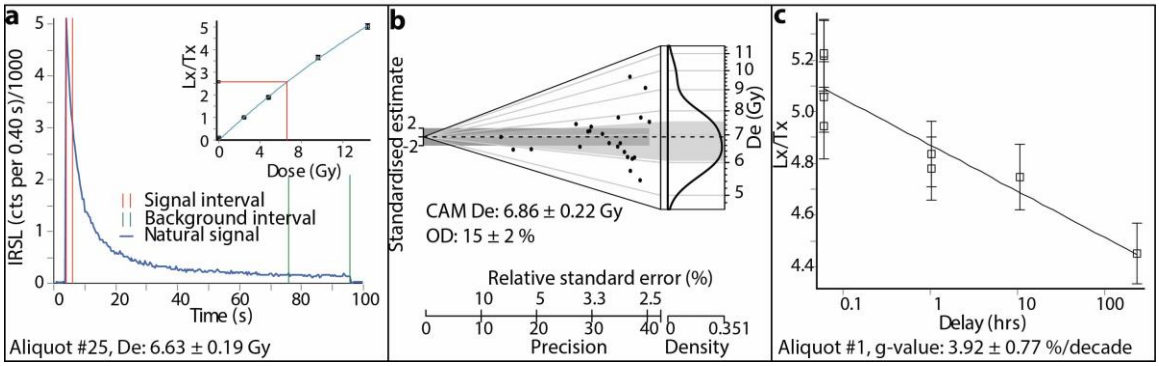

Figure C.6. 1956-TG-03

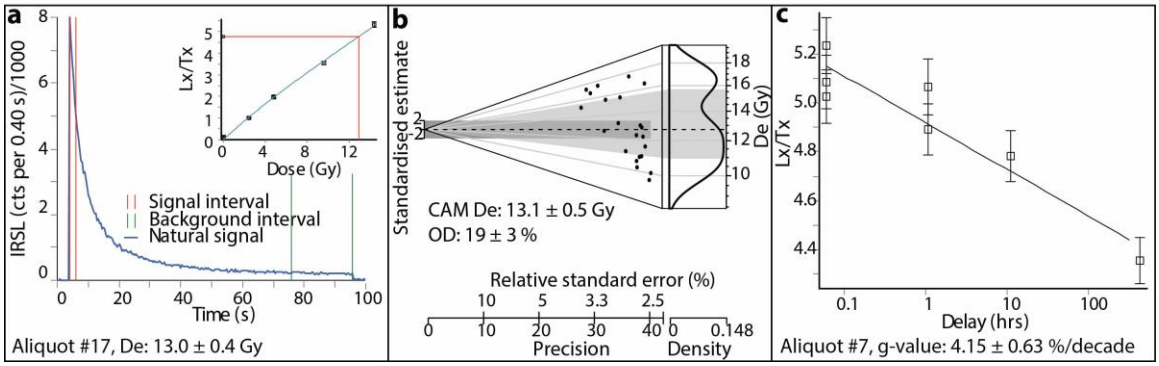

Figure C.7. 1958-TG-01

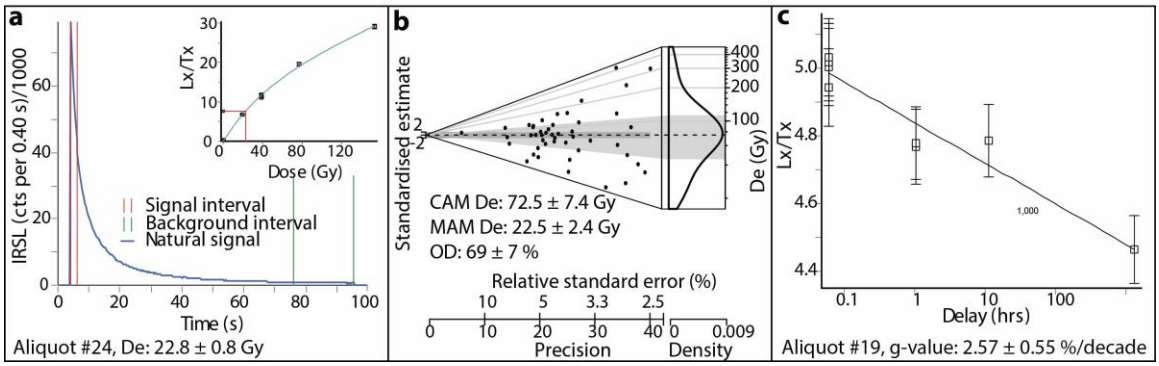

Figure C.8. 1960-TG-01

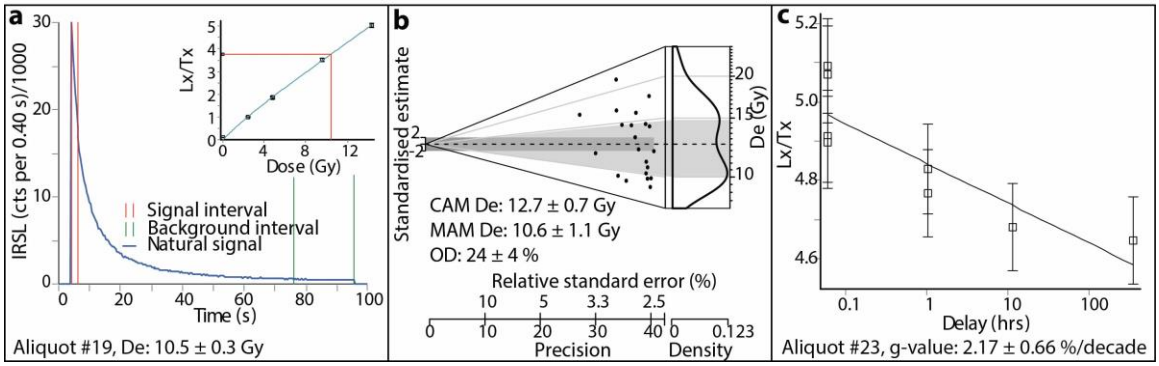

Figure C.9. 1961-TG-01

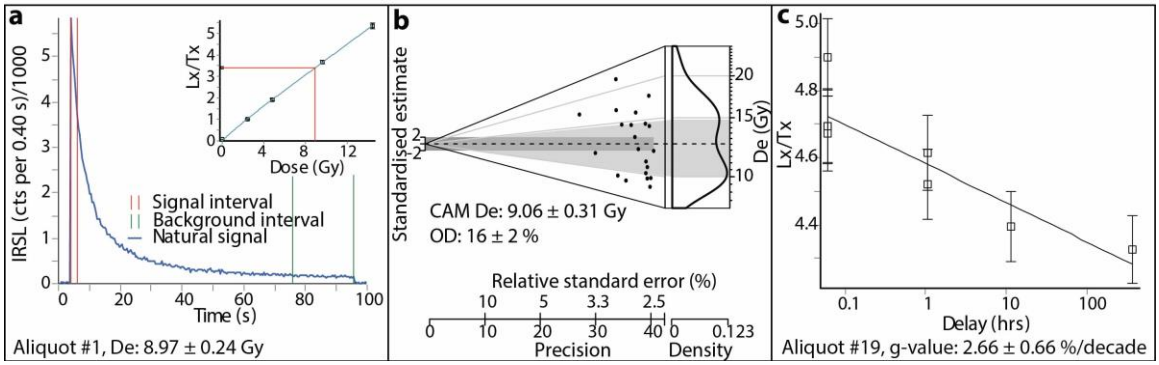

Figure C.10. 1962-TG-02

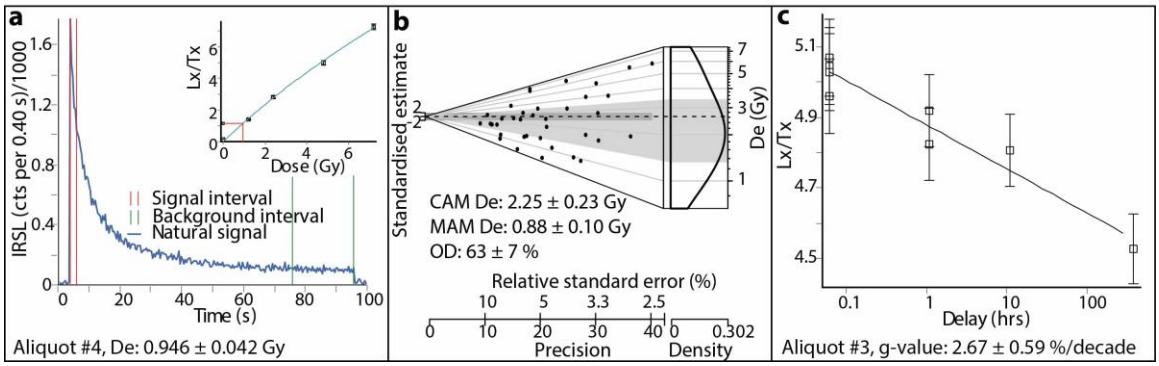

Figure C.11. 1966-TG-02

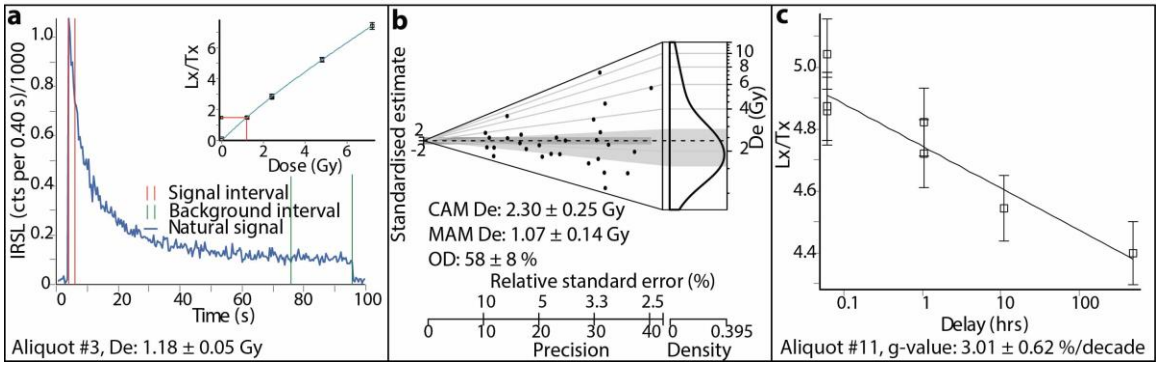

Figure C.12. 1966-TG-03

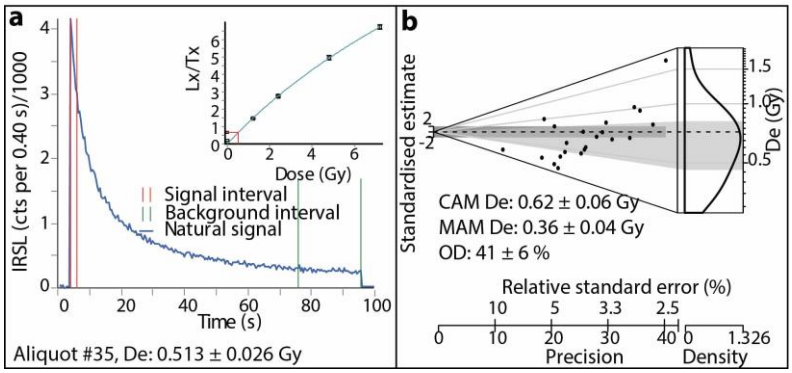

Figure C.13. BBL19. A fading test was not performed for this sample.

LM-OSL test

Linearly-modulated OSL (LM-OSL, Bulur 1996) was performed on quartz of 1951-TG-01 to determine if a thermally stable fast component, which is quickly reset (bleached) in daylight and thus makes quartz suitable for optical dating, was present. Five aliquots were tested with a 220° C preheat, with only one of the aliquots possessing a sufficient fast component (Figure C.14b). Quartz was thus abandoned and KF was used for dating in this study.

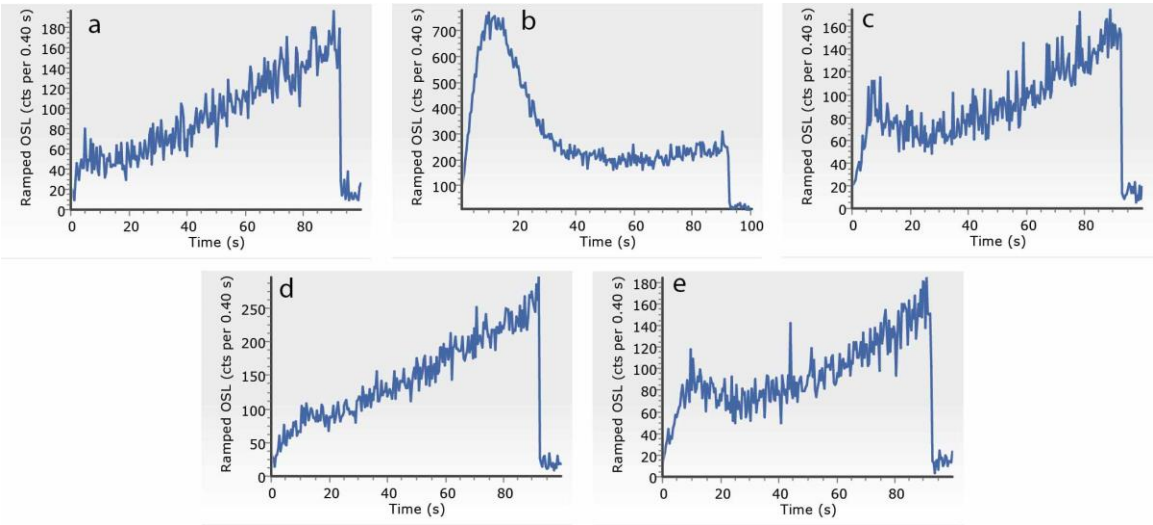

Figure C.14. LM-OSL results from 5 aliquots of sample 1951-TG-01. Only aliquot b possesses a fast component that is rapidly bleached in the first 20 s of stimulation.

Appendix D.

Valley cross-section data

Composite valley cross-sections for Big Bar and Watson Bar were compiled from seven and eight DEM-derived cross sections, respectively. Cross sections were derived in ArcGIS, then overlaid in Illustrator, using Fraser River as the base elevation. Cross-sections were selected to ensure as many terrace elevations as possible were visually represented in each cross-section. DEM-derived cross-sections are shown in the following figures.

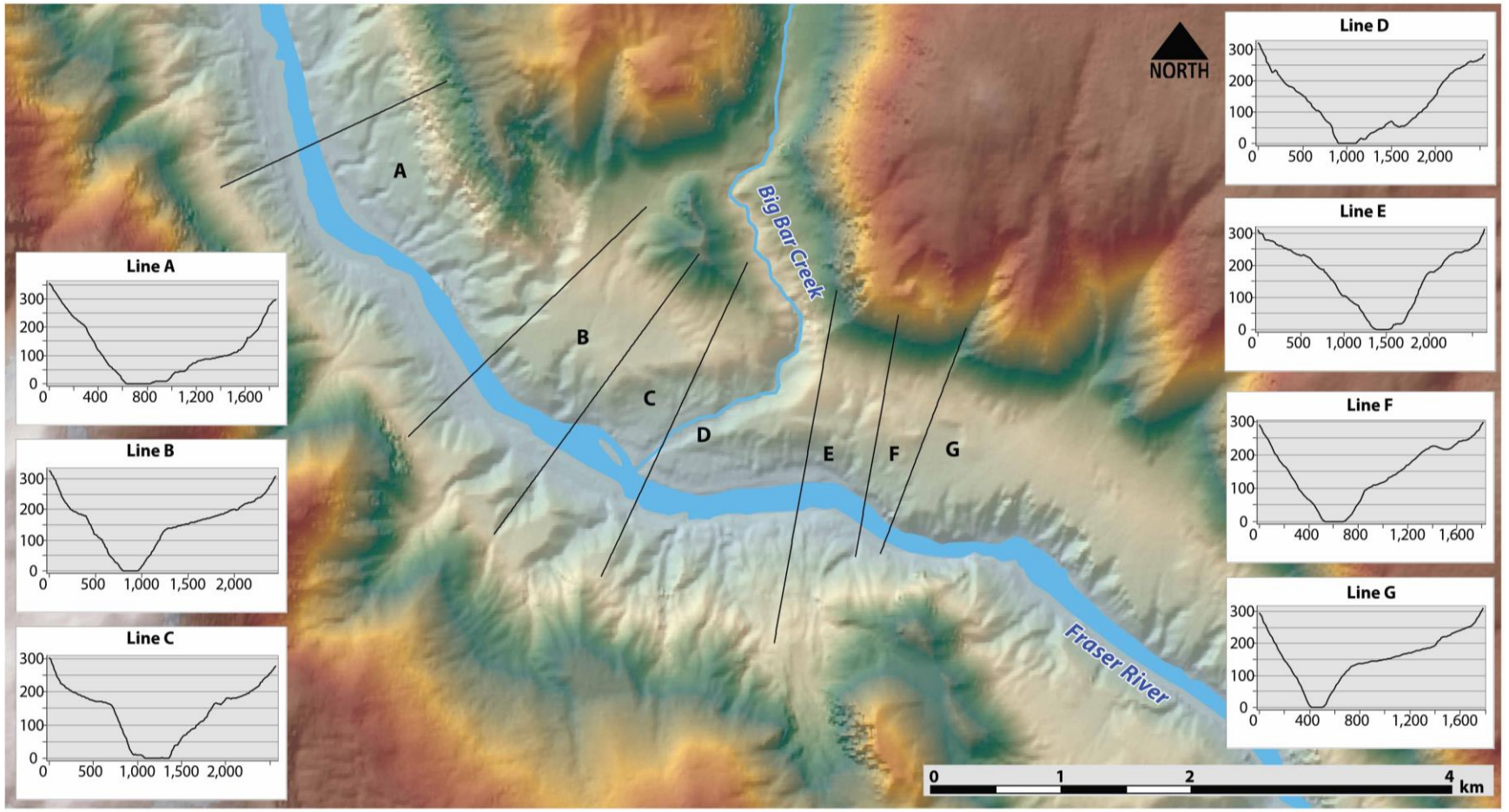

Figure D.1 Cross-sections from Big Bar used to create composite cross-section. X and Y axes are in metres, with X axis being ground distance and Y axis being height above river.

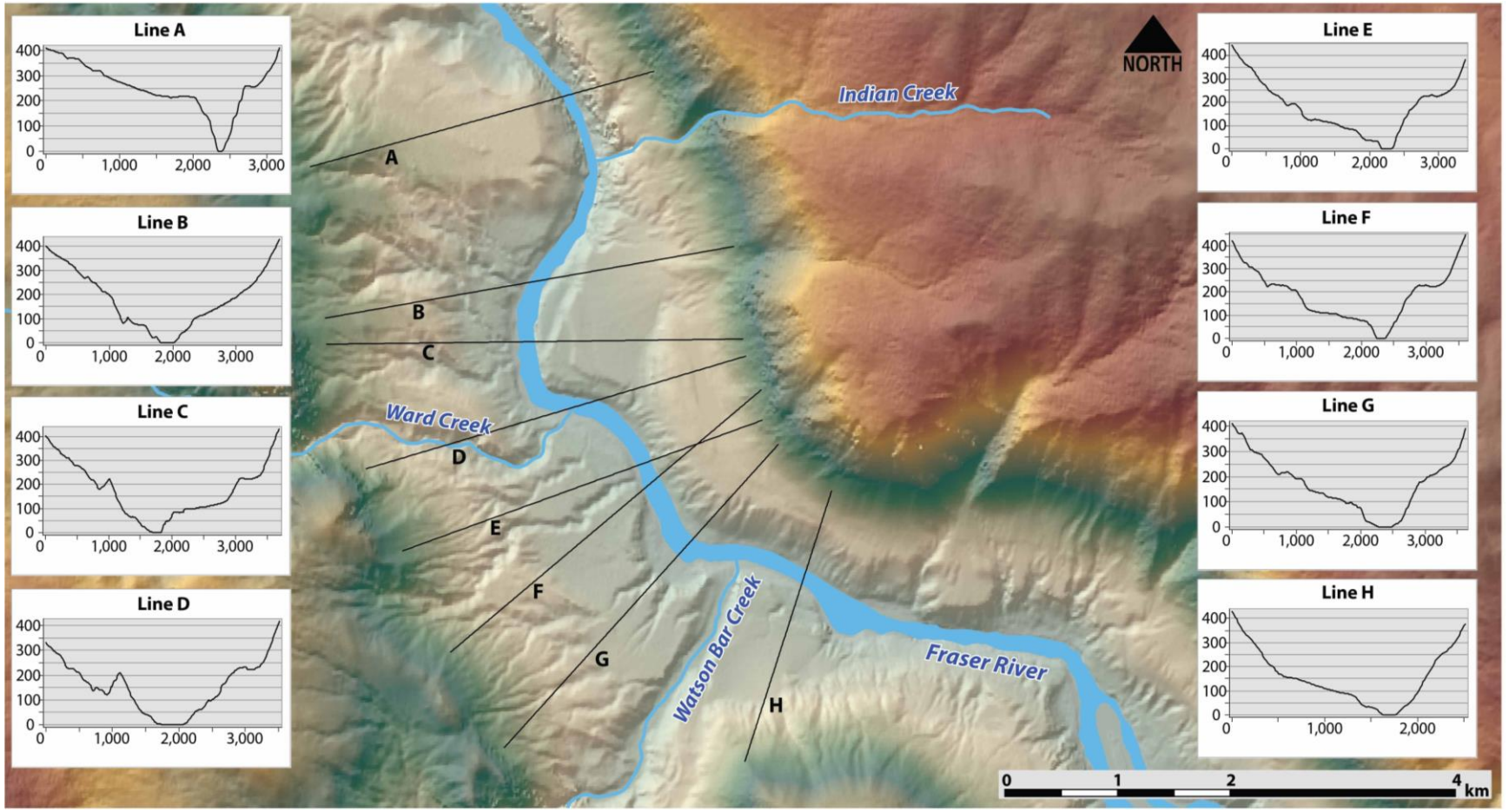

Figure D.1 Cross-sections from Watson Bar used to create composite cross-section. X and Y axes are in metres, with X axis being ground distance and Y axis being height above river.

Appendix E.

Optical dating sample collection photos

Figure E.1. Optical dating sample 1938-TG-01 was collected from unit 2c, 5 cm below the contact with unit 3 diamicton.

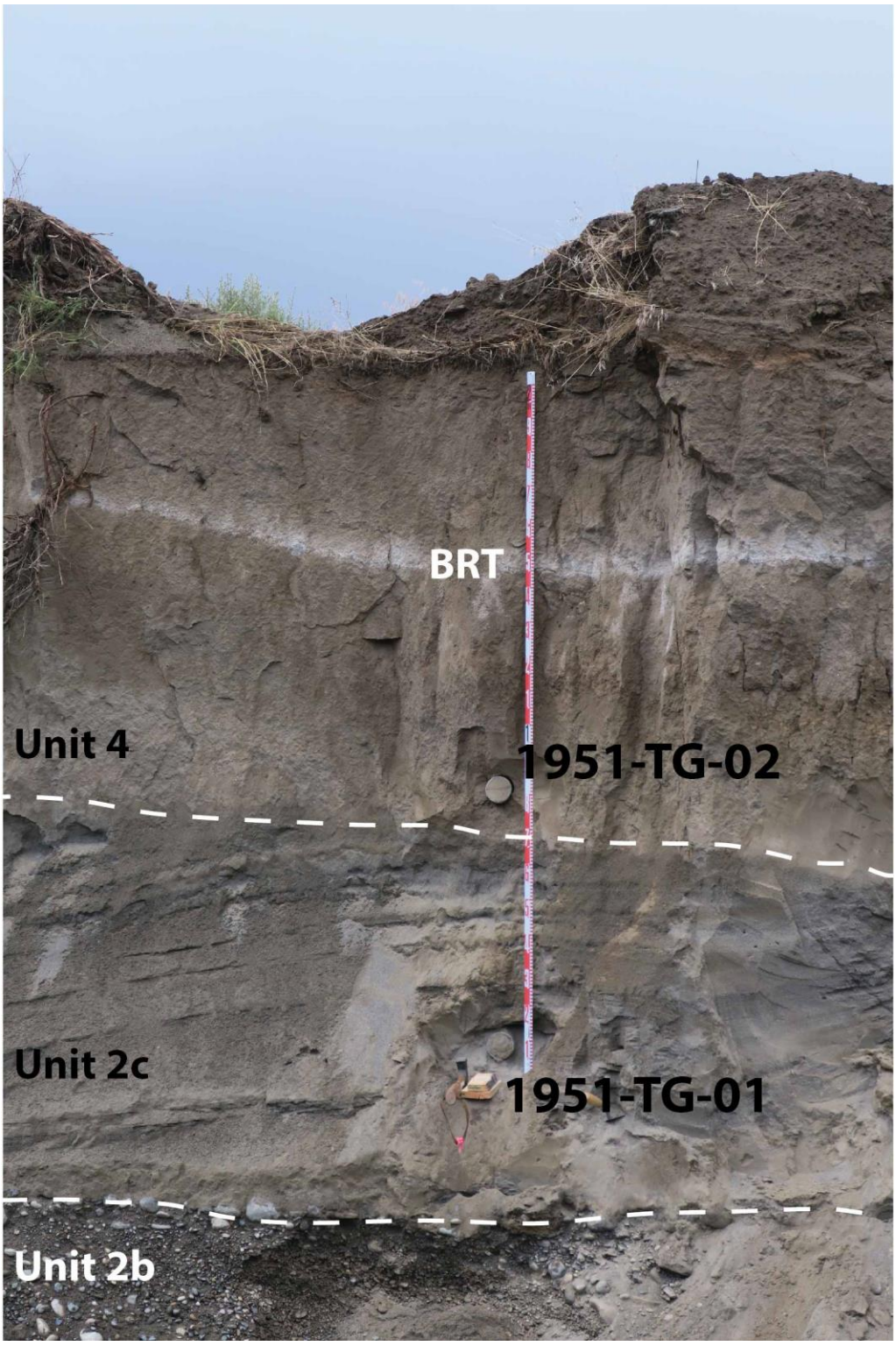

Figure E.2. Optical dating sample 1951-TG-01 was collected from unit 2b, 50 cm below the contact with unit 4. Optical dating sample 1951-TG-02 was collected from unit 4, 1 m below surface. Bridge River Tephra (BRT) (Clague *et al.* 1995) is clearly visible in unit 4 above 1951-TG-02.

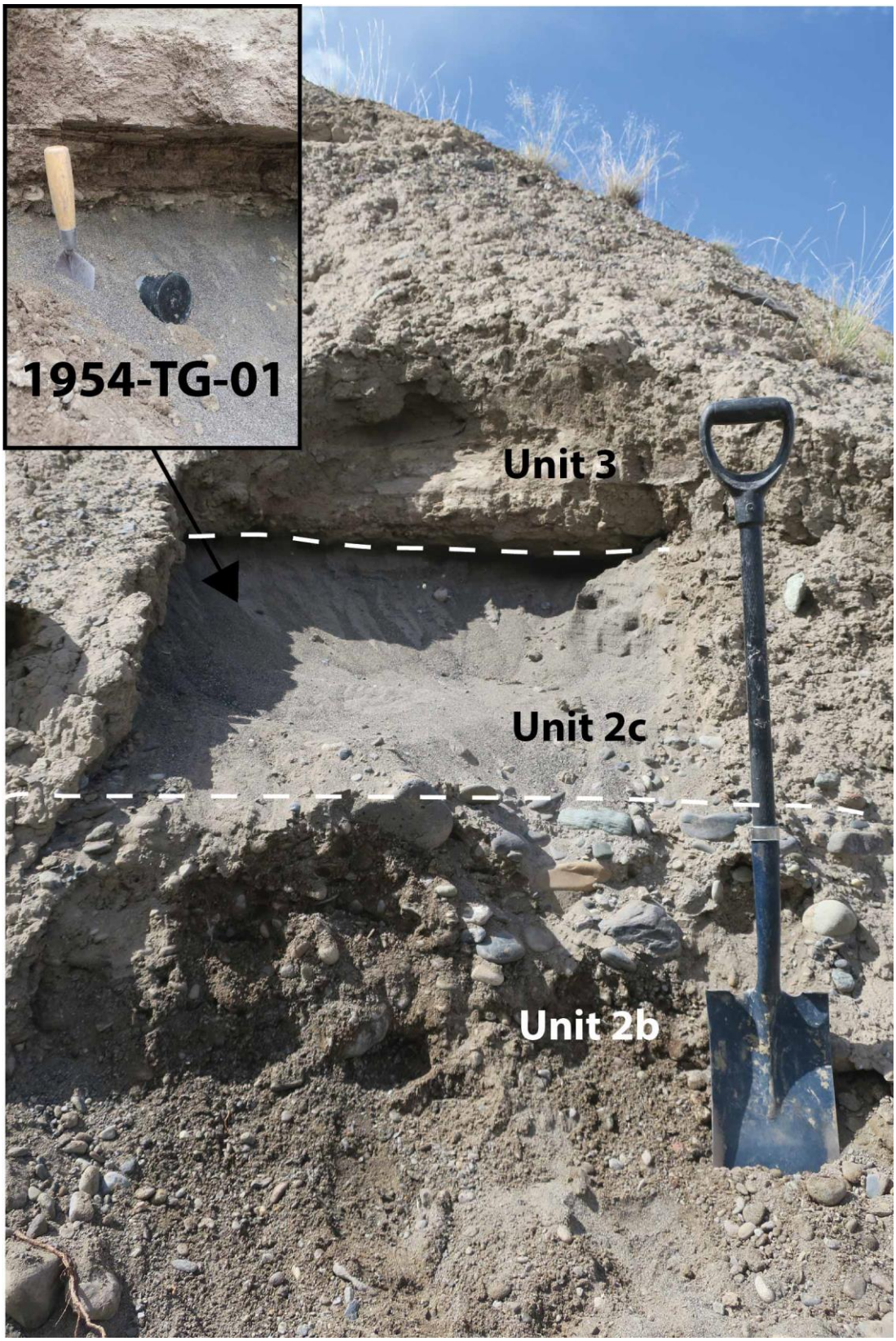

Figure E.3. Optical dating sample 1954-TG-01 was collected from unit 2c, 15 cm below the contact with unit 3.

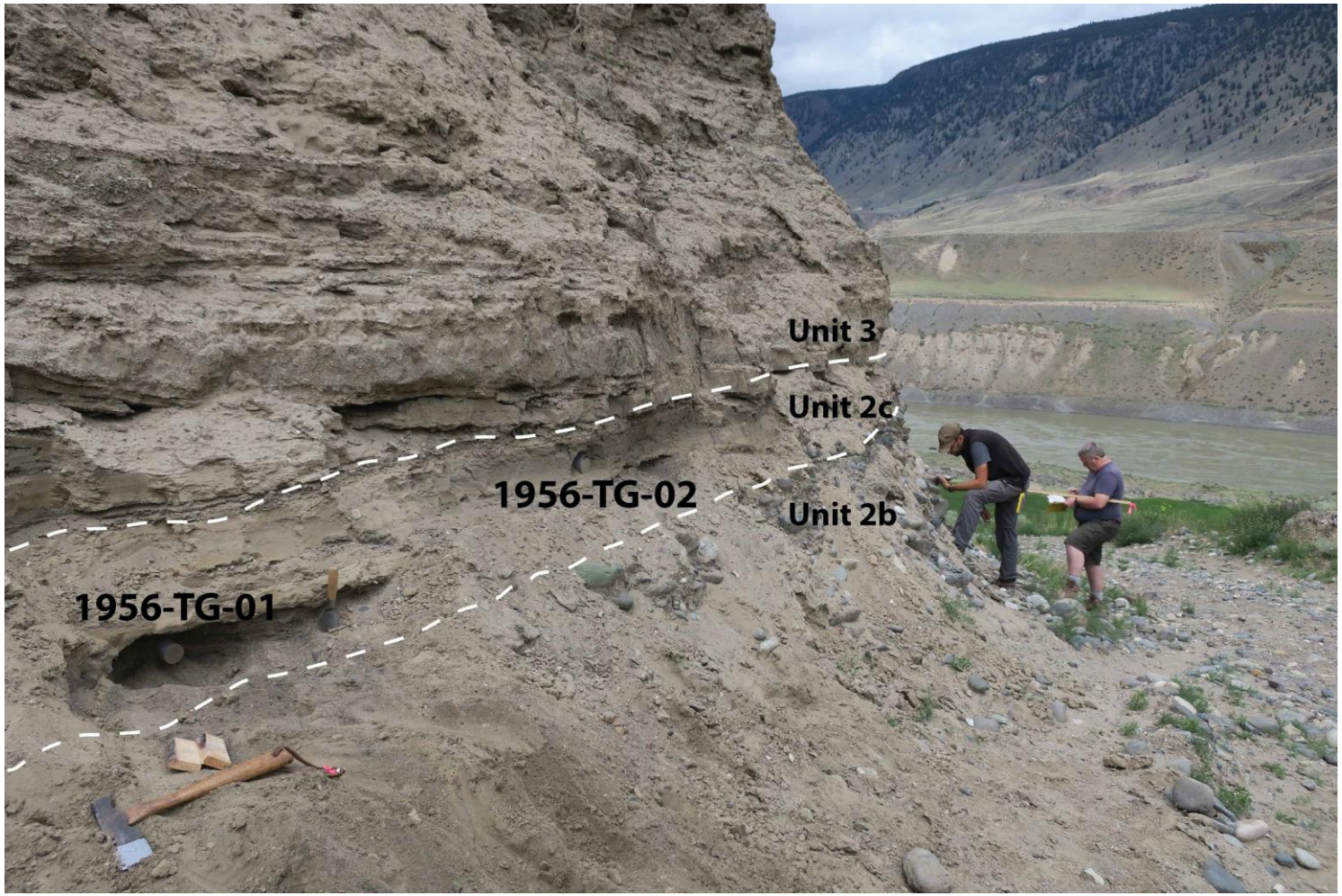

Figure E.4. Optical dating sample 1956-TG-02 was collected from unit 2c, which is interbedded with unit 3. It was collected from the centre of a 20 cm thick sand bed. Optical dating sample 1956-TG-01 was not used for dating in this study, but was collected in unit 2c, 10 cm above unit 2b and ~4.5 m from the surface.

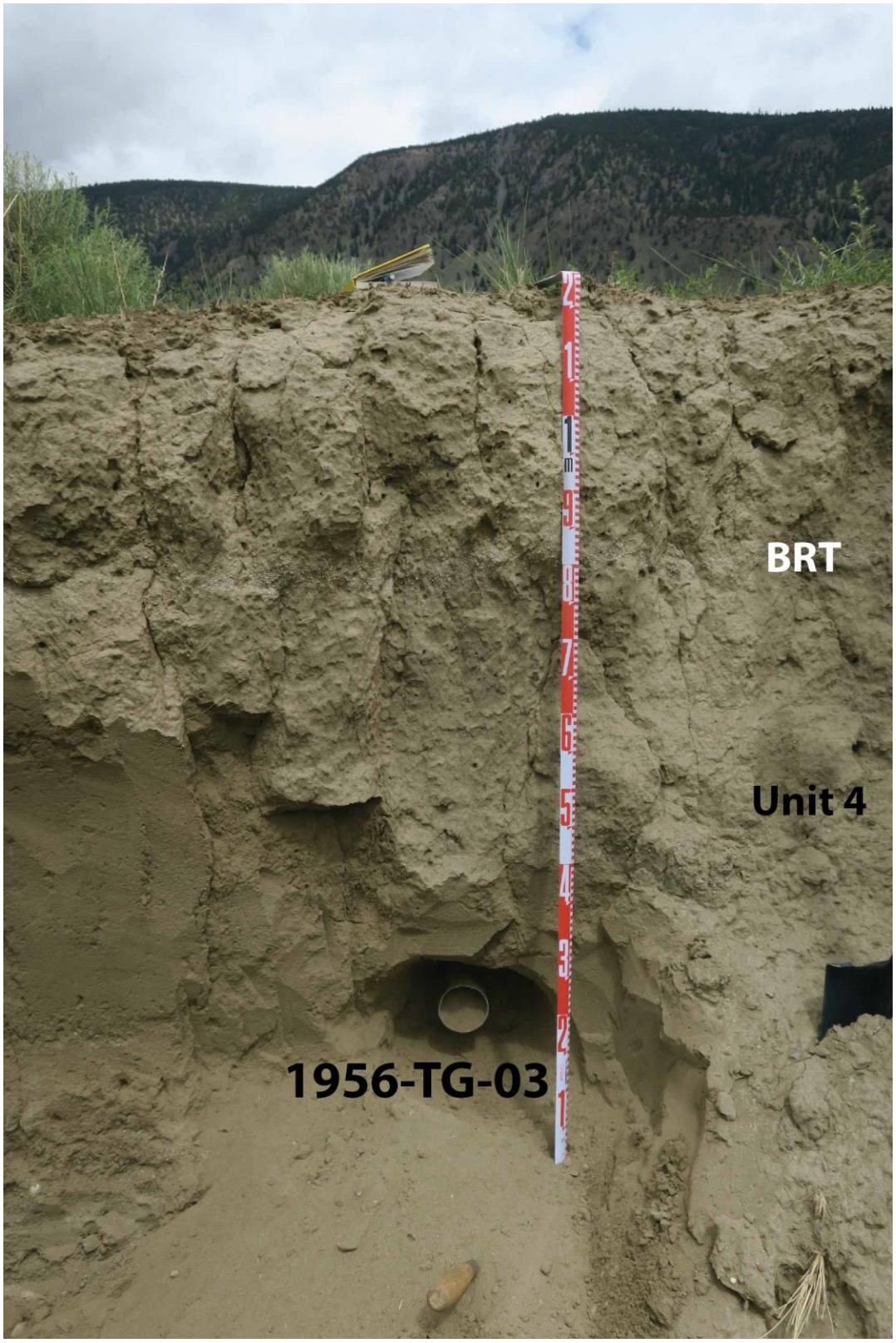

Figure E.5. Optical dating sample 1956-TG-03 was collected from unit 4, 1.2 m below the surface. Bridge River Tephra (BRT) (Clague *et al.* 1995) is faintly visible above 1956-TG-03.

Figure E.6. Optical dating sample 1958-TG-01 was collected from unit 2c (3.5 m thick), 1 m below the contact with unit 3.

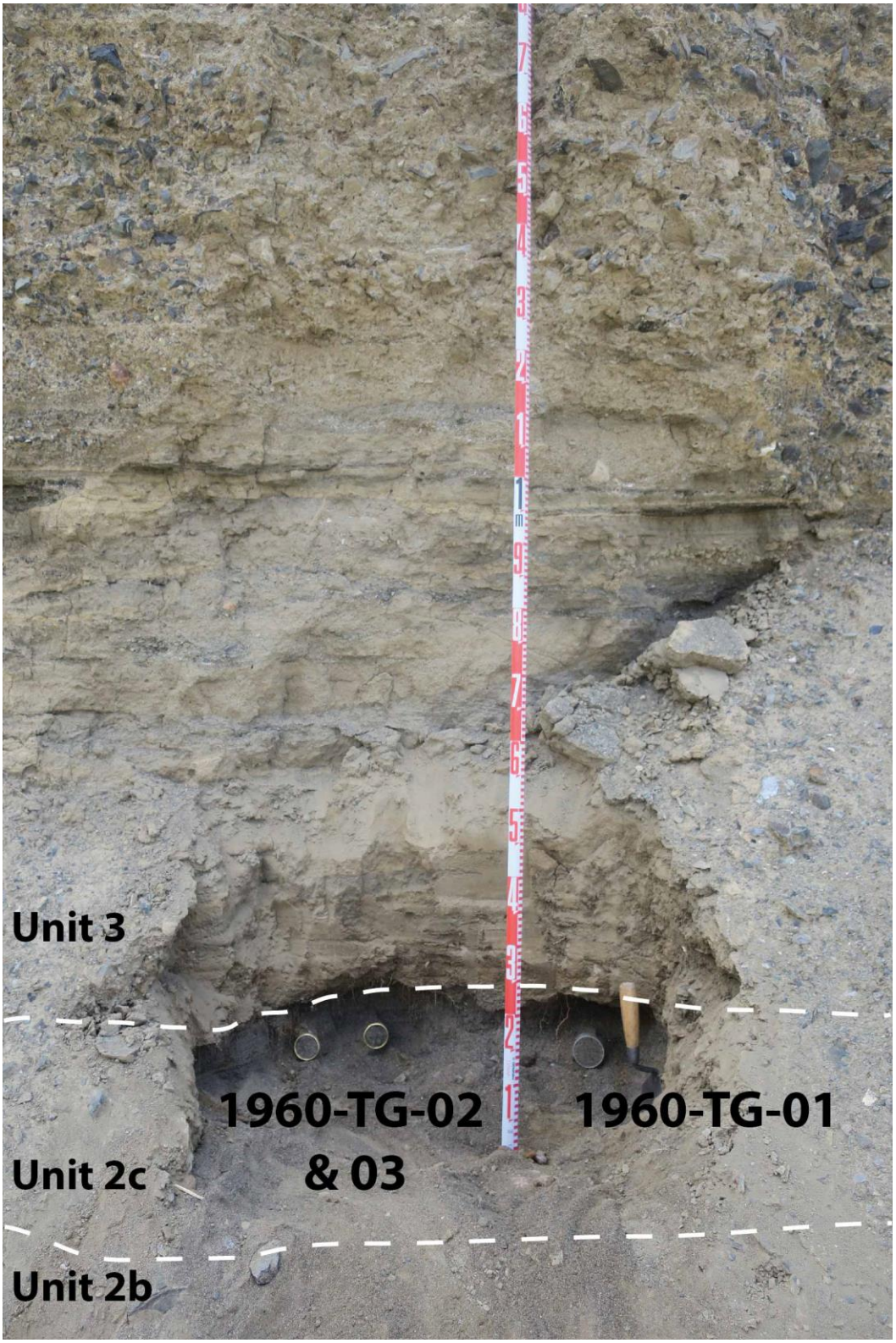

Figure E.7. Optical dating samples 1960-TG-01, 02, and 03 were collected from a 15 cm thick bed of unit 2c, 10 cm below the contact with unit 3. Only 1960-TG-01 was used for this study, with 1960-TG-02 and 03 collected to ensure there was sufficient material to date.

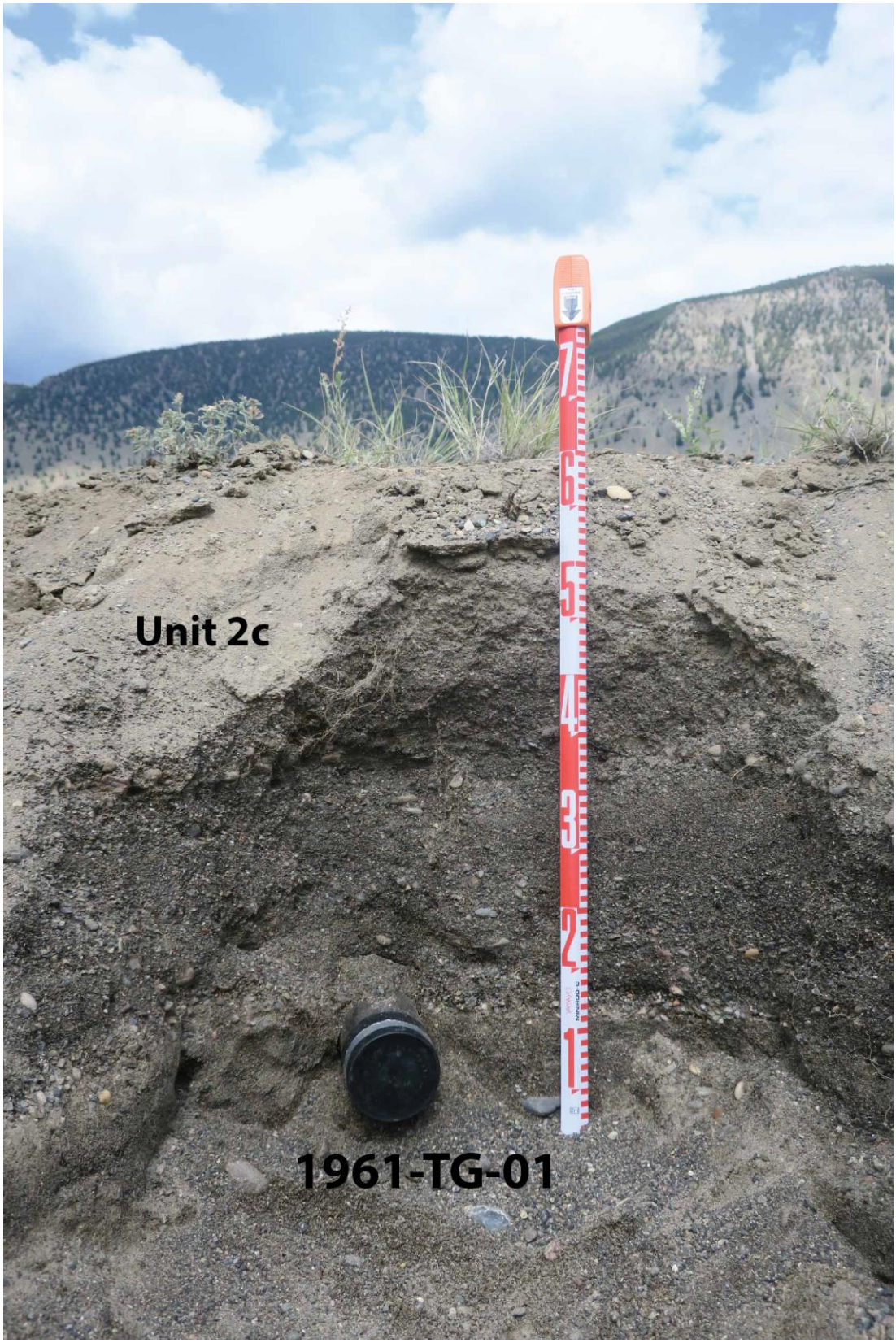

Figure E.8. Optical dating sample 1961-TG-01 was collected from a coarse sand and granule bed of unit 2c, 60 cm below the land surface.

Figure E.9. Optical dating sample 1962-TG-01 was collected from unit 2c medium sand directly above a bed of pebble gravel and 2.5 m below the land surface. 1962-TG-01 was not dated in this study.

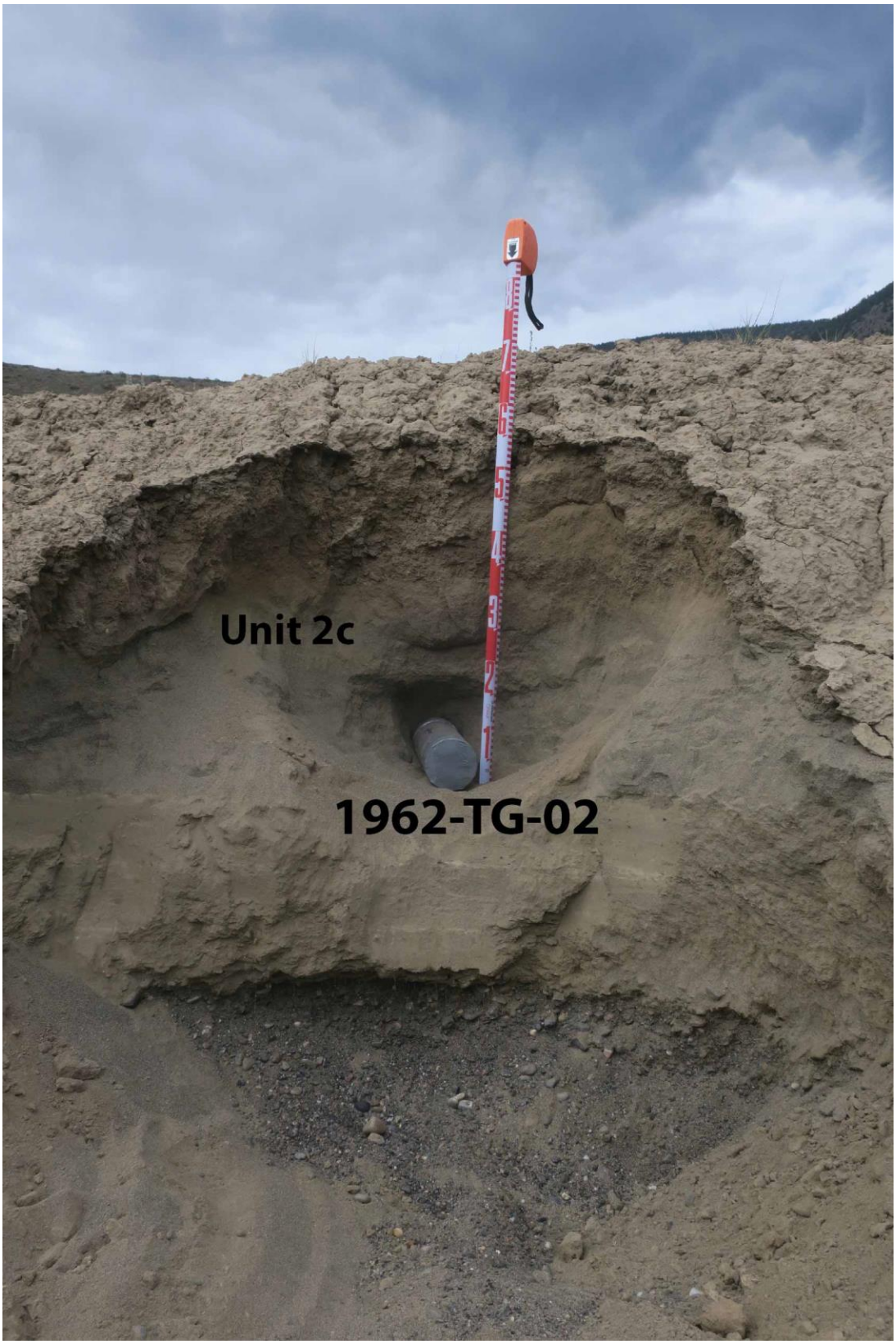

Figure E.10. Optical dating sample 1962-TG-02 was collected from a 50 cm thick sand bed in unit 2c, 80 cm below the land surface.

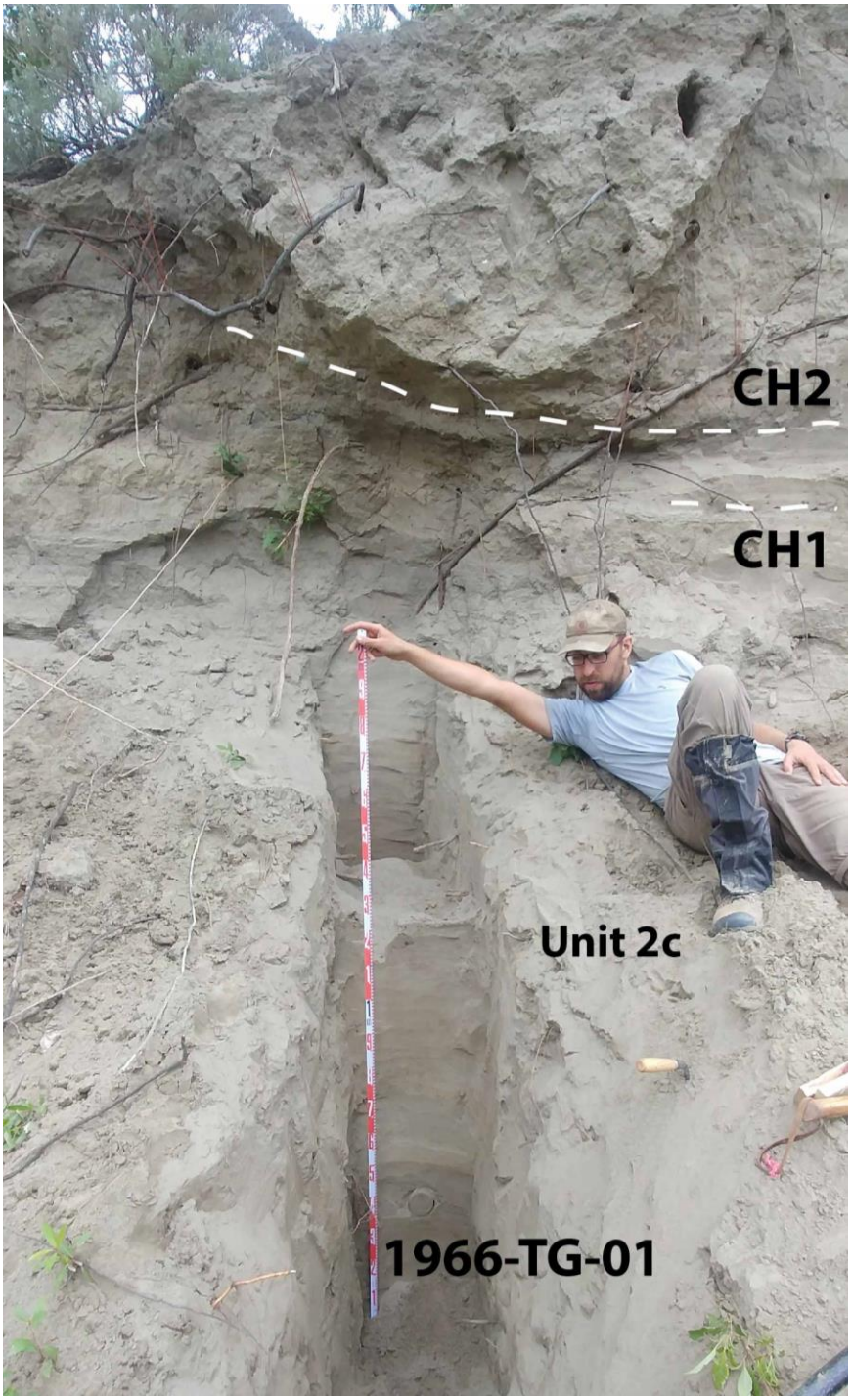

Figure E.11. Optical dating sample 1966-TG-01 was collected from a sand rhythmite in unit 2c, 4 m below the land surface. Charcoal lens and bed associated with radiocarbon samples CH1 and CH2, respectively, are denoted by white dashed lines. This sample was not used for dating.

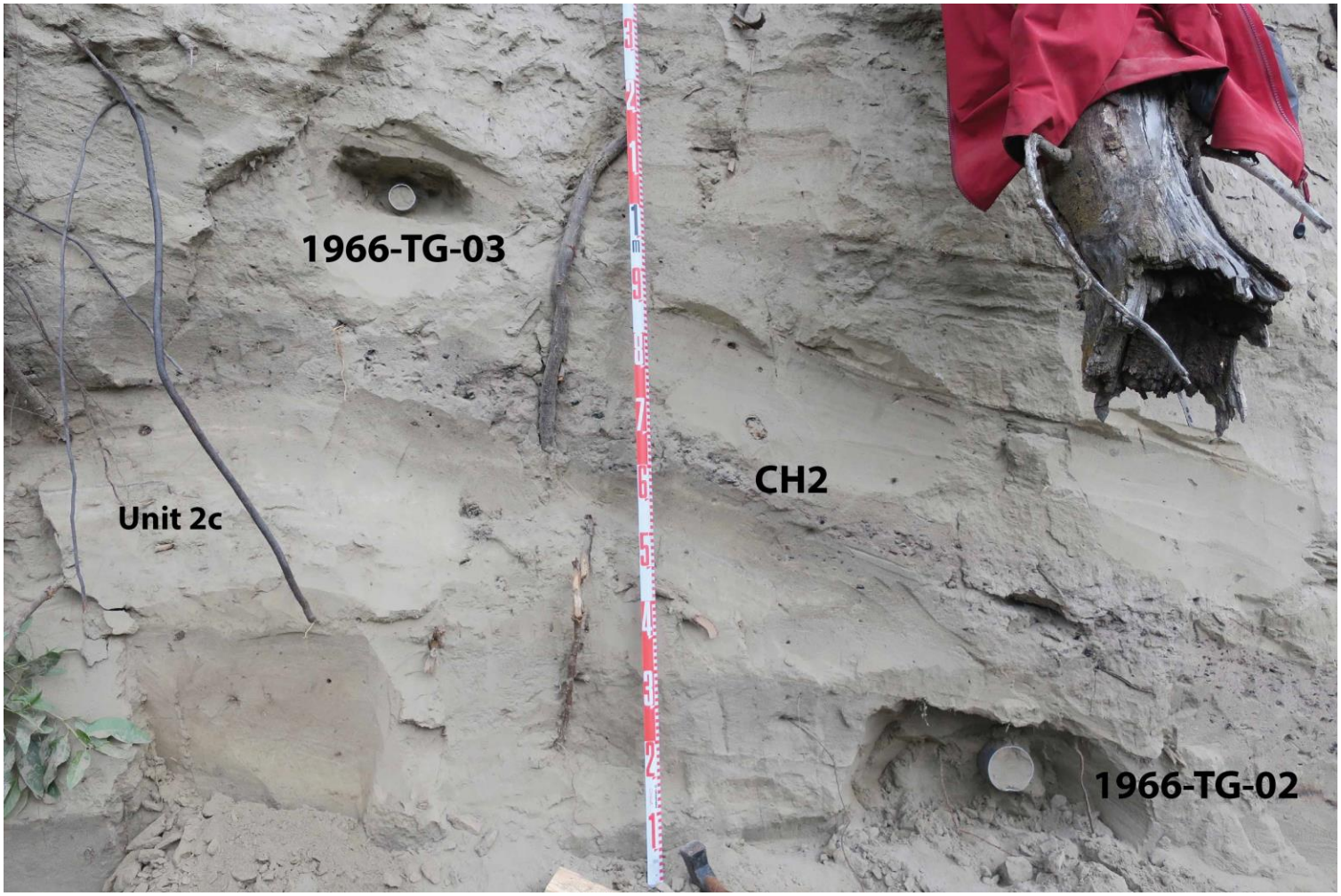

Figure E.12. Optical dating sample 1966-TG-02 was collected from a sand rhythmite in unit 2c below radiocarbon sample CH2 and stratigraphically above radiocarbon sample CH1 (not pictured, to left of frame). Optical dating sample 1966-TG-03 was collected from a sand rhythmite in unit 2c above radiocarbon sample CH2 and below all other charcoal beds.